ADVANCED FUNCTIONAL MATERIALS
www.afm-journal.de

3D (Bio) Printing Combined Fiber Fabrication Methods for Tissue Engineering Applications: Possibilities and Limitations

*Waseem Kitana, Indra Apsite, and Leonid Ionov**

Biofabrication is an emerging interdisciplinary field of engineering that aims to develop technologies for applications in tissue engineering and regenerative medicine. A progressing biofabrication technology is 3D (bio) printing (3DBP), which allows for controlled spatial deposition of cell-laden bioinks in a layer-by-layer approach to fabricate biologically active constructs. Although 3DBP can create some biologically relevant structures, it uses hydrogels, which are isotropic in nature and do not provide sufficient mechanical properties to reconstruct many tissues, such as cartilage, bone, and skin. Additionally, hydrogels alone do not replicate the complex hierarchical buildup of native tissue extracellular matrix (ECM), which contains both gel-like and fibrous components. Replicating native tissue's structure both mechanically and biologically by incorporating fibers would result in enhanced biological performance. This is possible by integrating biofabrication technologies such as 3DBP and fiber fabrication techniques. Thus, harnessing the strengths of each technique and eliminating their limitations. This will enable the fabrication of hybrid 3D constructs with multiscale hierarchy and enhanced mechanical and biological performance comparable to native tissue. This review aims to highlight attempts to combine fiber fabrication methods with 3DBP for tissue engineering applications. Additionally, different fiber fabrication techniques are discussed, showcasing their limitations and possible integration with 3DBP.

1. Introduction

Biofabrication technologies allow the fabrication of both biologically and mechanically relevant 3D tissue-like constructs for tissue engineering and regenerative medicine applications using additive manufacturing technologies. The ultimate aim of biofabrication is to fabricate tissue-like 3D scaffolds that can closely resemble the intricate 3D multiscale, multi-material, and multi-cellular architecture of many native tissues and organs. Thus, biofabrication provides the tools and technologies for the fabrication of such 3D constructs to produce fully functional tissues that ultimately solve the issue of donor tissue and organ shortage worldwide.[1] Biofabrication involves the use of various technologies covering a wide range of fabrication scales ranging from nano to macroscale, such as electrospinning (ES), melt electrowriting (MEW), and 3D (bio) printing (3DBP), respectively. There are also many other less common biofabrication techniques, such as particulate leaching, freeze drying, and many others. Although these biofabrication technologies can individually produce some tissue-relevant constructs, they cannot solely resemble many natural tissues' complex multiscale, multi-material, and multi-cellular hierarchical structures. Indeed, the native tissue extracellular matrix (ECM) of many tissues is composed of intricate hierarchical fibrillar structures embedded within a gel-like ground material. Replicating the complex architecture of native tissues as closely as possible by harnessing the capabilities of different biofabrication technologies would further advance the field of biofabrication toward fully functional tissue and organ development (**Figure 1**).[1b,c,f,2] While each biofabrication technology has its own strengths and weaknesses, selectively integrating or combining different biofabrication technologies unravels more freedom in the fabrication and design of biomimetic 3D scaffolds. For instance, integrating 3DBP with fiber fabrication methods would allow for both the automated patterning of 3D cell-laden biomaterial inks in the macroscale as well as the fabrication of mechanically anisotropic fibers in the nano-and/or microscale. This will result in a hybrid or composite construct that

W. Kitana, I. Apsite, L. Ionov
Professorship of Biofabrication
Faculty of Engineering Science
University of Bayreuth
Ludwig-Thoma-Straße 36A, 95447 Bayreuth, Germany
E-mail: leonid.ionov@uni-bayreuth.de
L. Ionov
Bavarian Polymer Institute
University of Bayreuth
Universitätsstraße 30, 95447 Bayreuth, Germany

The ORCID identification number(s) for the author(s) of this article can be found under https://doi.org/10.1002/adfm.202500450

DOI: 10.1002/adfm.202500450

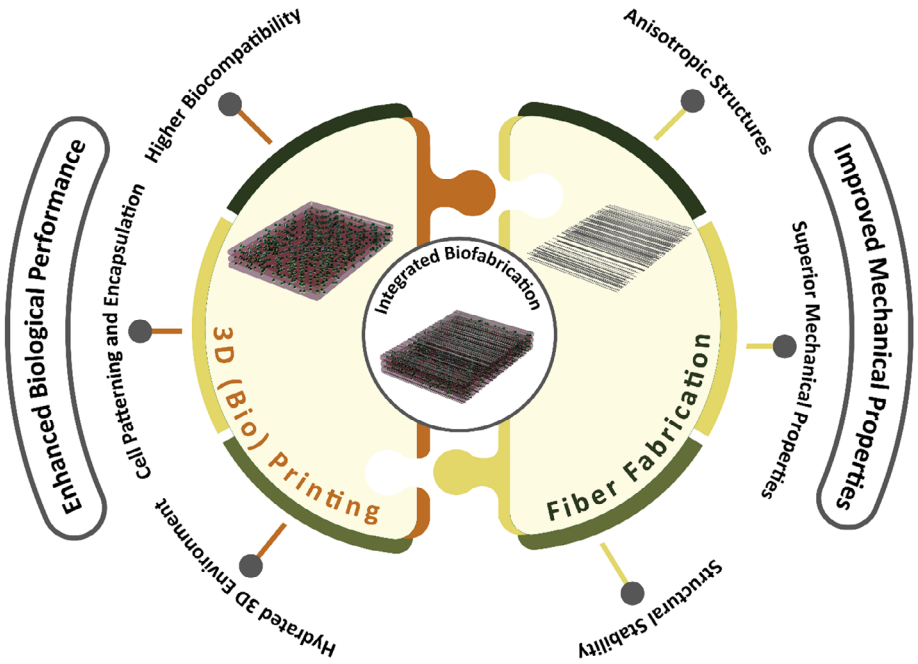

Figure 1. Graphical abstract showing the added advantages of integrating 3D (bio) printing of cell-laden hydrogel precursors with synthetic- and natural-based fiber fabrication methods to yield a composite 3D construct for tissue engineering applications.

better mimics the mechanical and biological properties of ECM of many biological tissues. Furthermore, this integration of hydrogel and fiber systems would improve the overall structural stability of the fabricated 3D constructs both in vitro and in vivo. This review discusses the integration of 3DBP of hydrogel precursors with the most commonly used fiber fabrication methods in the nano, microscale, and macroscale. ES as a conventional fiber spinning method, MEW as an emerging fiber fabrication technology, and melt thermoplastic/FDM 3D printing as an advancing fiber fabrication technique. Additionally, other fiber fabrication techniques that have already been or would be of interest to be integrated with 3DBP for tissue engineering applications are discussed, highlighting their strengths and limitations from the combined approach perspective.

2. Anisotropy of Biological Tissues

Native biological tissues are characterized by their biological and mechanical anisotropy, which provides tissues with functions and properties that are orientation dependent. This anisotropy is provided through the intricate hierarchical structure of tissues' ECM or due to the orientation of cells themselves. Besides water, tissue ECM mainly comprises two main components: i) fibrous component comprising predominantly of collagen and elastin fibrils as structural and mechanical support and ii) gel-like ground materials mainly including proteoglycans (PGs) and glycosaminoglycans (GAGs) such as hyaluronic acid and keratan sulfate. The gel-like component of ECM provides an aqueous hydrated environment for cell proliferation and migration and contributes to the ECM's compressive mechanical properties.[3] The synergy between the different components of the ECM regulates a plethora of cellular activities, such as cell differentiation, cell migration, and mechanotransduction, through a wide range of biophysical, biomechanical, and biochemical cues that regulate tissue function and remodeling.[2c,3a–c,4] In addition to that, the mechanical anisotropy is mainly governed by the fibrous components of the ECM, in which collagen, the most abundant fibrous protein in ECM (up to 85% of total protein mass), is mainly responsible for the tensile properties of tissues. In contrast, elastin gives elasticity to the overall structure that is, in turn, modulated by the orientation of the ECM fibers.[3a,b,d,5] Moreover, these fibers cover a wide range of scales ranging from a few nanometers (e.g., collagen fibrils 10–500 nm) to a few hundred micrometers (collagen fibrillar fibers 1–300 µm) in diameter. This size scale depends on tissue type, fibrillar organization, and tissue function, which modulate tissue mechanical properties and act as guidance cues for cell adhesion, alignment, and direct tissue development.[3c,5,6]

Fiber alignment and arrangement (individual fibers or bundles of fibers) mainly determine the mechanical and structural anisotropy as well as the mechanical strength of several majorly divergent tissues. This includes the musculoskeletal system (skeletal muscles, tendons, ligaments, and articular cartilage), other types of muscles (smooth muscles and myocardium), and many other tissues and/or organs (e.g., skin and stroma of the cornea). Examples include the skeletal muscle,[7] heart myocardium,[8] articular cartilage,[9] meniscus,[10] and corneal stroma.[11] For instance, skeletal muscles show a high degree of alignment of their myofibrils that originates from the alignment of precursor muscle cells called myocytes and their subsequent differentiation into myotubes. Finally, these myotubes fuse into myofibers that, in turn, bundle into tightly packed parallel muscular fascicles. This alignment is induced by both mechanical and structural properties of skeletal muscles governed by the direction of the generated forces and collagen fibers' main

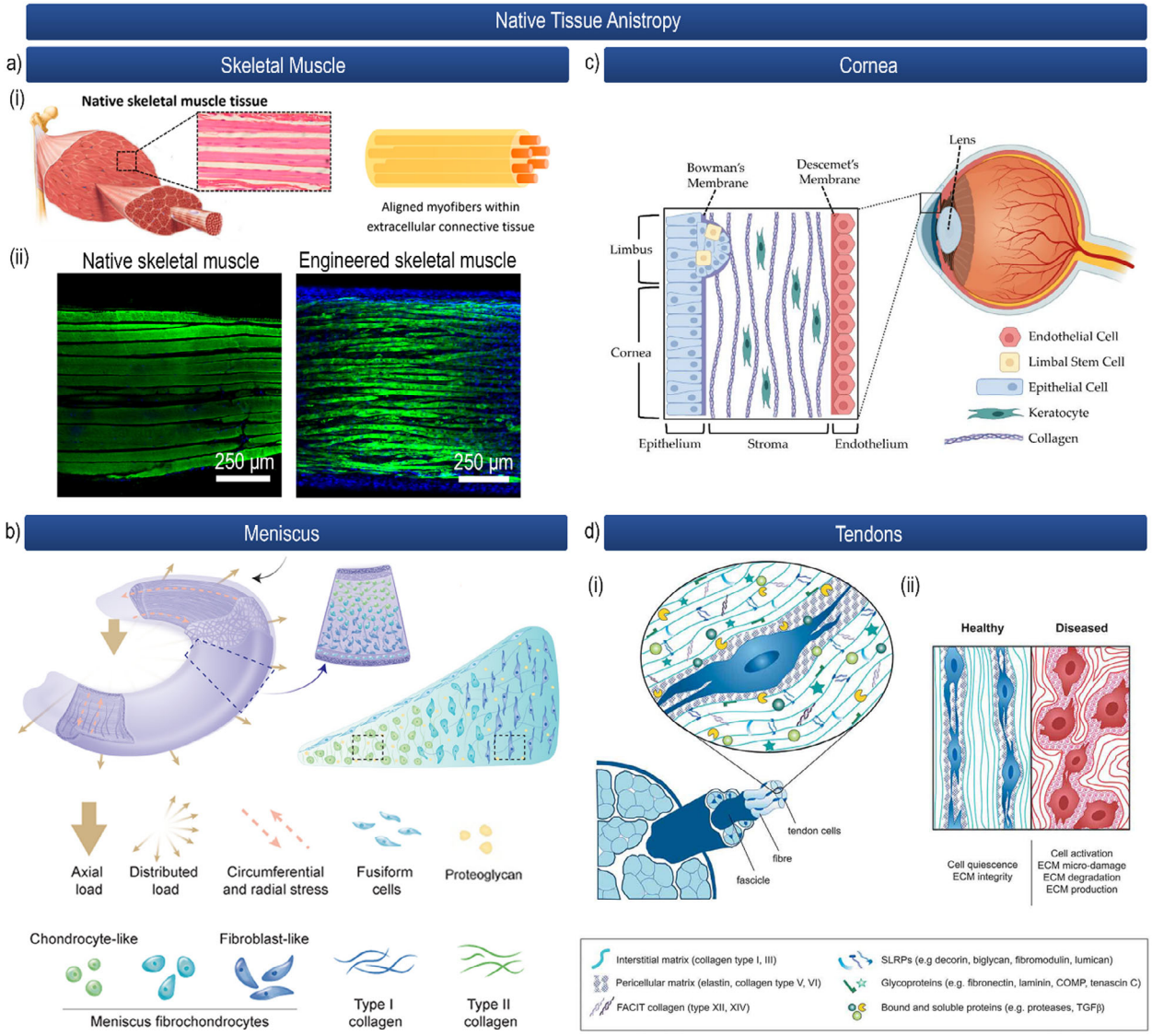

Figure 2. Native tissue anisotropy, where a) native skeletal muscle tissue organization, i) skeletal muscle is composed of aligned myofibers along the direction of extracellular matrix fibers orientation and force generation, adapted with permission from.[12a] Copyright 2015, American Chemical Society, and ii) fluorescence microscope images of native skeletal muscle tissue compared to engineered counterpart, adapted with permission.[7a] Copyright 2015, Acta Materialia Inc. Published by Elsevier Ltd. b) Meniscus tissue cell and fiber anisotropy from different views, which is composed of collagen fibers at different orientations in the radial and circumferential orientations as well as a mesh-like network of fibers and different types of cells are present at different orientations and with different biological functions, adapted under terms of the CC-BY license.[14b] Copyright 2024, The Authors. Publishing services by Elsevier B.V. on behalf of KeAi Communications Co. Ltd. c) Schematic representation of the human cornea anisotropy, where the corneal stroma composed of highly aligned collagen fibers with the keratinocytes aligned along the direction of the collagen fibers, adapted under terms of the CC-BY license.[28] Copyright 2021 by the authors, Licensee MDPI, Basel, Switzerland. d) Tendon extracellular matrix (ECM) composition and anisotropy, where i) tendons are composed of aligned collagen fibers with tendon cells (i.e., tenocytes) showing orientation along the main axis of tension and ii) the difference between healthy and diseased tendon tissues, in which in diseased tissue, both the collagen fibers and tenocytes orientation is disrupted, adapted under terms of the CC-BY license.[16e] Copyright 2020, The Author(s). Published by Informa UK Limited, trading as Taylor & Francis Group.

orientation. At the cellular level, this orientation is fundamental for the differentiation of oriented myoblasts, and at the tissue level, it allows for synchronized skeletal muscle contraction along the generated forces (**Figure 2**a).[7a,b,12] The myocardium is also composed of highly aligned muscular fibers oriented in a wrap-like structure in different orientations along the different layers of the myocardium. This orientation of the fibers is crucial for the proper functioning of the heart through synchronized electrical and mechanical signal propagation along the cardiac myofibers' main direction.[8a,13] Fibrocartilaginous meniscus is also characterized by its highly dense and anisotropic nature. In the meniscus, collagen fibers are organized into three different orientations in three different layers along the circumference, the radius, and at an angle (mesh). These orientations of collagen fibers give rise to the impressive mechanical properties of the meniscus in resisting high loads, for instance, in tension, compression, and

torsion, from all directions. On the other hand, the gel-like content within the different layers of collagen fibers, along with the water content of the meniscus, mainly aids shock absorption and acts as a lubricant. Moreover, the different regions of the meniscus have different types of cells that dominate over other cell types, providing different regional functions (Figure 2b).[4a,10,14] Corneal stroma is another example, where collagen fiber alignment, along with their interaction with other ECM components such as proteoglycans, is vital for the proper physiological behavior of the eye. In the cornea of the eye, the optical transparency, mechanical anisotropy, and mechanical strength of the cornea are highly governed by the arrangement of the collagen fibers in the stroma. These collagen fibers are arranged orthogonally between stromal cells such as keratocytes and further assemble into tightly packed lamellas within a proteoglycan-rich substrate and highly aligned cells. In addition to that, the localized differences in collagen fibers' interfibrillar distances regulate functional properties of the cornea, such as light attenuation and refraction. Moreover, any loss of collagen fiber alignment due to scar formation or other pathophysiological diseases can lead to vision loss or blindness (Figure 2c).[11,15] Tendons and ligaments are types of connective tissues in which the collagen fiber organization is crucial for its considerable mechanical properties. In tendons and ligaments, collagen fibers are aligned in an organized hierarchical manner in the longitudinal, transversal, and horizontal directions. This will allow tendons and ligaments to withstand forces from different directions, including rotational ones. Although collagens are the major component of tendons (up to 85% of total dry weight), other non-collagenous components are present, such as elastin, proteoglycans, and glycoproteins. Proteoglycans play a major role in tendon tissue integrity, compressive properties, and tissue lubrication. Moreover, the major cell type present is called tenocytes, which are highly elongated cells aligned along the tissue's main axis of load, and the disruption of the alignment of tenocytes could lead to tissue dysfunction and tendon degenerative diseases (Figure 2d).[16] In connective tissues, the fraction of total collagen, the main structural protein in ECM, varies widely depending on the tissue type and its main function. For that, it is important to have knowledge about the composition of collagen and other ECM components in the human tissue ECM. In addition to that, connective tissues are characterized by their high content of fibrous components such as collagen and elastin (**Table 1**).

3. 3D (Bio) Printing (3DBP) Techniques

3DBP, as a propitious biofabrication technology, uses a set of different techniques that involve the spatial deposition of cells, biomaterials, and/or bioactive components or molecules with high-level of precision and accuracy to build heterogenous 3D constructs for tissue engineering, pharmaceutical, and regenerative medicine applications.[29] This technique uses computer-aided additive manufacturing (AM) techniques for the automated sequential patterning of cell-encapsulated (bioink) and/or cell-free (biomaterial ink) hydrogel precursors in a layer-by-layer approach, yielding a geometrically relevant and functional 3D tissue-like construct.[29,30] For the fabrication of such constructs, 3DBP uses different modalities such as extrusion, inkjet (droplet-based), volumetric (light-based) /digital light processing (DLP) (light-based), laser-assisted (light-based), and stereolithography (SLA) 3DBP.[29a,c,31]

Extrusion 3DBP is the most commonly used variant due to its simple and cost-effective setup that is based on the direct extrusion of bioinks or biomaterial inks through a nozzle into continuous filaments or strands using either mechanical or pneumatic extrusion methods (**Figure 3a**).[29b,c,32] In contrast, Inkjet 3DBP is a droplet-based bioprinting technique that uses different approaches to control the deposition of bioinks in a droplet-by-droplet manner. These approaches include using thermal, piezoelectric, or electromagnetic stimulation to control the frequency of bioink jetting in the picolitre range of individual droplets (Figure 3b).[29a,33] On the other hand, volumetric 3DBP involves the use of light-sensitive biomaterial formulations known as bioresins for the fabrication of 3D constructs. This is done by controlled light exposure in space (volume) that crosslinks the bioresin at predefined positions through a series of predefined light patterns while the building platform is rotating (Figure 3c-i).[2a,31] Another 3DBP set of techniques, which uses light to crosslink light-sensitive bioinks in a layer-by-layer approach, is stereolithography (SLA)/digital light processing (DLP). SLA is a conventional method in which a scanning raster laser beam is used to photocrosslink the photopolymer in a single spot following a predefined pattern to form a layer. Once the first layer is done, the platform usually moves a certain distance in the *z*-direction to form the subsequent layers. In the case of DLP, a set of digital mirrors or digital display light projections (digital masks) are used to form a complete single layer. Next, the platform moves a certain distance in the z-direction, followed by the formation of the next layers, making it significantly faster than the conventional SLA. One drawback of these techniques (SLA/DLP) is that the 3D (bio) printed structure requires post-treatment, and it is limited only to low-viscosity bioinks that should be as well readily photo-cross-linkable. Another drawback is the difficulty of using multi-material SLA/DLP 3DBP since the 3D (bio) printing process occurs inside a reservoir of liquid bioink, where the 3D (bio) printed structure is submerged in the bioink reservoir. Although SLA/DLP multi-material 3D (bio) printing has been introduced, this leads to higher chances of cross-contamination when transferring between different bioink reservoirs, and it requires additional rinsing or cleaning steps between each transfer (time factor) (Figure 3c(ii,iii)).[34] The major difference between SLA/DLP and volumetric 3DBP is that volumetric 3DBP is a digital light processing unit with a rotating platform to generate light patterns that cure the photopolymer in 3D rather than layer-by-layer 2D patterns. This makes it remarkably faster than both SLA and DLP techniques. Laser-assisted 3DBP (LAB) is a nozzle-free 3DBP technique based on laser-induced forward transfer (LIFT) technology. This technique uses a pulsating focused laser beam to transfer the energy to an energy-absorbing layer. Directly beneath this energy-absorbing layer, there is a layer of a cell-containing biomaterial solution. Due to energy transfer, a high pressure is generated and the cell-containing biomaterial ink is deposited on a substrate located at a distance from the cell-biomaterial layer in drop-by-drop manner (Figure 3c(iv)).[29c,35]

Irrespective of the 3DBP technique used, 3DBP mainly uses naturally derived hydrogel precursor polymer solutions (biomaterial inks) for the biofabrication of hydrogel-based 3D

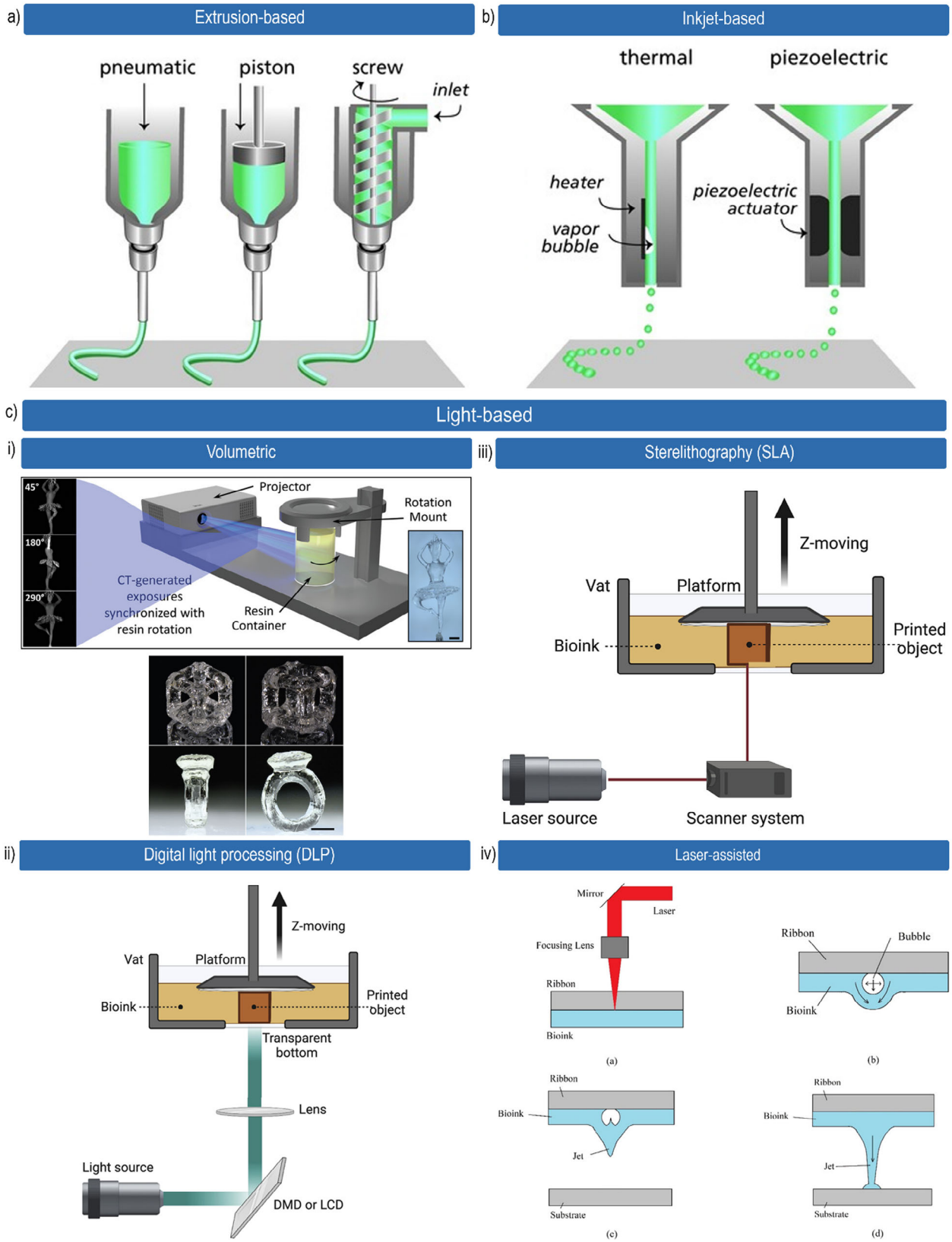

Figure 3. Schematic representation of the different 3D (bio) printing techniques, where a) extrusion-based 3D (bio) printing, in which bioinks are extruded using various methods such as pneumatic, mechanical piston, or screws, reproduced with permission.[1b] Copyright 2013, Wiley-VCH. b) Inkjet 3D (bio)

tissue-like constructs. Although hydrogels are able to mimic the ECM gel-like hydrated microenvironment of many tissues (crucial for cell growth and migration), hydrogels are usually characterized by their poor mechanical properties and low structural integrity. These properties are usually inappropriate for many tissue engineering and regenerative medicine applications that require mechanical robustness, such as bone, cartilage, and tendons.[1a,2c,36] Despite the fact that the mechanical properties of hydrogels can be enhanced by increasing the crosslinking density of the hydrogel and/or by increasing the concentration of the hydrogel precursor. This would have detrimental adverse effects on cells' bioactivity and survival, in which oxygen and nutrient diffusion, as well as cell motility and migration, would be hindered. Moreover, hydrogels are inherently isotropic, which does not resemble the anisotropic nature of ECM of many tissues. Thus, hydrogels require reinforcing components that elevate their wide applicability to further tissue engineering applications.[1a,2c,36b]

4. Fiber Fabrication Methods for Tissue Engineering

Fibers are present in abundance in nature, such as in plants (e.g., wood) and in animals (e.g., silk), and have been used throughout human civilization for many different applications, such as building materials and textile manufacturing. Thanks to the impressive mechanical properties of fibers and their inherent anisotropy, they contribute to the inspiring mechanical properties of human tissues, such as muscles and fibrocartilaginous tissues (e.g., meniscus). In tissues, these fibers either show distinct orientation/unidirectional alignment, such as in skeletal muscles, disordered orientation, such as in the skin, or a combination of different orientations (unidirectional, circumferential, and mesh-like), such as in the knee meniscus. These kinds of orientations contribute to a set of various mechanical and structural properties in different tissues serving different unique functions.

Fiber-shaped structures can serve as a fundamental building block to form complex functional 3D objects for various applications, such as tissue engineering applications. These fibers are characterized by a set of distinct properties; they are long and thin (have an incredibly high aspect ratio), flexible, and have higher elastic modulus and strength compared to their bulk counterpart due to the alignment of polymer chains. This makes their organization into ordered structures of interest for building complex hierarchical 3D constructs. This can be done using different techniques such as weaving, braiding, wrapping, folding, winding, and reeling.[38] In tissue engineering, there are other types of processing techniques to fabricate fibers of different sizes ranging from a few nanometers to hundreds of micrometers as continuous single fibers as in melt electrowriting (MEW) or continuous jetted fibers as in electrospinning (ES). These fibers are also collected using different collection methods depending on the fabrication technique and collector type used. For living cells, it is essential that the fabricated microenvironment closely resembles their native ECM environment, in which they should have an appropriate aspect ratio and fiber diameter size that corresponds to the fibrous proteins found in ECM, such as collagen fibers. For instance, native collagen fibrils have a diameter range of ≈10–500 nm and an estimated aspect ratio of 14–50 × 10^4 (see section 2 above for more details on the native collagen organization and structure in native tissues).[39]

The fiber formation process usually consists of i) pulling of polymer solution or melt, ii) its solidification by either evaporation of solvent (dry spinning), precipitation in poor solvent (wet spinning), or solidification below glass transition temperature or due to crystallization (melt spinning). The polymer can be formed into fibers from the state when it is fluid, either in solution or melt state. Different forces or sets of forces can be involved in the fiber fabrication process: electrostatic, mechanical, and/or magnetic. The advantage of using electrostatic forces is that they can be applied to any polymeric material and cause its polarization. But on the other hand, the precise or localized application of electrostatic forces is challenging. Furthermore, high electrostatic potential is harmful and needs special safety precautions. In contrast to electrostatic forces, magnetic forces are considered not harmful, allowing them to be used without any special safety measures. Nevertheless, the polymers used should be sensitive to the magnetic field by including magnetic particles in the polymer composition. In addition to that, the local application of magnetic forces is also challenging. In the case of mechanical forces, mechanical forces can be applied to the entirety of the polymer to be fabricated into fibers, such as centrifugal spinning, which allows for fast fiber fabrication. However, mechanical forces can also be applied locally, allowing for precise fabrication of individual fibers with a low fiber production rate. Independent from the fiber fabrication method and applied force, fiber formation highly depends on the rheological properties of the polymer solution or melt, which in turn depends on the type of interaction between polymer chains, molecular weight, concentration, temperature, and magnitude of applied force. In this chapter, the most commonly used fiber fabrication techniques used in tissue engineering are discussed: electrospinning (ES), melt electrowriting (MEW), and thermoplastic/fused deposition modeling (FDM) 3D printing, as well as other fiber fabrication techniques that would be of interest to be combined with 3DBP.

4.1. Common Fiber Fabrication Techniques

4.1.1. Electrospinning (ES)

Currently, ES is the most commonly used technique for the fabrication of fibrous mats and meshes for tissue engineering

printing, in which droplets of the bioinks are deposited using different drop-based mechanisms such as thermal and piezoelectric; and light-based 3D (bio) printing such as i) volumetric 3D (bio) printing, in which a bioresin is cross-linked using light projections in volume while the platform is rotating, reproduced with permission.[37] Copyright 2020, Lawrence Livermore National Security, LLC. Published by Wiley-VCH GmbH. ii) Digital light processing (DLP) and iii) stereolithography (SLA), in which the bioresin is cross-linked in a layer-by-layer approach, using digital mirrors (DMD or LCD) or focused scanning beam, respectively, with permission.[34a] Copyright 2023, the Author(s), Elsevier. And iv) laser-assisted 3D (bio) printing, in which laser is used to deposit a bioink droplet by directing the laser into a layer of bioink attached to a ribbon or an absorbing layer, reprinted with permission.[35] Copyright 2021, Wiley-VCH GmbH.

Table 1. Structural and organizational properties of collagen fibers in different tissues.

	Total collagen	Fibrillar collagen	Interfibrillar space	Fibrillar diameter [μm]	Fibrillar fiber (bundles) diameter [μm]	Fiber orientation	Refs.
Skeletal muscle	70% of total protein	52% of total protein	Densely packed	0.01–0.3	0.6–50	Aligned along the main axis (parallel arrangement)	[3d,17]
Articular cartilage	59% of total protein	45% of total protein	Highly variable (Superficial, middle, deep, and calcified zone)	0.02–0.24	n.a.	Parallel, perpendicular, and random.	[3d,18]
Tendon	81% of total protein	66% of total protein	0.05 μm (densely packed)	0.02–0.15	1–300	Aligned along the main axis (parallel arrangement)	[3d,19]
Bone	n.a.	90% of total protein	Highly variable (dense or trabecular)	0.03–0.12	1–3	Parallel arrangement (non-uniformly distributed, transverse, longitudinal, and a combination of transverse and longitudinal)	[3d,20]
Adipose tissue	Below 45% of tissue dry mass	n.a.	Loosely dense	0.01–0.06	30	Parallel arrangement in the septa follows a circular-like pattern (around lobules)	[21]
Intervertebral disk	Annulus fibrosus: 60% of tissue dry mass; Nucleus pulposus: 15% of tissue dry mass	n.a.	Variable (Periphery to center gradient)	0.02–0.19	5	Annulus fibrosus: Parallel with alternating angles ±30° (ply-angled)	[22]
Meniscus	85% of tissue dry mass	n.a.	Highly variable between different layers	0.03–10	150–300	Mesh-like, circumferential, and transverse	[23]
Skin	80% of tissue dry mass	n.a.	1–20 μm	0.05–0.12	20–50	Multilayered organization: Reticular dermis: aligned (follows Langer's lines); Papillary and periadnexal dermis: random orientation	[24]
Cornea	82% of total protein	51% of total protein	0.06 μm	Stroma: 0.03–0.07; Sclera: 0.03–0.3	5–35	Orthogonally stacked (central cornea) and circumferential alignment (periphery)	[25]
Blood vessels	n.a.	40% of tissue dry weight	n.a.	0.01–0.1	Media: 2–4; Adventitia: 15–26; Lumina: 5–30; Ablumina: 4–25 (Aorta)	Media: Circumferential (Parallel arrangement); Adventitia: longitudinal (Parallel arrangement)	[26]
Myocardium	42% of the total protein in the heart	n.a.	n.a.	0.05–0.15	1–10	Multilayered organization: Longitudinal and circumferential to the myofiber direction (Parallel arrangement)	[27]

applications. This technique is based on drawing fibers from a polymer solution droplet by applying an extremely high electric voltage, usually in the range of tens of kilovolts (kV), between the oppositely charged electrode within a distance ranging from 5 to 30 cm. The process starts with applying a voltage difference between the tip of the needle and the collector, which depends on the dielectric properties of the polymer solution used. In addition to that, it highly depends on the formation of a proper Taylor cone of the polymer solution at the electrified (usually positively charged) tip of the needle for the proper fiber jet formation and subsequent fiber collection in the range from tens of nanometers to few micrometers in diameter (10 nm–10 μm) on the oppositely charged collector with relatively large linear rate (several m s^{-1}) (**Figure** 4a and **Table** 2). This requires the fine adjustment of the contents of the spinning dope, voltage applied, needle tip to collector distance, and type of collector to achieve the required droplet surface tension and subsequent fiber jet initiation.[1b,40] Additionally, any instabilities in the electric field and environmental conditions, such as temperature and humidity, cause uncertainties in the fiber fabrication process.[41] Moreover, the polymer solution's initial viscosity is an important factor for smooth bead-free fiber formation. The reported viscosity range of the ES polymer solution is 1 – 5000 mPa·s.[42] Although electrospinning provides several advantages for several tissue engineering applications, such as a high surface area for cell adhesion and proliferation as well as a high degree of porosity at the cellular level, it usually results in 2D fibrous structures with limited thicknesses (usually <1 mm) rather than 3D structures with

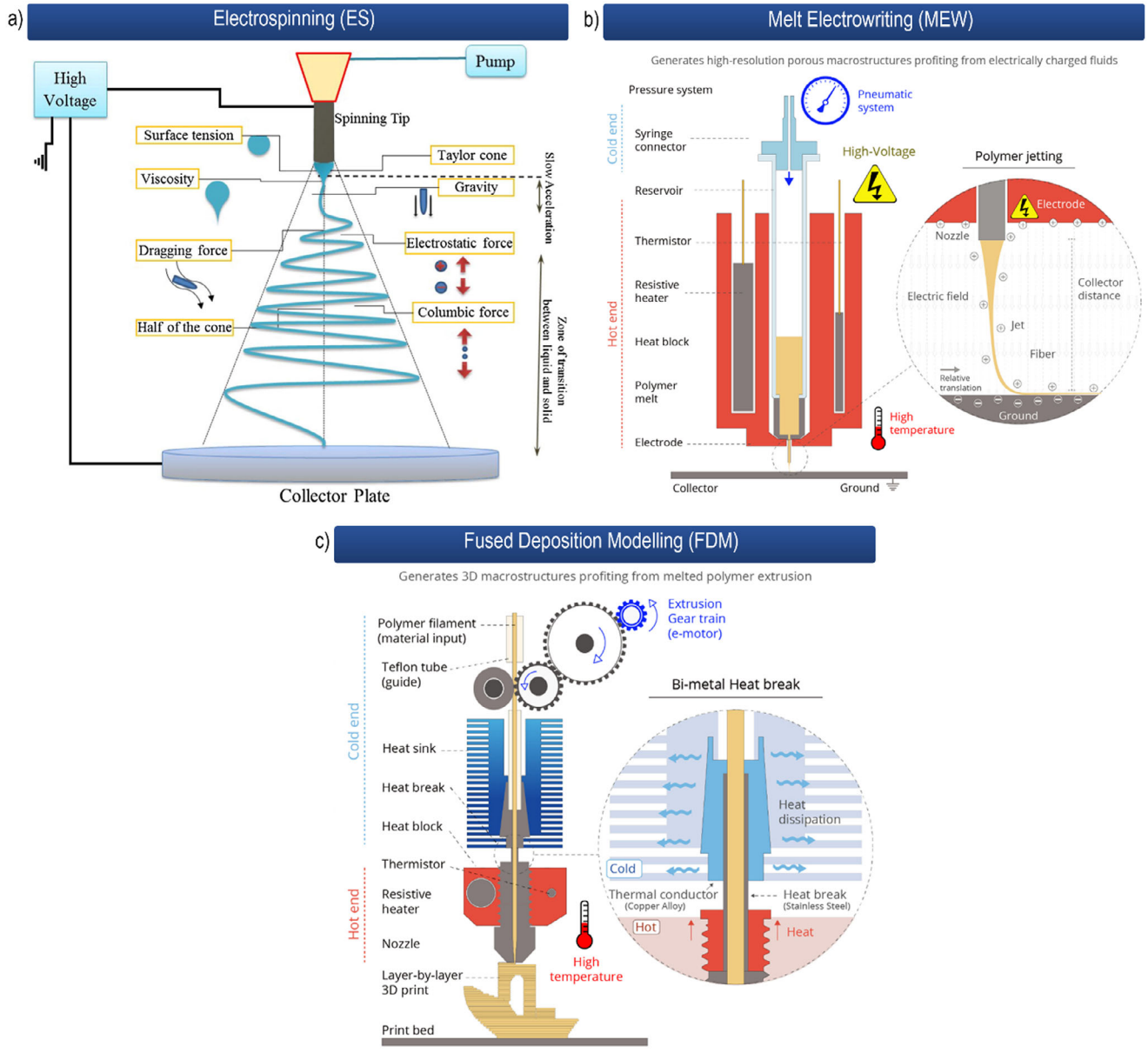

Figure 4. Comparison between the most common fiber fabrication methods working principle showing the most common setup, where a) electrospinning (ES). Reproduced with permission.[54] Copyright 2016, Elsevier B.V. All rights reserved. b) Melt electrowriting (MEW). Reproduced under terms of the CC-BY license.[51a] Copyright 2023, The Authors, Published by Elsevier B.V. And c) fused deposition modeling (FDM) 3D printing, reproduced under terms of the CC-BY license.[51a] Copyright 2023, The Authors, Published by Elsevier B.V.

controlled 3D architecture mimicking the 3D architecture of many tissues ECM.[11b,14a,43] Additionally, increasing the electrospun fibrous mat thickness usually leads to denser structures with limited porosity for cell infiltration and nutrient and oxygen diffusion. While having a dense fibrous structure could be beneficial for some tissue engineering applications, where it acts as a physical barrier for limiting bacterial penetration[44] or limiting surrounding fibrotic tissue infiltration.[45] Having less dense fibers with controlled porosity is beneficial for other tissue engineering applications where cell infiltration and light transmittance are crucial, such as for corneal tissue engineering applications.[11b] Besides that, the fabrication of commercially relevant fibrous structures is limited due to the relatively slow fabrication process and high energy consumption, which might take several hours to a few days to fabricate fibrous structures in the range of a few cm^3.[36a,46] Moreover, due to the use of high electrical fields, the orientation of the polymer chain in the fabricated fibers cannot be precisely controlled, resulting in fibers with poorly predictable mechanical properties compared to that provided by other fiber fabrication techniques.[47] Another drawback of ES is the limited ability to fabricate constructs with complex geometrical structures, which are anatomically relevant.[14a,43] A further major drawback of the ES process is the poor control over fiber deposition on the substrate, which leads to polymer losses

Table 2. Comparison between the most commonly used fiber fabrication methods based on different process parameters showing the most common configuration and reported ranges.

	Electrospinning (ES)	Melt electrowriting (MEW)	Fused deposition modeling (FDM)
Voltage needed	8–40 kV	1–15 kV	n.a.
Common material feeding system	Pneumatic	Pneumatic	Mechanical
Nozzle to collector distance	5–30 cm	0.1–3 cm	Direct contact
Maximum temperature	n.a.	150 °C	350 °C
Maximum thickness	1 mm	10 mm	Limited to printer height
Fiber diameter	10 nm–100 µm	0.8–150 µm	50–600 µm
Typical viscosity range	1–5000 mPa·s	100–1000 Pa·s	10–100 000 Pa·s
Polymer feed	Solution (most commonly used solvents: chloroform, DMF, and DMSO)	Melt	Melt
Volumetric flow rate (fabrication rate)	10–5000 µL h^{-1} (10–2000 mm^3 h^{-1})	0.5–50 µL h^{-1} (0.5–50 mm^3 h^{-1})	10 000–115 000 µL h^{-1} (10 000–115 000 mm^3 h^{-1})
Head movement speed	n.a.	100–6000 mm min^{-1}	600–30 000 mm min^{-1}
Material loss	high	low	Depending on the amount of support needed
Main features	Fibers are stretched; In the basic setup, fibers are disordered; Alignment of the fibers can be obtained by using a parallel plate or rotating collector.	Fibers are not stretched; Nearly any pattern is possible; Continuous fiber formation occurs for complex geometries, where fiber overlapping occurs.	Fibers are not stretched. Any pattern or geometry is possible. High dimensional accuracy. Do not use extremely high voltages for fiber fabrication.

and inhomogeneous fiber distribution along the collector with regions having larger fiber thickness compared to other regions on the substrate. Besides that, by nature, ES produces disordered fibrous structures in which the fibers are randomly oriented. For the fabrication of aligned fibers for tissue engineering applications, usually a highly rotating mandrel is used. In this case, the mandrel is rotating at a tangential rotational rate higher than the fiber production rate, producing fibers mainly oriented in the direction of rotation. On the other hand, at lower rotational speeds (lower than fiber fabrication rate), the fibers crimple and lose orientation. Generally, these rotational speeds generate high centrifugal forces, which limits its integration with other biofabrication techniques that deposit materials on stationary flat surfaces, such as 3DBP. Although there are less commonly used methods to produce aligned fibers using ES, each approach has its own limitations. For further information on different methods to produce aligned fibers using ES, please refer to the review paper of Robinson et. al.[40b] In summary, the extremely high voltage used, poor control over fiber orientation and deposition, sensitivity to polymer solution conductivity and environmental conditions, low fabrication rate for commercial applications, and the limited thickness to fabricate 3D structures limit its wide application in advanced tissue engineering applications.[48] Thus, the combination of ES with 3DBP would resolve the majority of the abovementioned limitations, yielding more complex 3D geometries.

4.1.2. Melt Electrowriting (MEW)

MEW also known as melt-based electrohydrodynamic (EHD) printing is one of the most commonly used biofabrication techniques for the fabrication of fibers in a controlled deposition manner. This technique is based on using high electrical voltage in the range of a few kV (usually 1–15 kV) over a collector-to-nozzle distance of 0.1–3 cm to draw a single continuous fiber in the range of a few micrometers in diameter (usually 1–150 µm) from an extruded polymer melt using AM techniques (Figure 4b and Table 2).[49] Although the viscosity is dependent on the temperature and the shear rate used, the typical melt shear viscosity is in the range of 100–1000 Pa·s, with the highest zero shear viscosity reported at 1×10^6 Pa·s[50] and the lowest melt shear viscosity of 3 Pa·s at a shear rate below 30 s^{-1} and temperature of 190 °C.[50] Unlike ES, MEW uses a high-viscosity polymer melt with a low flow rate rather than a low-viscosity polymer solution. MEW was first introduced by Brown et al. in 2011 with the name melt electrospinning writing. Since then, there has been an increased number of publications highlighting the use of MEW for the fabrication of tissue engineering scaffolds. This technique was introduced to solve the problem of non-controlled and random deposition of fibers provided by solution ES, which usually results in non-controlled pore geometry and size as well as non-controlled fiber diameter and fibrous mat thicknesses. Although MEW results in a relatively larger fiber diameter compared to solution ES, it provides superior control over fiber spatial deposition. This results in an automated controlled fabrication of high-resolution 3D fibrous constructs with controlled pore geometry for tissue engineering applications. In this technique, a close consideration of the polymer flow rate/jet speed and extrusion head/collector movement rate is crucial for the formation of straight fibers rather than buckled or lagged ones (critical translational speed). Additionally, in MEW, the polymer flow rate/jet is controlled by the synergy between extrusion temperature (governing polymer viscosity), nozzle inner diameter,

extrusion pressure, and voltage. The extrusion head and collector movement can be precisely controlled by the MEW setup hardware and software.[49b,c,51] From the rheological point of view, the movement rate should be lower than the reciprocal relaxation time of the polymer melt. If the movement rate exceeds this limit, the fiber will lose its ability to adhere to the substrate properly, and the fibers will be stretched between the nozzle and substrate without adhering to the substrate. Although MEW provides enhanced spatial control over the deposition of fibers compared to ES, the thickness of the fabricated constructs using the most common setup is limited to ≈7 mm due to charge dissipation with increased height and does not provide clinically relevant thicknesses alone.[14a,49c,52] Recently, using a modified setup of MEW, the thickness limitation has been increased to ≈10 mm. This was achieved by incorporating a charge neutralization module besides the MEW extrusion head.[52a] In addition to that, MEW is characterized by its slow fiber fabrication rate and, more specifically, for the fabrication of fibers in the lower fiber diameter limit of this technique, in which polymer flow rate in the range of from hundreds of nL h^{-1} to few µL h^{-1} is crucial.[51a] Additionally, MEW provides a limited material choice, since it requires polymers with low melting point, relatively low viscosity, and high degradation temperature, such that PCL with molecular weight of up to 100 kDa. By far, PCL is the most commonly used polymer for MEW due to its low melting point and its preferable crystallization dynamics.[51a] Adding to that, in the MEW process, reversing the movement direction rapidly is challenging due to the mass of the electrical and mechanical components involved in the fabrication process. The rotation or movement of the rotor of the stepper motor, lead screw, and extruding unit must be reversed rapidly to change the movement direction effectively. This fast motion will result in vibrations, which require the gradual deceleration of the fabrication process, leading to a further reduction in the fabrication rate. Even though this effect can be reduced by fabricating considerably larger sample sizes, the limiting factor will be controlling the flow rate of the polymer by decreasing the polymer melt viscosity (i.e., increasing temperature).[52b] In a typical MEW setup, the polymer melt is deposited in a relaxed state (i.e., the polymer chains are not oriented), meaning that the MEW fibers have a lower modulus than fibers produced with stretched chains. The use of polymers with low molecular weights that are needed to have a viscosity in a proper range also limits the strength and toughness of fabricated structures. Another limitation of MEW is that it requires a conductive substrate, and the deposition of free-hanging fibers is not possible, and for that it requires support for deposited fibers. In summary, the main limitation of the MEW process lies in its relatively slow fabrication process, the limited thickness of its fabricated substrates, the requirement of a conductive substrate and support for deposited fibers, and the limited material choice. This can be solved, for instance, by integrating MEW with other biofabrication techniques to yield 3D constructs with clinically relevant thicknesses and with an increased fabrication rate. It is also noteworthy to mention that there is also a variant of EHD printing (solution-based EHD printing) that uses polymer solutions for fiber fabrication. Solution-based EHD printing is less commonly used in tissue engineering applications since it usually yields fibers in diameter ranges (>tens of micrometers) higher than melt-based EHD printing. For detailed information on EHD printing possibilities and limitations, please refer to J. He, et al. 2020.[52b]

4.1.3. Fused Deposition Modelling (FDM) 3D Printing

FDM 3D printing, also known as thermoplastic melt 3D printing, involves the heating of a thermoplastic polymer above its melting point and subsequently pushing the melted polymer through a nozzle (0.1–1.5 mm in diameter) into filaments or strands onto a heated bed (30–120 °C) by direct contact between the nozzle and the heated bed. Through computer-aided manufacturing (CAM) processes, these filaments are deposited in a layer-by-layer approach to fabricate 3D constructs based on a predesigned model using computer-aided design (CAD) tools (Figure 4c and Table 2). Although FDM 3D printing is superior to other fiber fabrication techniques for the fabrication of reproducible and geometrically relevant 3D structures in the macro range, it is technically challenging to produce fibrous structures at the cell level that replicates the fibrous structure of native ECM, which is in the range of nanometers to few micrometers.[14a] For instance, depending on the 3D printing settings and nozzle size used, FDM 3D printing can produce fibrous structures as small as 50 µm—although challenging—using 0.1 mm nozzle up to hundreds of micrometers using larger nozzle sizes (Table 2).[1a,14a,51b] This would limit the interaction of cells with FDM 3D printed fibers due to the lack of proper mechanical and spatial cues at the cell level provided by the FDM 3D printed fibers, which limits cell alignment and its subsequent differentiation.[53] In conclusion, the main limitation of FDM 3D printing is the limited resolution and the need for elevated fabrication temperatures.

4.2. Other Fiber Fabrication Techniques

In this section, other fiber spinning techniques that have the potential to be or have already been integrated with 3DBP methods for the fabrication of hybrid structures composed of fibers and hydrogels are discussed.

4.2.1. Mechanical Pulling

In mechanical pulling, straight fibers can be fabricated by stretching at a rate larger than the reciprocal relaxation time of polymer when it is in an elastic state and behaves as a rubber. In this case, a close consideration of the applied strain degree is highly important, as considerably large strains (fiber stretching during spinning) occur at large extension rates when the material is in a rubbery state, resulting in the failure of the fibers. In addition to that the stretched fibers require a collection or deposition step to be deposited on a platform or substrate. For that, a wide range of fiber collection methods have been proposed and discussed. **Table 3** shows a direct comparison between the different fiber fabrication methods that will be addressed in this section based on fiber fabrication conditions, and **Table 4** shows the polymer state and main force used to fabricate the fibers in comparison with ES and MEW.

Touch Spinning (TS): TS was first introduced as a promising technique for the fabrication of nanofibrous constructs as

Table 3. Comparison between other fiber fabrication methods showing the reported processing parameters and polymers investigated, including the main feature of each technique and tissue engineering applications.

Fiber fabrication technique	Viscosity range	Fiber diameter range	Fiber production rate	Main fiber fabrication force	Fiber arrangement	Collector type for aligned fibers	Polymer state	Polymers investigated	Cell type and tissue engineering applications investigated	Main features
Touch spinning (TS)	–	0.04–5 µm	Up to 40000 mm^3 h^{-1} (with a fiber diameter of 10 µm and 100 cm rotating stage)	Mechanical pulling	Random and aligned	Stationary	Solution/melt	PCL, PE, PCL-PU, PEO, PAN, and PVA	C2C12 (skeletal muscle tissue engineering), NIH 3T3 (fibroblasts), and NSCs (neural stem cells; neural tissue engineering)	• Highly aligned fibers. • Patterned fibers are possible. • No need for high voltage.
Handspinning (HS)	–	0.1–1 µm	–	Mechanical pulling	Aligned	Stationary	Solution/melt	PVAc and PP	–	• Simple and inexpensive setup. • No need for high voltage. • Slow fiber fabrication rate.
Pull Spinning	0.1–1 Pa·s	0.2–1.2 µm	130 mm^3 h^{-1} (0.15 g h^{-1})	Mechanical pulling and centrifugal force	Random, aligned, and threaded	Stationary or rotating	Solution/melt	PCL, PU, blend of nylon and PU	C2C12 and primary human vascular smooth muscle cells (muscle tissue engineering)	• Both aligned and random fibers are obtained at the same time.
Spinneret-based Tunable Engineering Parameters (STEP)	–	0.05–0.5 µm	–	Mechanical pulling	Aligned	Stationary or rotating	Solution/melt	PS, PMMA, PLA, and PLGA	C2C12 (skeletal muscle tissue engineering) and C3H10T1/2 (multipotent fibroblastic cells)	• Highly aligned fibers. • Patterned fibers are possible. • Fiber spacing can be controlled.
3D Melt Blowing (3DMB)	–	1–100 µm	5250 mm^3 h^{-1} (6 g h^{-1})	Air force	Random and aligned	Rotating	Melt	PCL, PLA, PU, and PC elastomer	NIH 3T3 (fibroblasts), hernia plug, and meniscus tissue engineering	• Highly organized and aligned fibers in 3D. • Use of a multi-axis robotic arm-controlled platform. • High fabrication rate.
Track Spinning	–	0.45–40 µm	–	Mechanical pulling	Aligned	Stationary	Solution/melt	PVAc and PU	–	• Highly aligned fibers. • Fibers with variable lengths. • Fibers from high-viscosity solutions or melts can be produced.
Centrifugal/rotary jet spinning	0.05–113 Pa·s	0.03–15 µm	55 000 mm^3 h^{-1} (60 g h^{-1})	Centrifugal force	Random and aligned	Stationary	Solution/melt	e.g., PLA, PLLA, PAA, PEO, PVP, and gelatin.	Primary rat cardiomyocytes (cardiac tissue engineering) and Human dermal fibroblasts	• Extremely high fiber fabrication rate. • Circumferentially aligned fibers.

(*Continued*)

Table 3. (Continued)

Fiber fabrication technique	Viscosity range	Fiber diameter range	Fiber production rate	Main fiber fabrication force	Fiber arrangement	Collector type for aligned fibers	Polymer state	Polymers investigated	Cell type and tissue engineering applications investigated	Main features
Magnetospinning	6–90 Pa·s	0.05–5 µm	Up to 450 mm^3 h^{-1} (with fiber diameter of 2.5 µm and 100 cm rotating stage)	Magnetic force and mechanical pulling	Random and aligned	Rotating	Solution/melt	PCL, PTFE, PEO, PS, PVDF, and PMMA (mixed with nickel oxide or iron oxide)	NIH 3T3 (fibroblasts)	• Fibers with magnetic properties. • Simple and inexpensive setup. • Fibers can be produced independent of their other properties, such as dielectric point.
Gravity Fiber Drawing (GFD)	–	0.1–100 µm	–	Gravitational force	Aligned	Stationary	Solution/melt	PCL	RAW264.7 cells (macrophage)	• Aligned and patterned fibers. • Freestanding single fibers. • Precise control over individual fiber orientation and fiber spacing. • A wide range of fiber diameters are covered.
In Situ Fiber Tethering via Orbital spinning	50 Pa·s	0.5–10 µm	–	Mechanical pulling	Aligned	Stationary or rotating	Solution	HA with high molecular weight PEO (PEDOT:PSS as a conductive component)	In Situ fiber spinning on chicken embryo	• Single fiber drawing. • Substrate-free. • Surface curvature and topography adaptation (in situ spinning).

Table 4. Polymer state and main force are used for fiber drawing using different fiber spinning techniques.

		Main force				
		Electric	Mechanical	Magnetic	Air jet	Gravitational
State	Melt	Melt electrowriting	• Touch spinning • Centrifugal spinning • Handspinning • Pull Spinning • Spinneret-based Tunable Engineering Parameters (STEP) • Track Spinning • In Situ Fiber Tethering via Orbital spinning	Magnetospinning	3D Air Blowing	Gravity Fiber Drawing (GFD)
	Solution	Electrospinning				

scaffolds for tissue engineering and regenerative medicine applications in 2015 by Tokarev et. al. TS can be described as a simple, controllable, customizable, and scalable method for the fabrication of biomimetic scaffolds by mechanically drawing fibers from a polymer solution or melt using a shaft with high rotational speeds into fibrous meshes with fibers in various orientations, controlled densities, varying thicknesses, and fibers from different polymers combined or alone. In this technique, a polymer solution/melt is usually introduced using a syringe pump through a needle with a consistent droplet formation in close proximity to a collecting rod that is attached to a rotating disk. Once the rod touches the polymer solution droplet, it mechanically pulls the droplet and extends it into fibers that are collected on a static or rotating collector (**Figure 5a**). This will eliminate the need for extremely high voltages that are commonly used in other fiber fabrication techniques, such as ES and MEW. The fabricated fiber diameter is usually uniform in the range of a few nanometers to a few micrometers and can be accurately adjusted by varying the used polymer concentration or molecular weight, the spinning speed, and the polymer flow rate.[40a,55] In solution TS, the fiber formation is based on the use of highly volatile or fast-evaporating solvents that evaporate during the fiber formation process by creating a larger surface area upon polymer droplet stretching. Meanwhile, in the case of melt TS, the fiber formation is based on polymer cooling during the fiber spinning process. Thus, this technique allows for fiber formation from a wide range of polymer solutions and/or melts without the need for adjusting the dielectric properties of polymer solutions, which is usually needed in the case of ES. Examples of polymers that have been investigated for TS include polycaprolactone (PCL), polyethylene (PE), polycaprolactone polyurethane (PCL-PU) copolymers, Polyethylene glycol (PEO), polyacrylonitrile (PAN), and polyvinyl alcohol (PVA). Another advantage of TS is the ability to produce fibers in different orientations (aligned or random) due to the nature of this technique, which allows for enhanced control over fiber alignment and orientation, although the fibers are straight.[40a,41,55] Additionally, using this technique, the polymer crystallinity and polymer chain alignment in the amorphous phase can be better regulated in comparison to ES, which will enhance the mechanical properties of the fibers in the case of TS.[41,55] Moreover, TS shows enhanced stability of the fibers and, hence, better alignment in extended cell culture experiments in comparison to ES.[41] Another advantage of TS, in contrast to the conventional ES, is that the deposition of fibers is relatively precise, in which the location of the deposited fibers is determined by the point where the droplet touches the rotating rod. This will allow for better control over the spatial deposition of fibers on the substrate compared to ES techniques. However, the limitation of TS lies in the fact that the rod rotates around the substrate where the fibers are collected. This will impose restrictions on the total thickness of the substrate that can be produced but would still allow for a larger thickness compared to that achieved by ES and MEW. In TS, there is also a size limitation, in which the width and length of the sample are limited to the length of the fiber-spinning rotating rods and the radius of the rotating disk. Adding to that, as the size and the rotation speed of the fiber-spinning rods increase, the free end of the rods starts to deflect considerably from their long axis. This will negatively influence the consistent contact between the formed droplet and the fiber-spinning rotating rods, which will affect the quality of the fabricated fibers.

The applicability of the TS approach for the biofabrication of fibrous meshes or mats for tissue engineering applications was confirmed by multiple studies.[36b,40a,41,55,56] In one study, it has been proven that simultaneous cell deposition and fiber TS is possible by spraying mouse NIH-3T3 fibroblast cells and touch spinning of PCL. Therefore, it was demonstrated that sprayed cells were homogeneously distributed throughout the fibrous construct. To further demonstrate the capability of TS to fabricate fibrous structures for tissue engineering applications, a TS mat spun out of PCL was prepared, and mouse 4T1 breast tumor cells were cultured on top of it, observing the cell alignment.[40a] Similarly, PCL nanofibrous scaffolds with varied mechanical properties were prepared by TS, and NE-4C neural cells were cultured on top of the highly aligned fibers to study their differentiation phenotype. It has been found that the mechanical properties of the TS fibers have an effect on the differentiation pathway of the neural stem cells into either neuronal or glial cells. Thus, fibers with higher crystallinity and chain alignment and, hence, higher mechanical properties stimulate neuronal differentiation, whereas fibers with lower mechanical properties promote glial differentiation.[41] Likewise, in another study, TS was used to fabricate highly aligned TS fibers using PCL in chloroform as a spinning solution, and NE-4C neural cells were seeded on top of the fibers. Additionally, electrospun fibers were fabricated with a comparable fiber alignment and diameters to the TS fibers as a control. In this case, a higher degree of neurite alignment with smaller cell aggregates and more extended neurites on the TS fibers was observed compared to the electrospun fibers. This difference in neural cells' behavior was attributed to the enhanced crystallinity and, hence, the higher mechanical properties of the touch-spun fibers.[55] One study used a PCL-PU copolymer as a touch-spinning solution to fabricate highly aligned fibrous mats with soft and elastic properties for muscle tissue engineering applications. It has been shown that C2C12 mouse myoblasts cultured on top of the fibrous scaffolds are able to elongate along the highly aligned touch-spun fibers with a preferred orientation along the main axis of the fibers.[56–57] TS has been recently integrated with 3DBP in a single setup (Please see section 5.1.4.).

Handspinning (HS): Another fiber fabrication technique that is promising for the fabrication of highly oriented fibers in combination with 3DBP is called handspinning (HS). HS relies on pure mechanical drawing or stretching of fibers by placing a viscous polymer solution or melt between two parallel plates that are in direct contact with each other. Thus, the fibers are formed by the controlled displacement of the parallel plates from each other creating a stretching force pulling the polymer solution. Next, the well-oriented fibers in the sub-micrometer range (hundreds of nanometers) are directly deposited on a flat surface, and this process can be repeated (push and pull motion) with a controlled and consistent polymer supply (Figure 5b). Compared to ES, HS does not require the use of highly toxic and environmentally unfriendly solvents common for electrospinning of chemically resistant polymers. In the studies exploring the HS technique, polyvinyl acetate (PVAc) and polypropylene (PP) were used for the fiber fabrication. Although HS is a relatively simple, low-cost, and straightforward fiber fabrication technique that produces fibers with diameters comparable to ES, HS

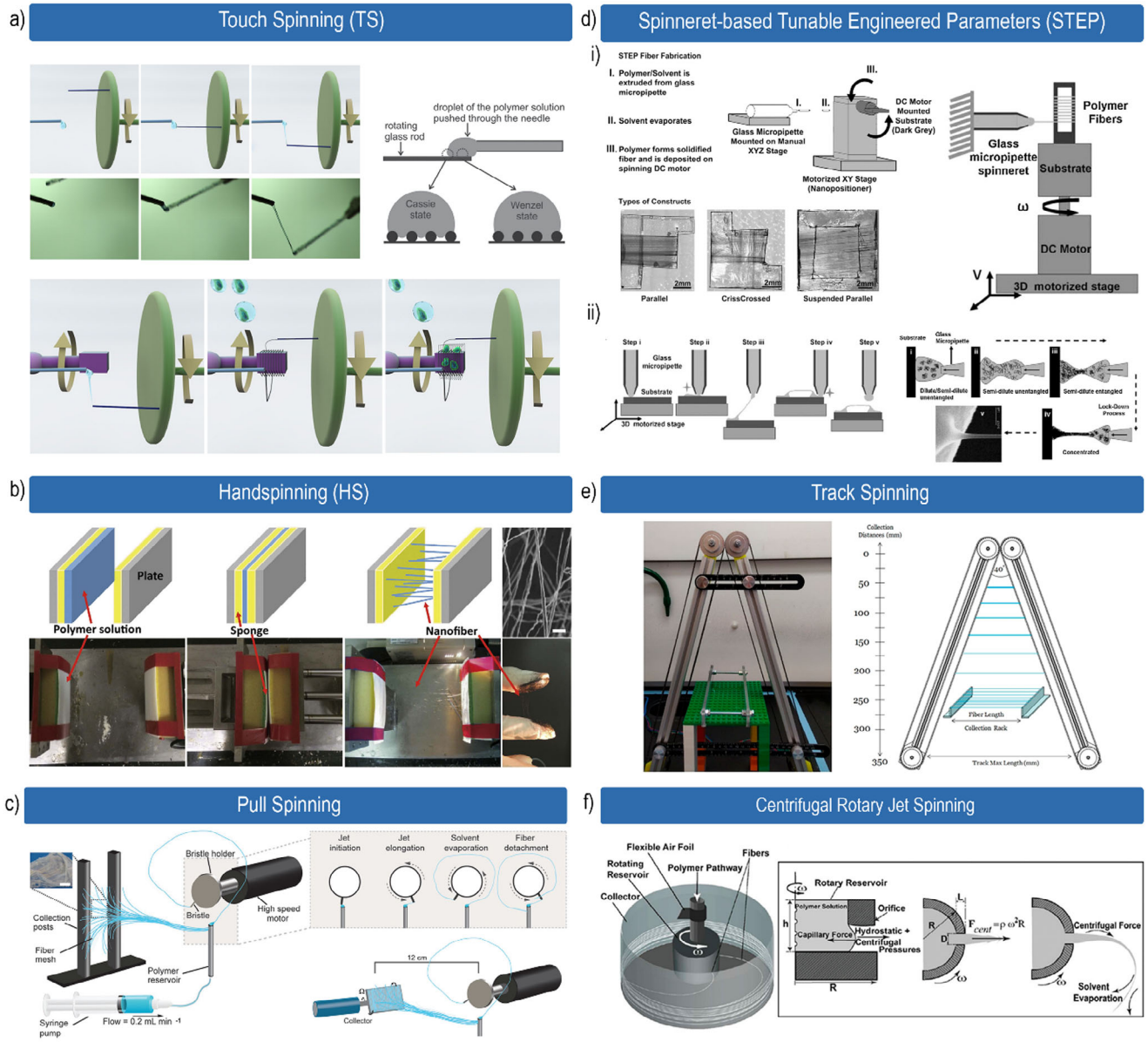

Figure 5. Other fiber fabrication techniques and the possible integration with 3D (bio) printing using dry spinning techniques, where a) the working principle of solution touch-spinning where the process starts with a rotating rod touching a polymer droplet and extending it into a continuous fiber upon solvent evaporation. This technique allows simultaneous cell spraying for tissue engineering applications. Reproduced with permission.[40a] Copyright 2015, Wiley-VCH. b) The handspinning (HS) technique, in which the process starts with having a polymer solution placed between two plates, followed by moving the plates away from each other, stretching the polymer solution with the plates moving further away from each other, and depositing fibers on a flat surface, adapted under terms of the CC-BY license.[47] Copyright 2016, The Author(s), published by Springer Nature. c) The pull spinning process, in which a highly rotating bristle touches a polymer solution feed while rotating, creating a polymer jet that is elongated into fibers that are stretched between the polymer feed and oppositely placed posts or rotating collector, creating aligned suspended fibers, adapted with permission.[59] Copyright 2017, Wiley-VCH. d) the spinneret-based tunable engineered parameter (STEP) technique, in which the process starts with a polymer solution droplet making initial direct contact with a collector followed by translating away from the collector, stretching the polymer droplet. The fibers are collected using two approaches: i) a rotating collector to create wrapped fibers or ii) the point-to-point approach on a flat surface to create suspended fibers yielding different types of fibrous constructs. Reproduced with permission.[60a] Copyright 2011, Elsevier Ltd. Reproduced with permission.[60b] Copyright 2009, Wiley-VCH. and adapted with permission from.[60c] Copyright 2008, Wiley-VCH Verlag GmbH & Co. KGaA, Weinheim., e) The track spinning technique, in which fibers are fabricated using rotating tracks that converge at a single point, where polymer solution is fed at the intersection point. The fibers are formed by stretching the polymer solution while the tracks diverge from each other, thinning the fibers further and depositing them on a flat surface, adapted with permission.[65] Copyright 2019, American Chemical Society., f) Centrifugal rotary spinning, in which the fibers are formed mainly by centrifugal forces. The process starts with jetting a polymer through a set of nozzles while the polymer reservoir is rotating at high rotating speeds, forcing the polymer jet to stretch and deposit on a set of polls located at the circumference at a distance from the nozzles, adapted with permission.[48] Copyright 2010, American Chemical Society.

currently has low throughput compared to other fiber fabrication methods.[47,58] This fiber fabrication technique is still not well characterized and needs improvements on the setup to increase the fiber fabrication throughput, among others, including its applicability for tissue engineering applications. Although HS has not been explored for its integration with 3DBP or 3D printing in general in a single setup, from the technical point of view, it is feasible to integrate through simple alternation between fiber deposition and 3DBP. This can be done, for instance, by introducing a printing stage or platform that can move up and down along the z-axis (common for FDM 3D printers) to collect fibers and allow for the 3DBP step to occur by raising the platform beyond the parallel plates.

Pull Spinning: A fiber spinning technique based on both centrifugal spinning and TS was also developed and termed pull spinning. In pull spinning, a highly rotating bristle of several tens of thousands of rounds per minute (rpm) makes initial contact with a polymer solution supply. Subsequently, the bristle pulls fibers out of the polymer solution and stretches them into thin fibers while completing a full rotation. Finally, fibers are jetted directly onto a collector at a certain distance from the rotating bristle, creating suspended fibers between the collector and the polymer solution supply reservoir (Figure 5c). This fiber fabrication technique is able to produce sub-micrometer fibers from synthetic and natural polymers with aligned orientations and random meshes on a rotating or static collector using a synergy between centrifugal and viscous forces. Different polymer solutions have been tested, including PCL, nylon, PU, and a blend of nylon and PU. The applicability of pull spinning for muscle tissue engineering was confirmed by the fabrication of highly aligned fibers that support myoblast and smooth muscle cells alignment, fusion, maturation, and contraction.[59] This technique can also be integrated with 3DBP by modifying the current setup to allow for the automated collection of fibers. This can be done, for instance, by using a movable platform that approaches the fiber mat from below, stretching the fibers slightly. This will allow for fixing the fibers on a flat surface, which allows for straightforward 3DBP in a subsequent step. Finally, the fibers can be cut at both ends, and the whole platform moves away from the fiber spinning setup, allowing for the next layer of fibers to form.

Spinneret-based Tunable Engineering Parameters (STEP): Another technique is called Spinneret-based Tunable Engineering Parameters (STEP), a fiber fabrication technique that is able to deposit and stack highly aligned fibers either sequentially or continuously with a controlled distance between individual fibers through automated movement.[60] This technique is based on the dry spinning of fibers in the micro-/nanoscale using a glass micropipette that extrudes a viscous polymer solution into a droplet that comes into contact with the collecting platform. Next, the fiber is drawn by vertical movement away from the building platform, followed by either the rotational movement of the collector to form continuously wrapped fibers around the substrate (Figure 5d(i)) or by the horizontal movement of the building platform forming a suspended fiber with two attachment points (Figure 5d(ii)).[60b,c] As for other fiber fabrication techniques that are based on mechanical pulling, this technique is based on using a highly volatile solvent to form fibers through complete evaporation of the solvent and subsequent mechanical drawing of fibers through automated movement. This creates fibers in the range from nanometers to sub-micrometers (50–500 nm) and fiber spacings in the range from sub-micrometer to micrometer. This technique has been tested on different polymer materials, including PS, Polymethyl methacrylate (PMMA), polylactic acid (PLA), and poly(lactic-co-glycolic) acid (PLGA).[60b,c] The major difference between TS and STEP techniques is that in the case of TS, the fibers are formed by a rotating collector that deposits the fibers directly on a stationary substrate. In contrast, the STEP technique uses attachment points to create suspended fibers on a stationary substrate or directly wrap fibers around a rotating substrate.

This fiber fabrication technique was also investigated for tissue engineering applications, in which the adhesion, alignment, and migration of C2C12 myoblasts were studied. The results showed that myoblasts were able to instantly adhere to, migrate along, and align to the highly aligned fibers, showing elongated morphologies.[60a,c] In addition to that, STEP integration with 3DBP was also investigated.[60a] For that, highly aligned fibrous structures were first fabricated using PS, followed by inkjet 3DBP of growth factors into the desired pattern. Finally, cells were seeded on top of the prepared construct. It has been found that by controlling the inkjet (bio) printing pattern of different growth factors can be used to control cell differentiation into different fates on a single construct.[60a] Additionally, the STEP technique was applied for the nanopatterning of already prepared 3D substrates using a technique called spun-wrapped aligned nanofiber (SWAN) lithography. The fabricated nanostructures using the SWAN technique can be used to guide cell adhesion and orientation for tissue engineering applications.[61]

3D Melt Blowing (3DMB): The melt-blowing fiber fabrication method was recently adapted for the biofabrication of high-throughput scalable tissue-relevant fibrous scaffolds for tissue engineering applications, which is called 3D melt blowing (3DMB). In this technique, highly organized fibers ranging from a few to tens of micrometers (1–100 μm) are fabricated using AM techniques and robotics.[14a] In this fiber fabrication method, the thermoplastic polymer is heated up and extruded in a controlled flow through a die (set of coaxial nozzles) with flow and temperature-controlled coaxial airflow. By precisely controlling the heated airflow and the rheological properties of the polymer melt, the air pressure forces the polymer jet formation and its subsequent drawing into fibers. The fibers are then collected on a multi-axis robotic arm-controlled platform with various fiber collection geometries that can be attached to the platform (e.g., flat and cylindrical).[14a,46,62] Moreover, synchronization between the collector movement rate and the fiber jet is of high importance to obtain fibers of preferred orientation rather than buckled fibers. Moreover, 3DMB has been investigated for fiber production using PCL, PLA, PU, and thermoplastic polyester elastomer (TPC-ET). Additionally, 3DMB applicability for tissue engineering applications was demonstrated by fabricating a bioresorbable hernia plug composed of PCL and PLA fibrous layers at different aligned orientations with proper mechanical characteristics for surgical manipulations. In addition to that, a patient-specific meniscus scaffold was fabricated using PCL to demonstrate the capability of 3DMB to fabricate complex tissue-relevant geometries.[14a] Although 3DMB has the capability to fabricate fibrous scaffolds at high throughput, several limitations need to be addressed. For instance, unlike other fiber fabrication

techniques, 3DMB requires significantly higher amounts of polymer to fabricate a single scaffold. In addition to that, the 3DMB setup is relatively complex and large in size compared to other fiber fabrication techniques since it uses a robotic arm with multi-axis control.[14a,58] This technique can also be applied to polymer solutions (solution blowing), in which, in solution blowing, the fiber formation is governed by solvent evaporation by the pressurized air jet.[14a,63] Solution blowing has recently shown its promising applicability for several tissue engineering applications.[64] From the technical point of view, 3DMB can be combined with 3DBP since it involves using a multi-axis robotic arm for fiber collection on different collector types, including flat surfaces.

Track Spinning: Track spinning is a fiber fabrication technique based on a direct drawing of fibers using two rotating tracks that come into contact at a single point, where the polymer solution or melt is fed. Starting from the point of contact, the tracks diverge at an angle, pulling fibers with increased distance between the tracks. The pulled fiber diameter is further reduced while the distance between the tracks further increases, producing highly aligned fibers in the range from hundreds of nanometers to a few micrometers in diameter that are directly deposited on a collection platform (Figure 5e). In principle, track spinning is similar to the handspinning (HS) technique, with the difference that track spinning is able to produce continuous fibers in an automated manner through rotating tracks that diverge at a variable angle. In addition to that, track spinning possesses the same advantages as the HS technique, with the additional advantage of being able to have a higher fiber fabrication throughput by using automated rotating tracks and the ability to fabricate fibers of variable lengths. Moreover, similar to HS, track spinning is able to produce fibers from a wide range of polymers with high and low viscosities and from composites with magnetic and electric nanoparticles. This technique has also been tested for a few polymer solutions, including PVAc and PU, and its applicability with tissue engineering applications has not yet been tested.[65] Track spinning can be relatively easily integrated with 3DBP in a straightforward manner by incorporating a 3DBP head that can move in all axes while the track can slide in one axis. For instance, once the fiber fabrication step is done, the dual-track setup slides away, leaving the collected fibers below. This will allow the 3DBP head to move freely and start the 3DBP layer.

Centrifugal/Rotary Jet Spinning: Centrifugal/rotary jet spinning uses extremely high rotational speeds (≤75 000 rpm) to produce high-throughput circumferentially aligned nano-/microfibers on a static collector.[48,59,66] In this process, the polymer solution or melt is loaded in a rotational container and fed through an orifice or set of orifices at high rotational speeds. This forces the polymer to eject and subsequently stretch due to shear forces led by a combination of centrifugal forces, air resistance, and solvent evaporation/polymer melt cooling. The jetted polymer fibers are then collected on a stationary platform located at a variable distance from the center of the rotating polymer container shaft (Figure 5f). Due to the extremely high rotational speeds used, this technique is characterized by a high production rate, which is significantly higher than ES and MEW.[48,66–67] This technique has been tested on a variety of polymer solutions, including PLA, poly(L-lactide) (PLLA)–polyacrylic acid (PAA), PEO, polyvinylpyrrolidone (PVP), and gelatin. Centrifugal/rotary jet-spun fibers were also investigated for tissue engineering applications, including cardiac tissue engineering[48] and other tissue engineering applications.[66] Although this technique has a high fiber fabrication rate, its combination with 3DBP of bioinks might be limited due to the use of extremely high rotational speeds.

Magnetospinnng: Magnetospinning uses a combination of magnetic field forces and mechanical forces applied to a polymer solution mixed with magnetic nanoparticles (i.e., ferrofluid) to deform the polymer droplet, forming a liquid bridge that is further elongated into fibers while the permanent magnet is displaced and the solvent evaporates. This yields nano-/microfibers in the range from 50 nm to 5 µm. This approach can be applied to a wide range of polymer solutions independent of the dielectric properties of the polymer and/or the solvent by simply incorporating stabilized magnetic nanoparticles to the polymer solution made of, for example, PCL, Polytetrafluoroethylene (PTFE), PEO, PS, polyvinylidene difluoride (PVDF), and PMMA mixed with nickel oxide or iron oxide nanoparticles as well as polymer solutions incorporated with Ag nanowires or multiwalled carbon nanotubes mixed with nickel oxide or iron oxide nanoparticles. Similar to rotary jet spinning, the fibers are collected circumferentially on a pillar or set of pillars located around the center of a rotating stage that either additionally angularly rotates, rocking a magnet sphere around for pulling fibers, or the magnet itself acts as a rotating pillar.[68] This technique can be considered as a variant of touch spinning, in which an additional force is used, that is, the magnetic force to pull fibers through direct contact with the polymer droplet by continuous rotation of the magnet and the fiber fabrication platform. This technique has been explored for its compatibility with tissue engineering applications by seeding fibroblasts on top of the collagen-coated magnetic fibers, demonstrating the magnetic fibers' biocompatibility. Magnetospinning can be combined with 3DBP by modifying the current setup[68b] to be similar to the current TS setup[36b] in which the fibers are collected on a stationary substrate located in between the rotating magnet and the rods.

Gravity Fiber Drawing (GFD): GFD is a technique used to draw vertical freestanding single fibers ranging from a few hundred nanometers to tens of micrometers in diameter from a polymer solution supply with precise control over individual fiber orientation and interfibrillar spacing. This will allow for the building of 3D architectures using AM techniques. In this technique, a polymer solution is supplied through a nozzle at a certain vertical distance from a platform. The droplet free falls by gravitational forces, producing a single fiber suspended between the tip of the nozzle and the platform. The solidified fiber is formed by the evaporation of the solvent during the free-falling process. The fiber diameter can be precisely controlled by controlling the distance between the nozzle tip and the platform, polymer solution properties (e.g., viscosity), and solvent evaporation rate. The formed freestanding fibers can be used as building blocks to fabricate 3D constructs with controlled fiber organization using custom-made fiber handling machinery or other well-known fiber handling techniques such as weaving or braiding. Compared to other fiber spinning/drawing techniques mentioned earlier, including the most commonly used techniques (ES and MEW), this technique has a superior capability in controlling single fibers 3D organization (alignment and interfibrillar spacing)

and covering a wide range of diameters (100 nm–100 µm) fabricating freestanding fibers with controlled fiber drawing ratio. This will allow for the biofabrication of ECM mimetic 3D constructs with a wide range of fiber diameters and porosities, crucial for cell infiltration and nutrient and oxygen diffusion. For that, PCL grid-like structure of fibers with porosity of 99%, interfibrillar space of 50 µm, layer gap of 45 µm, and thickness of 430 µm were fabricated using GFD. The fabricated structures were seeded with cells, showing that the cells were able to proliferate, infiltrate, adhere to the fibers, and follow the fiber pattern.[69] Thus, the main advantage of GFD is that it allows for the deposition of freestanding fibers on a platform with no limitation on the thickness of the fabricated construct, with a relatively high production rate and controlled fiber organization. Unlike other methods that have limitations on sample thickness and size, GFD can produce fibrous constructs of varying thicknesses and dimensions. Nevertheless, a limitation of this technique is that the vertically oriented platform may not be suitable for applications that require true integration with 3DBP.

In Situ Fiber Tethering via Orbital Spinning: In situ solution fiber tethering using orbital fiber spinning is a technique based on fabricating fibers directly on the surface of any living biological structures or tissues (e.g., skin, chicken embryo, and human hair) with the ability to precisely control fiber density and organization. In this technique, the fiber deposition is guided by the target object's macro- and microscale surface topography, allowing the fibers to accommodate the shape of the substrate, whether it is curved or irregular. The setup is composed of an extrusion head that moves in all axes with a rotating fiber-pulling arm that mechanically draws or pulls a single fiber at a time from an aqueous viscoelastic polymer solution supplied through a needle (i.e., non-continuous fiber formation). Next, the fiber is wrapped around the substrate located in between using low rotational speeds (≈55 rpm) that allow the fiber to accommodate the substrate shape and/or surface topography (estimated fiber deposition force 10 µN). With each rotation, a single fiber in the range of sub-micrometer to micrometer in diameter (0.5–10 µm depending on contact state) is drawn, and due to the movement of the fiber spinning head, the fiber density and coverage area can be controlled. Initially, the fiber is deposited in a solution or wet state on the target object or substrate surface, and then the fiber dries within a few seconds at ambient conditions. This technique has been tested for bioelectronic applications using PEDOT:PSS (poly (3,4-ethylenedioxythiophene):polystyrene sulfonate) as a conductive component with PEO and sodium hyaluronate (HA) as a fiber-forming component. Thus, this approach is mainly characterized by its ability to produce fibers in the sub-micrometer to a few micrometer range at precise locations and various orientations on any substrate. The fibers are also able to follow the curvature and topography of the surface while applying extremely low fiber deposition forces in the micro Newton range. The applicability of this technique has been investigated for tissue engineering applications by fiber spinning directly on chicken embryo, in which the fiber spinning approach did not affect the normal growth and development of the embryo.[70] Although this technique is able to produce fibers in a highly aligned manner, it wraps fibers around the substrate, as for touch spinning, which could limit its broad applicability in tissue engineering, where, in some cases, fibers are needed to be deposited on top of the surface rather than wrapping around. Similar to touch spinning, this technique can be combined with 3DBP.

4.2.2. Wet-Spinning Techniques

Microfluidic Fiber Spinning: In contrast to other fiber fabrication methods mentioned earlier (i.e., ES, MEW, TS, etc.) in microfluidic fiber spinning, fiber is not pulled from the end but rather pushed like in extrusion 3D printing, which essentially influences the diameter of the formed fiber and its production rate, which are connected to each other by Hagen-Poiseuille equation. Microfluidic fiber spinning is based on using microfluidic channels for manipulating small volumes of solutions through mixing and separation for the fabrication of fibers (50 nm–100 µm) with various structures such as hollow fibers,[71] core–shell,[38,72] and structures with spatiotemporal contrasts in chemical make-up and morphology (e.g., grooved fibers and nanopatterned fibers) (**Figure 6**a(i)).[71a,73] Fiber formation is based on the instant gelation or precipitation of a hydrogel precursor directly before extrusion, such as using chemical, physical, and/or photo-crosslinking.[38,73–74] This fiber fabrication technique is particularly of interest for fabricating fibers made of natural biomaterials that are challenging to fabricate using other fiber fabrication methods. For instance, microfluidic systems were able to replicate the silk fiber fabrication process seen in spiders.[73,75] Furthermore, this fiber fabrication technique allows for direct encapsulation of cells using a cell-friendly environment and in situ fiber spinning.[38,73] Besides that, different fiber collection methods can be used to handle the fibers and collect them in different orientations using, for instance, braiding and weaving techniques (Figure 6a(i)).[38,73] In order to harness the capabilities of microfluidic fiber spinning, microfluidic 3DBP heads were developed and used to biofabricate 3D constructs with anisotropic properties for several tissue engineering applications (Figure 6a(ii)).[71b,74,76] This technique has been also used to fabricate fibers out of alginate by direct gelation using divalent ions. Thus, this approach offers a wide range of advantages but needs further investigations and improvements to be widely applicable in the biofabrication field.[74]

Computer-Aided Wet Spinning (CAWS): Similar to microfluidic spinning, in computer-aided wet spinning (CAWS), fiber is not pulled from the end but rather pushed like in common extrusion 3D printing. CAWS uses AM techniques for the fabrication of highly ordered fibers through the extrusion of a polymer solvent directly into a coagulation bath. This will form solidified fibers through phase separation in a layer-by-layer approach, yielding a 3D structure similar to FDM 3D printed ones. Compared to FDM 3D printing, CAWS introduces the added advantage of the ability to 3D print polymers that are not processable by high temperatures and need post-processing to form stable fibers such as polysaccharides and collagen as well as polymers with loaded bioactive molecules such as inorganic ceramics (e.g., hydroxyapatite) (Figure 6b).[77] This approach was applied for several tissue engineering applications such as bone tissue engineering, in which geometrically accurate critical bone size defect was fabricated and implanted in vivo.[77d,e] Although alginate was wet spun in a calcium chloride ($CaCl_2$) coagulation bath,[78] one

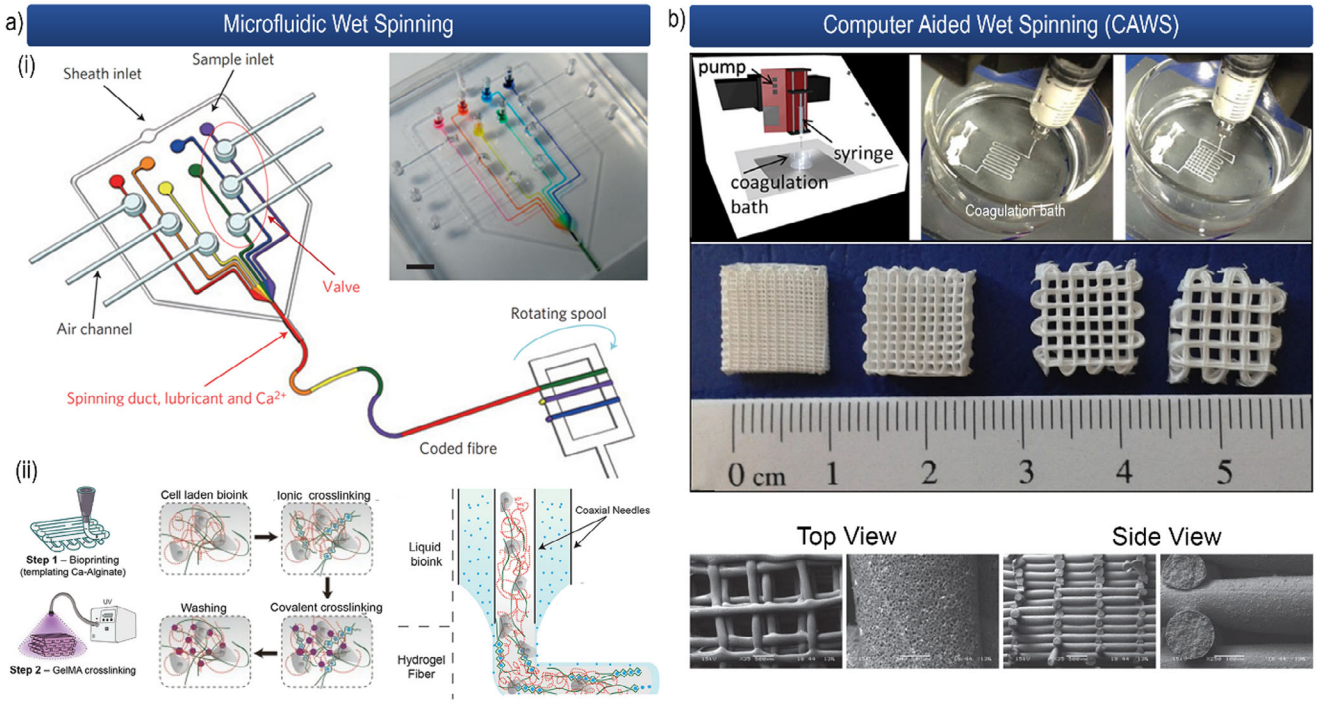

Figure 6. Other fiber fabrication techniques and the possible integration with 3D (bio) printing using wet spinning/fiber fabrication techniques: a) microfluidic wet spinning, in which microfluidic channels or printheads (e.g., coaxial nozzle) are used for mixing two or more materials in small volumes and thus providing control over the extruded fiber contents forming fibers with spatiotemporal contrasts in morphology and chemical content. The fibers can be either i) collected using different collection methods such as wrapping, braiding, and weaving or in situ fiber deposition. Reproduced with permission.[73] Copyright 2011, Springer Nature Limited, or can be ii) directly deposited on a platform using additive manufacturing (AM) techniques (coaxial 3D (bio) printing). Reproduced with permission.[76c] Copyright 2015, WILEY-VCH Verlag GmbH & Co. KGaA, Weinheim. b) Computer-aided wet spinning (CAWS), in this technique, the polymer solution is 3D printed directly into a coagulation path to form fibers due to the insolubility of the extruded polymer in the coagulation bath and its precipitation. Reproduced with permission.[77b] Copyright 2016, Society of Chemical Industry, John Wiley and Sons.

limitation of potential integration of CAWS with 3DBP is that it usually uses toxic or cell-noncompatible coagulation baths such as ethanol for the fabrication of microfibers.

A unique feature of the above-mentioned wet spinning methods is that they are used to produce hydrogel-based fibers or precipitated fibers. In the first case, the hydrogel, in any case, has poor mechanical properties that cannot be improved by drawing – the isotropic structure is restored after drawing due to the mobility of the polymer chain segments, even if the drawing was applied. The hydrogel fibers also cannot be used to enforce 3D (bio) printed hydrogels. In the second case, the deposited fibers are porous due to solvent leakage, and they have not been drawn, resulting in poor mechanical properties.

5. 3D (Bio) Printing with Integrated Fiber Fabrication/Spinning Methods

Hydrogel-fiber composites for tissue engineering applications are expected to enhance the overall mechanical and biological properties of the hybrid or composite 3D construct due to the inclusion of mechanically anisotropic fibrous structures in the cell-encapsulating hydrogel. In this system, the hydrogel provides the cells with a hydrated environment that nurtures cell growth and migration within a contained environment, whereas fibers act as mechanical and structural support for the overall construct and act as mechanical guidance for a preferred cell orientation. This section discusses the literature-reported integrated fiber fabrication methods (i.e., ES, MEW, and FDM 3D printing (ranging from nanoscale to macroscale)) with 3DBP for tissue engineering. In addition to that, TS will be highlighted as a promising technique for the direct automated sequential fabrication of hybrid constructs in combination with 3DBP. It is also noteworthy that not in all cases to be mentioned or discussed, 3DBP was integrated with fiber fabrication methods in a single device or setup. **Table 5** shows a summary of the majority of the studies that use the combined or integrated approach of integrating or combining 3DBP with fiber fabrication techniques, including biological and mechanical characterizations performed, highlighting the main findings. Additionally, **Table 6** discusses the possibilities and limitations of the true or actual integration of the dry fiber fabrication methods, including ES, MEW, and other fiber fabrication methods with 3DBP.

5.1. . Overview of the 3DBP/Fiber Spinning Integration Approach

5.1.1. Electrospinning (ES)

3DBP was combined with electrospinning for several tissue engineering applications,[36a,44,45,79] including cartilage,[36a]

Table 5. Summary of work in literature, where 3DBP was integrated with different fiber fabrication techniques (true integration highlighted in grey).

(Bio) printing technique	Fiber fabrication	Bioink/hydrogel	Fiber	Biological analysis	Mechanical and morphological analysis	Single setup	Refs.
EBP	ES	Collagen type I (cell-laden; BMSCs, 6×10^6 cells mL^{-1}). Crosslinking: physical (thermal; 37 °C).	PCL with CNTs (random and aligned fibers). Solvent: chloroform and DMF. Fiber diameter: 368 nm. Treatment: oxygen plasma. Sterilization: 70% ethanol + UV.	• BMSCs cell viability (>80%).	• Compression test: • Strain rate: 2 mm min^{-1} • Modulus: 20 kPa (2 – 3x higher than gel alone). • Shape fidelity: <2% size mismatch (19% less size mismatch compared to gel alone). • Shrinkage: 2% (18% less compared to gel alone).	No	[79a]
EBP	ES	Alginate with $CaCl_2$ (cell-laden; NIH 3T3 fibroblasts 5×10^6 cells mL^{-1}). Crosslinking: physical (Ionic; $CaCl_2$).	PCL (random fibers). Solvent: methylene chloride and DMF. Fiber diameter: 420 nm. Treatment: oxygen plasma.	• High cell viability and proliferation (2 x increase in proliferation compared to gel alone).	• Compression test: • Strain rate: 1 mm min^{-1}. • Modulus: 89 kPa (4x higher than hydrogel alone). • Higher shape fidelity. • Shrinkage: 13 – 20% less shrinkage after crosslinking. • Higher structural stability in vitro.	No	[79b]
rEBP	ES	GelMA blended with gelatin and HA (cell-laden; SMCs 10×10^6 cells mL^{-1}). Crosslinking: chemical (UV light).	PCL (aligned fibers). Sterilization: 70% ethanol + UV. Fiber diameter: 1 µm. Cells seeded: HUVECs 30×10^6 cells mL^{-1}.	• SMCs and HUVECs viability (>90%) and proliferation (increased with time). • Blood vessel-like structure formation with collagen secretion and endothelilization.	• Burst pressure (2000 mmHg, 60 x higher than hydrogel alone). • Suture retention strength (2.2 N; 44 times higher than hydrogel alone). • High structural stability.	No	[79c]
EBP	ES	Collagen type I (cell-free). Treatment: neutralization with ammonia vapor. Crosslinking: Physical (thermal; 37 °C).	PLCL (random fibers). Solvent: HFIP. Fiber diameter: 645 nm. Cells seeded: PC12 cells; $10^3 - 10^4$ cells cm^{-2}.	• Differentiation into neuron-like cells (10.7%) compared to ES mat alone (0.8%). • Nerve tissue regeneration with dense and organized axons as well as remyelination. • Functional motor recovery in rat models (comparable results to that of the nerve autograft ones).	• High structural stability.	No	[79d]
SL	ES	PEG or PEGDA (cell-free). Crosslinking: chemical (UV light).	PCL or PCL blended gelatin (aligned fibers). Solvent: Chloroform or TFE. Treatment: prewetting with poly-L-lysine at 37 °C and laminin coating. Sterilization: 70% ethanol + UV. Cells seeded: NSCs and primary embryonic rat cortical; 30000 cells per scaffold.	• Improved primary neuronal cell adhesion, cell growth, neurite alignment, and directional neurite outgrowth compared to gel alone. • Improved NSC adhesion and proliferation compared to gel alone.	• Tensile test: • Young's modulus is 1.3 MPa (3x higher compared to gel alone). • Ultimate tensile strength: 0.6 MPa (2x increase compared to gel alone).	No	[79e]

(*Continued*)

Table 5. (Continued)

(Bio) printing technique	Fiber fabrication	Bioink/hydrogel	Fiber	Biological analysis	Mechanical and morphological analysis	Single setup	Refs.
EBP	ES	PVA blended alginate and chitosan (cell-free). Crosslinking: physical (Ionic; $CaCl_2$). Treatment: cycles of freezing and thawing. Seeded cells: fibroblast; 10000 cells per scaffold.	PCL blended PLA (random fibers). Solvent: DCM and DMF. Treatment: lyophilization. Sterilization: UV. Fiber diameter: 756 nm. Cells seeded: fibroblasts; 5000 cells per scaffold.	• Human dermal fibroblast cell viability (high viability) and proliferation (increased with time). • Antibacterial properties and bacterial penetration (no bacterial penetration).	–	No	[44]
EBP	ES	PCL blended gelatin and nano-hydroxyapatite (cell-free). Seeded cells: BMSCs; 0.02 × 10^6 cells mL^{-1}.	PCL blended gelatin (random fibers). Solvent: TFE and acetic acid. Crosslinking: 1-ethyl-3-(3-dimethylaminopropyl) carbodiimide/N-hydroxysuccinimide (EDC/NHS) ethanol. Sterilization: gamma irradiation. Fiber diameter: 380 nm. Seeded cells: fibroblasts; 0.02 × 10^6 cells mL^{-1}.	• Enhanced tissue formation and improved integration into the surrounding native tissue compared to gel alone (25% bone volume to total volume; 1.25x increase compared to fibers alone). • Fibrotic tissue was not present at the defect site.	–	No	[45]
EBP	ES	Alginate blended gelatin (cell-free). Treatment: Freeze drying.	PCL (random fibers) Solvent: DCM Sterilization: 70% ethanol + UV. Fiber diameter: 190 nm. Seeded cells: hASCs; 1 × 10^6 cells cm^{-2}.	• hASCs cell morphology, adhesion, and proliferation.	–	Yes	[79f]
EBP	ES	Gelatin blended chitin (cell-free). Crosslinking: Physical (thermal; 22 °C).	PVA blended gelatin (random fibers). Solvent: acetic acid. Sterilization: 70% ethanol + UV. Seeded cells: fibroblasts; 25000 cells cm^{-2}.	• High cell viability (90%).	–	Yes	[79g]
EBP	ES	GelMA (cell-free) Crosslinking: chemical (UV light).	PCL.	–	–	Yes	[79h]

(*Continued*)

Table 5. (Continued)

(Bio) printing technique	Fiber fabrication	Bioink/hydrogel	Fiber	Biological analysis	Mechanical and morphological analysis	Single setup	Refs.
EBP	ES	GelMA (cell-free). Seeded cells: HUVECs; 30000 cells per sample. Crosslinking: chemical (405 nm light).	PCL and PCL/PLCL blends (random fibers). Solvent: HFP Sterilization: 70% ethanol. Fiber diameter: around 400 nm. Seeded cells: HUVECs; 10000 cells per sample.	• Direct cell viability on GelMA: 8.5 x increase in resorufin fluorescence intensity between days 1 and 3. Indirect cytocompatibility on fibers: non-significant difference in viability in PCL-only fibers, a significant decrease in viability in PCL/PLCL blends)	• Tensile test (50 N load cell, circumferential and longitudinal axis) strain rate: 11 mm min^{-1}. Modulus: ~ 0.12 – 1.65 MPa (circumferential modulus is lower than longitudinal, comparable anisotropy to native blood vessels) Ultimate tensile strength: 1 – 4.1 MPa (significantly higher than GelMA alone). • Burst pressure (50 N load cell) Rate: 2.1 mL min^{-1}. Burst pressure: 1000 – 2352 mmHg (significantly higher than GelMA alone). • Compliance test (three pressure ranges, minimum 50 and maximum 15 mmHg with 10 mmHg increments). Compliance: ~ 6 – 40%/100 mmHg (lower range is comparable to native blood vessels).		[81]
cEBP	ES	Alginate blended gelatin and hyaluronic acid (cell-laden; PC12 10×10^6 cells mL^{-1}). Crosslinking: Physical (thermal; 4 °C).	PLLA blended gelatin (random fibers). Solvent: HFIP. Fiber diameter: 500 nm.	• PC12 cell viability (93%). • High cellular activity and proliferation by self-organization into tissue-like structures, expression of PC-12 specific biomarkers, and stable secretion of PC-12 specific neurotransmitters (in vitro). • Generation of tissue-like structures with angiogenic blood vessels formation, immune infiltration, and neovascularization in mouse models (in vivo).	• Compression test: • Modulus: 50 kPa (1.2x increase compared to gel alone). • High structural stability.	Yes	[79i]
Inkjet BP	ES	Collagen Type I blended fibrinogen (cell-laden; rabbit-derived chondrocytes 3 – 4×10^6 cells mL^{-1}). Crosslinking: chemical (thrombin).	PCL (random fibers). Solvent: acetone. Fiber diameter: 422 nm.	• Cell viability (80%). • Cartilage-like tissue structure with enhanced cell organization and major cartilage ECM proteins secretion (collagen and glycosaminoglycans) compared to the control both in vitro and in vivo.	• Tensile test (0.2 mm s^{-1} strain rate): • Young´s modulus: 1.76 MPa (4.3x increase compared to gel alone). • Ultimate tensile strength: 1.11 (4.3x increase compared to gel alone). • High structural stability in vitro.	Yes	[36a]
EBP	ES	GelMA-based (cell-free). Crosslinking: chemical (UV light).	PU-based (random fibers). Solvent: HFIP. Fiber diameter: 1 µm. Seeded cells: HUVECs (0.01×10^6 cells per scaffold).	• High cell viability (>95%). • HUVECs migration (18.3 – 44%) and wound closure on rat diabetic model (>90% closure at day 14).	• Tensile test (10 mm min^{-1}): • Modulus: 60 – 65 MPa. • Cyclic tensile test (10% strain max): • Plastic deformation was observed for all samples at 6% strain.	No	[80b]
EBP	ES	GelMA blended sodium alginate (cell-free). Crosslinking: chemical (UV light) and physical ($CaCl_2$).	Chitosan blended with PEO (random). Solvent: acetic acid. Crosslinking: chemical (GA vapors) Seeded cells: HeLa 0.3×10^6 cells cm^{-2}.	• High cell viability and proliferation (increased with time). • Excellent antibacterial properties. • Higher levels of proangiogenic factor (VEGF-A) were released compared to the control (promotes wound healing).	–	No	[80a]

(*Continued*)

Table 5. (Continued)

(Bio) printing technique	Fiber fabrication	Bioink/hydrogel	Fiber	Biological analysis	Mechanical and morphological analysis	Single setup	Refs.
4DB	MEW	AAMA (cell-free) Crosslinking: chemical (UV light).	PCL (110 °C). Sterilization: 70% ethanol + UV. Fiber diameter: 10 – 30 µm. Treatment: coating with FNC. Seeded cells: C2C12; 200000 cells cm^{-2}.	• High cell viability (80%), proliferation, and alignment.	–	No	[57,86]
Inkjet BP	MEW	BMSCs suspension (30×10^6 cells mL^{-1}).	PCL (100 °C).	• High cell viability. • Cartilage-like (hyaline-like) tissue formation and cellular organization with ECM proteins secretion (collagen fibrillar organization).	• Compression test (at 20% and 30% strain): Compressive modulus: 177 and 388 kPa; 50 and 76x increase post-implantation. Equilibrium modulus: 180 and 214 kPa; 20 and 27x increase post-implantation. Dynamic modulus: 1.4 and 2.6 MPa; 26 and 51x increase post-implantation. • Tensile test (0.3 mm min^{-1} strain rate): Tensile modulus: 1.4 MPa; no significant difference compared to control. Equilibrium modulus: 1.7 MPa; no significant difference compared to control. Yield stress: 132 kPa; 1.4x increase post-implantation. • Enhanced structural stability in vitro.	Yes	[49a]
EBP	MEW	GelMA-based (cell-laden; hiPSC-CM with hfCF 60×10^6 cells mL^{-1} and HUVECs with hfCF 30×10^6 cells mL^{-1}). Crosslinking: chemical (white light) and physical (thermal; 37 °C).	PCL (80 °C). Fiber diameter: 11 µm. Treatment: collagen or Matrigel coating.	• Cell patterned localization and adhesion to the MEW mesh. • Tissue-like and ECM formation with contractile cardiac tissue-like structure along the main axis of melt electrowritten fiber mesh. • Interface between vascular and myocardial regions.	–	Yes	[84]
VBP	MEW	GelMA (cell-laden; HUVECs 10×10^6 cells mL^{-1} and hBMSC $1–5 \times 10^6$ cells mL^{-1}). Crosslinking: chemical (405 nm light; UV), and physical (thermal; 37 °C).	PCL.	• hBMSC viability (>90%). • Cell localization in different tubular layers similar to blood vessels. • Tissue-like geometrical features were fabricated (valves, vascular bifurcations, internal struts, fenestrated blood vessels, and vascular stenosis model).	• Tensile test: Young´s modulus (10.8 – 3.2 kPa; 5 – 16x increase compared to gel alone). Ultimate tensile stress (20.3 – 73.0 kPa; 4 – 14x increase compared to gel alone). • Burst pressure (1.1 – 1.6 bar; 1.7 – 2.4x increase compared to gel alone). • Bending resistance at 25 mm gap (1 – 4 mm; 5 – 1.25x less bending compared to gel alone).	No	[2a]

(*Continued*)

Table 5. (Continued)

(Bio) printing technique	Fiber fabrication	Bioink/hydrogel	Fiber	Biological analysis	Mechanical and morphological analysis	Single setup	Refs.
EBP	MEW	GelMA (cell-laden; eMSCs 20×10^6 cells mL^{-1}). Crosslinking: chemical (UV light).	PCL (85 °C). Fiber diameter: 13 µm.	• eMSCs viability (>90%), proliferation, and chondrogenic differentiation. • ECM proteins secretion (collagen type II and GAGs).	• Compression test: Peak modulus: 247 kPa (12.4x increase compared to gel alone). Equilibrium modulus: 53 kPa (4.5x increase compared to gel alone).	Yes	[53]
Inkjet BP	MEW	GelMA (cell-laden; HaCaT cells 1×10^6 cells mL^{-1}). Crosslinking: chemical (UV light).	PCL (90 °C). Fiber diameter: 3 µm.	• High cell viability.	• Improved scaffold handleability through integration with MEW fibers.	Yes	[85b]
Inkjet BP	MEW/FDM	Alginate-based (cell-laden; BMSCs 30×10^6 cells mL^{-1}). Crosslinking: physical (Ionic; $CaCl_2$).	FDM: PCL (83 °C) and fiber diameter of 150 µm. MEW: PCL (85 °C) and fiber diameter of 15 µm.	• Excellent cell viability. • MEW-based scaffolds show higher levels of DNA and sGAG, and collagen secretion comparable to native tissue compared to FDM counterpart. • Tissue-organization was directed by both MEW and FDM fibrous structure.	• Compression test: Modulus: FDM 5 – 10 MPa and MEW 0.1 – 0.15 MPa. MEW-based scaffolds stiffness (after 4 weeks of incubation) is comparable to the native meniscus.	Yes	[85a]
EBP	TS	Alginate, SCMC, Laponite-RD and their blends (cell-laden; fibroblasts 60×10^6 cells mL^{-1}).	PCL (aligned fibers). Solvent: chloroform. Fiber diameter: 436 nm.	• Cell viability (>80%) and uniaxial alignment. • Time-lapse microscopy (cell adhesion and alignment dynamics).	–	Yes	[36b]
EBP	FDM	Gelatin blended with fibrinogen, HA, and glycerol (cell-laden; 3T3 fibroblasts, hAFSCs 5×10^6 cells mL^{-1}, chondrocytes 40×10^6, or C2C12 3×10^6 cells mL^{-1}). Crosslinking: chemical (thrombin).	PCL or PCL with TCP (92.5 °C or 112 °C). Fiber diameter: 130 and 200 µm.	• High cell viability (>91%) and proliferation (increased with time). • ECM formation (GAGs, proteoglycans, and collagen), vascularization, and innervation in vitro and in vivo. • Angiogenesis and tissue remodeling of transplanted hybrid structures in rat models. • Regenerated muscle-like tissue responded to applied electrical signal (similar to immature muscle function).	• Cyclic 3-point bending test (pre- and post-implantation with 0.02 mm s^{-1} for 4 cycles): Higher normalized load post-implantation. Higher resilience post-implantation. • Structural stability in vitro and in vivo.	Yes	[87f]

(*Continued*)

Table 5. (Continued)

(Bio) printing technique	Fiber fabrication	Bioink/hydrogel	Fiber	Biological analysis	Mechanical and morphological analysis	Single setup	Refs.
EBP	FDM	Alginate (cell-laden; hASCs (chondrocytes or adipocytes) 1×10^6 cells mL^{-1}). Crosslinking: physical (ionic; $CaCl_2$).	PCL (80 °C). Fiber diameter: 200 µm.	• Cell viability (>95% before 3D printing) and proliferation (increased with time; cell number and DNA content). • Chondrogenesis and adipogenesis differentiation confirmation by tissue-specific gene expression levels determination and immunofluorescence.	–	Yes	[87i]
EBP	FDM	Alginate (cell-laden; primary chondrocytes 1×10^6 cells mL^{-1}). Crosslinking: physical (ionic; $CaCl_2$).	PCL (80 °C). Fiber diameter: ~ 250 µm.	• High cell viability (>85%). • Cartilage-like tissue formation with secretion of GAGs and increased total collagen and DNA content both in vitro and in vivo.	–	Yes	[87e]
EBP	FDM	Alginate (cell-laden; primary chondrocytes or ATDC5 cells 5.68×10^6 cells mL^{-1}). Crosslinking: physical (ionic; $CaCl_2$).	PCL (65 – 80 °C). Fiber diameter: ~ 300 µm.	• High cell viability (>77%). • Cartilaginous differentiation and cartilage-like tissue formation: GAGs and collagen secretion (increased with time).	• High structural stability in vitro.	Yes	[87h]
EBP	FDM	Alginate blended with gelatin (cell-laden; MSCs 0.5×10^6 cells mL^{-1}) Crosslinking: physical (ionic; $CaCl_2$).	PCL (100 – 180 °C).	• Cell viability (40 – 70%; 72% for control).	• Compression test (1 mm min^{-1} strain rate): Modulus: 4.5 MPa; 150x increase compared to gel alone.	Yes	[32]
EBP	FDM	Alginate dialdehyde gelatin (cell-laden; stromal cell line ST2 2×10^6 cells mL^{-1}). Crosslinking: physical (covalent).	PCL-PEG (80 °C). Fiber diameter: 307 µm.	• Increased cell viability and proliferation with time (optical density) (70%). • Cell adhesion to and migration from the hydrogel to the FDM 3D printed structure.	–	Yes	[87c]
EBP	FDM	HA, gelatin, or atelocollagen (cell-laden; primary hepatocytes or pre-osteoblast MC3T3-E1 Cells 1×10^6 cells mL^{-1}). Crosslinking: physical (thermal; 37 °C and 22 °C).	PCL blended with PLGA (120 °C).	• Cell viability (>95%) with increased proliferation with time.	–	Yes	[87b]
EBP	FDM	Alginate (cell-laden; primary chondrocytes 5×10^6 cells mL^{-1}). Crosslinking: physical (ionic; $CaCl_2$).	PCL (160 °C).	• Cell viability (>70%).	• Compression test (0 – 18 N with 3N incremental step): Modulus: 6.2 MPa; ~ 300x increase compared to gel alone.	Yes	[36c]
EBP	FDM	Alginate (cell-laden; primary chondrocytes and osteoblasts 1×10^6 cells mL^{-1}). Crosslinking: physical (ionic; $CaCl_2$).	PCL (80 °C). Fiber diameter: 250 µm.	• Cell viability (>90%).	• Higher structural stability.	Yes	[87a]

(*Continued*)

Table 5. (Continued)

(Bio) printing technique	Fiber fabrication	Bioink/hydrogel	Fiber	Biological analysis	Mechanical and morphological analysis	Single setup	Refs.
EBP	FDM	Decellularized ECM from different tissues (cell-laden hASCs, hMSCs, and L6 myoblasts 1–5 × 10^6 cells mL^{-1}). Crosslinking: physical (thermal; 37 °C).	PCL (80 °C) Fiber diameter: 100 µm and 200 µm.	• Cell viability (>90%) and apoptosis. • Cell differentiation and tissue formation by evaluation of different collagens, cardiac myosin heavy chain, and F-actin, as well as gene expression levels of cardiogenic, adipogenic, and chondrogenic factors.	• High structural stability in vitro without chemical crosslinking.	Yes	[87d]
EBP	FDM	Decellularized ECM derived from heart tissue (cell-laden; hiPSC-CM and primary human cardiac fibroblasts (9:1) 50 × 10^6 cells mL^{-1}). Crosslinking: physical (thermal; 37 °C).	PEVA (150 °C).	• Very high cell viability (>99%) with uniaxial cell alignment. • Reproduction of human cardiac physiology: Synchronized and spontaneous contraction through contractile force and contraction direction analysis. Drug response is similar to native tissue. Cardiac tissue formation (presence of cardiac markers at high levels and high fusion index).	–	Yes	[13c]
EBP	FDM	Alginate-based (cell-laden; BMSCs 20 × 10^6 cells mL^{-1}). Crosslinking: physical (ionic; $CaCl_2$).	PCL (-). Fiber diameter: 437 µm.	• High cell viability after 1 h of printing. • Higher bone tissue formation levels in vivo: Higher levels of bone formation (~ 4% bone area; ~ 10x higher) and mineralization compared to gel alone (5% bone volume; 10x higher). Higher numbers of blood vessels formation compared to gel alone (30 blood vessels per cross-section compared to almost none).	• Compression test (1 mm s^{-1} strain rate): Modulus: 1.4 MPa; 360x increase compared to gel alone.	Yes	[87l]
EBP	FDM	Thiol-modified gelatin, hyaluronan, and heparin mixture or hyaluronan with gelatin mixture (cell-laden; hMSCs 10.5 × 10^6 cells mL^{-1}). Pre-crosslinking: chemical (thiol + acrylates). Post-crosslinking: chemical (thiol + alkynes + UV light).	PCL (90 °C).	• Cell viability (>95%). • Successful differentiation of hMSCs into smooth muscle and cartilaginous lineages in their distinct regions by modulating scaffold stiffness and growth factors.	• Tensile test (10 mm min^{-1} strain rate): Modulus: 1.3 MPa for smooth muscle region and 12 MPa for cartilage region Yield stress: 0.36 MPa for smooth muscle region and 1.39 MPa for cartilage region • Comparable mechanical properties of the smooth muscle and cartilage regions to native tracheal tissue´s smooth muscle and cartilage regions.	No	[87p]
EBP	FDM	Alginate-based (cell-laden; BMSCs 10 × 10^6 cells mL^{-1}). Crosslinking: physical (ionic; $CaCl_2$).	PCL (60 °C)	• Cell viability (~66% at day 1 and recovered to 100% at day 14). • Enhanced bone mineralization and construct vascularization compared to the acellular construct in vivo (subcutaneous implantation into mice)	–	Yes	[87o]
EBP and Inkjet BP	FDM	Micro extrusion: GelMA (cell-laden; BMSCs 20 × 10^6 cells mL^{-1} Inkjet BP: BMSCs and chondrocytes cell suspension 3:1 ratio (30 × 10^6 cells mL^{-1}). Sacrificial material: Pluronic. Crosslinking: chemical (UV light).	PCL (80 °C and 65 °C) Fiber diameter: 150 µm and 250 µm.	• Directed cell migration and tissue organization guided by PCL infill structure. • Secreted collagen fiber orientation guided by PCL infill structure similar to native tissue. • Tissue-like formation with ECM protein content similar to native tissue. • Spatially distinct tissue formation in the bone and cartilage designated regions.	• Compression test (1 mm s^{-1} strain rate): Modulus: 3 MPa; comparable to native tissue.	Yes	[87n]
Inkjet BP	FDM	BMSCs cell suspension (100 × 10^3 cells per microwell).	PCL (88 °C) Fiber diameter: 150 µm	• High cell viability. • Cartilage-like tissue formation with homogeneous proteins (sGAG and collagen) secretion. • Native tissue-like collagen fibers organization and alignment.	-	Yes	[87m]

- EBP: extrusion-based (bio) printing, VBP: volumetric (bio) printing, rEBP: rotational extrusion-based (bio) printing, cEBP: cryogenic extrusion-based (bio) printing, SL: stereolithography, 4DB: 4D Biofabrication, ES: electrospinning, TS: touch-spinning, MEW: melt electrowriting, STEP: spinneret-based tunable engineered parameters. – PCL: Polycaprolactone, CNTs: Carbon nanotubes, GelMA: methacrylated gelatin, PEG: Polyethylene glycol, PEGDA: Polyethylene glycol diacrylate, PVA: Polyvinyl alcohol, PLA: Polylactic acid, PLLA: Poly-l-lactic acid, PLCL: Poly(L-lactide-co-ϵ-caprolactone), PS: polystyrene, PEVA: polyethylene vinyl acetate, AAMA: methacrylated alginic acid (alginate), SCMC: Sodium carboxymethyl cellulose. – BMSCs: bone marrow-derived mesenchymal stem cells, SMCs: smooth muscle cells, HUVECs: human umbilical vein endothelial cells, PC12: pheochromocytoma cells, NSCs: neural stem cells, hASCs: human adipose stem cells, C2C12: immortalized mouse myoblast cells, hiPSC: human induced pluripotent stem cells, CM: cardiomyocytes, hfCF: human fetal cardiac fibroblasts, eMSCs: equine mesenchymal stem cells, hAFSCs: human amniotic fluid-derived stem cells.

Table 6. Possibilities and limitations of the true integration of dry fiber fabrication methods with 3D (bio) printing.

Fiber fabrication method	3D (bio) printing method	Single device possible	The main limitations of the true combination with 3D (bio) printing (3DBP)
Electrospinning	Extrusion	Yes	– Use of high voltage for an extended period: • Irreversible cell damage. • Bioink drying. – Limited thickness due to charge dissipation. – Random fiber orientation.
	Inkjet	Yes	
	DLP/SLA/Volumetric	No	
	Laser-assisted	Yes	
Melt electrowriting	Extrusion	Yes	– Use of high voltage for an extended period: • Irreversible cell damage. • Bioink drying. – Limited thickness due to charge dissipation.
	Inkjet	Yes	
	DLP/SLA/Volumetric	No	
	Laser-assisted	Yes	
Touch spinning	Extrusion	Yes	– Fibers are wrapped around the substrate. – At high spinning rates, fibers deform the bioink. – Thickness is limited to the rotating stage diameter.
	Inkjet	Yes	
	DLP/SLA/Volumetric	No	
	Laser-assisted	Yes	
Handspinning	Extrusion	Yes	– Slow fiber fabrication method.
	Inkjet	Yes	
	DLP/SLA/Volumetric	No	
	Laser-assisted	Yes	
Pull spinning	Extrusion	Yes	– Fibers are stretched between the tip of the spinneret and the collection posts (requires manual intervention to allow for combination with 3DBP).
	Inkjet	Yes	
	DLP/SLA/Volumetric	No	
	Laser-assisted	Yes	
Spinneret-based Tunable Engineering Parameters (STEP)	Extrusion	Yes	– Slow fiber fabrication method in case of using stationary substrate (point-to-point technique). – Rotating substrate does not allow for combination with 3DBP (centrifugal forces).
	Inkjet	Yes	
	DLP/SLA/Volumetric	No	
	Laser-assisted	Yes	
3D Melt Blowing (3DMB)	Extrusion	Yes	– Use of pressurized hot air stream could cause the drying of the bioink, leading to cell death.
	Inkjet	Yes	
	DLP/SLA/Volumetric	No	
	Laser-assisted	Yes	
Track Spinning	Extrusion	Yes	– Relatively slow fiber fabrication method. – Larger vertical and horizontal distances (larger than 350 mm) may be required to yield fiber diameters of tens to a few hundred nanometers.
	Inkjet	Yes	
	DLP/SLA/Volumetric	No	
	Laser-assisted	Yes	

(*Continued*)

Table 6. (Continued)

Fiber fabrication method	3D (bio) printing method	Single device possible	The main limitations of the true combination with 3D (bio) printing (3DBP)
Centrifugal/rotary jet spinning	Extrusion	Yes (by modifying the current setup)	– Fibers are deposited circumferentially on a stationary substrate (requires changing the setup to allow for 3DBP). – In order to yield fibers in the range of tens of nanometers to a few hundred nanometers, high rotational speeds are needed (higher than 10000 rpm).
	Inkjet	Yes (by modifying the current setup)	
	DLP/SLA/Volumetric	No	
	Laser-assisted	Yes (by modifying the current setup)	
Magnetospinning	Extrusion	Yes (by modifying the current setup)	– In the current setup, fibers are collected circumferentially around the rotating substrate (requires changing the setup to allow for 3DBP).
	Inkjet	Yes (by modifying the current setup)	
	DLP/SLA/Volumetric	No	
	Laser-assisted	Yes (by modifying the current setup)	
Gravity Fiber Drawing (GFD)	Extrusion	Yes (by modifying the current setup)	– Slow fiber fabrication method. – Requires a separate fiber collection mechanism or a multi-axis rotating stage setup to allow for direct combination with 3DBP.
	Inkjet	Yes (by modifying the current setup)	
	DLP/SLA/Volumetric	No	
	Laser-assisted	Yes (by modifying the current setup)	
In Situ Fiber Tethering via Orbital Spinning	Extrusion	Yes	– Slow fiber fabrication method. – Fibers are wrapped around the substrate.
	Inkjet	Yes	
	DLP/SLA/Volumetric	No	
	Laser-assisted	Yes	

bone,[45] skin,[44,80] nerve,[79d,e] vascular,[79c,h,81] meniscus,[79a] and neurosecretory[79i] tissue engineering. In most of the studies, the electrospun nanofibrous mats were first fabricated and then incorporated or inserted manually between the layers during the 3DBP process in a multi-step manner (**Figure 7a**).[44,45,79a–e] One disadvantage of this approach is the difficulty in the manual handling or manipulation of thin fibrous mats and the lack of an automated process for the fabrication of such constructs. This could limit the wide applicability of this approach in tissue engineering and regenerative medicine applications.[36a,79a] Another drawback of this approach is the need to treat the nanofibrous mats' surface to facilitate their adhesion to the hydrogel layers in case the fibrous layers are hydrophobic. Without adjusting the hydrophobicity of the fibrous layer, there would be a higher risk of construct delamination.[79a,b] On the other hand, few studies have integrated 3DBP with ES in a single setup for the fabrication of hybrid structures composed of both hydrogels and fibers in a multilayer approach (Figure 7b).[36a,79f–i,81] In such a case, the electrospun layer was composed of randomly oriented fibers rather than oriented fibers.[36a,44,45,79b,d,f,g,i,81] This is due to the technical difficulty in producing highly aligned fibers in combination with 3DBP, in which the most commonly used ES setup needs a highly rotating mandrel or disk (e.g., 11 m s^{-1}) to produce relatively highly aligned fibers.[40b] Additionally, using high rotational speeds of the collector to produce highly aligned fibers could distort the structure of the 3D printed hydrogel due to centrifugal forces,[79h] which could have detrimental effects on cells while undergoing high centrifugal forces. Although relatively aligned fibers can be achieved by parallel bars (gap electrospinning), the achieved fiber alignment is limited to the fiber mesh thickness limit in this approach. With increased thickness, the alignment is lost due to residual charge buildup, which leads to further polymer losses (poor fiber deposition on the substrate and increased fabrication time).[40b,82] Moreover, the fabricated structures in the abovementioned studies were limited to a few layers in thickness. This might be due to the reduced electrical field when increasing the thickness of the fabricated construct, which is a common issue in ES.[40b] Furthermore, increased thicknesses of the electrically non-conductive hydrogel layer will further distort the electrical field and hinder the successful ES of fibers, thus leading to further fiber losses by fibers being deposited away from the collector or substrate. In addition to that, the use of high electrical voltages in the range of tens of kV (usually 10–30 kV) with electrical current in the range of nano to milli amperes could have a detrimental effect on living cells and needs to be kept at a level, which does not cause irreversible damage to cells. Although this can be achieved by reducing the voltage level, it could limit the polymer choice that can be used for ES or result in inconsistent fiber formation.[83] Thus, combining 3DBP with ES is simple and straightforward—high voltage can be easily applied between nozzle and substrate—but achieving controlled deposition and formation of aligned fibers is rather challenging, and the applied voltage could have adverse effects on the cells.

5.1.2. Melt Electrowriting (MEW)

MEW was combined with different types of 3DBP, including volumetric 3DBP (**Figure 8a**),[2a] extrusion-based 3DBP (Figure 8b),[53,84] inkjet 3DBP (Figure 8c),[49a,85] and 4D biofabrication (Figure 8d)[57,86] for several tissue engineering applications. This includes skeletal muscle (Figure 8d),[57,86] articular cartilage (Figure 8c),[49a] myocardial (Figure 5b),[84] and vascular (Figure 8a)[2a] tissue engineering.[49b,53] Instead of fabricating a multilayered 3D construct with alternating melt electrowritten fiber layer and 3D (bio) printed hydrogel layers,[53] the majority of the studies,[2a,49a,57,84,86] where MEW was combined with 3DBP, the full thickness MEW construct was first fabricated followed by 3DBP of the cell-laden bioink filling the predefined pore geometry of the melt electrowritten construct. One reason could be that the deposited hydrogel layer could limit the fusion between the MEW fibers upon stacking the subsequent layers since MEW fiber's adhesion in the z direction is mainly based on the solidification of the molten polymer fiber on the previous layer. Another reason may be the poor or limited adhesion of the hydrogel precursor layer to the MEW fiber layer.[2a,53] Moreover, it might be due to the fact that MEW conditions are not fully compatible with cells. The extended exposure of cells to the high voltage used in MEW for a long time and the relatively long fabrication time to fabricate relatively large constructs could have a detrimental effect on cell viability and their metabolic activity. To investigate the effect of MEW voltage on cells, the effect of simultaneous MEW and cell-laden bioink on cell viability was investigated. For this, mesenchymal stem cell-laden GelMA bioink and PCL polymer melt were used to fabricate a 3D composite construct of alternating MEW and 3DBP. It was found that the metabolic activity of the stem cells decreased by 80% after 60 min of fabrication time, with no significant increase in the metabolic activity of cells upon incubation for 21 days in cell culture conditions. Moreover, to study the effect of the increased voltage on cell behavior, stem cell viability under the range of voltages from 0 to 15 kV was investigated. It was found that the applied voltage did not have a considerable effect on the cell viability (>90% on day 14) under the testing conditions used, and the cells were able to recover during cell culture with time. Moreover, it has also been confirmed that the effect of applied voltage on stem cells' metabolic activity and differentiation ability compared to a control (without fibers) was non-significant by quantifying the ECM proteins secretion (glycosaminoglycans and collagen II).[53]

5.1.3. Fused Deposition Modeling (FDM)

FDM 3D printing was also integrated with 3DBP of bioinks for several tissue engineering applications.[13c,32,36c,85a,87] From the technical point of view, the integration of FDM 3D printing of synthetic polymers with 3DBP of bioinks is the most forward of all the other fiber fabrication techniques. This is due to the fact that both FDM 3D printing and 3DBP are based on the same family of AM processes, in which materials are deposited directly on a building platform using mere extrusion of materials into filaments through a nozzle in a layer-by-layer approach (Figures 4c and 9a). In most of the studies where the integration of FDM 3D printing and 3DBP is investigated, the FDM 3D printed layers are not intended to act as a biologically active component but rather as a mechanical or structural support for the mechanically poor bioink or biomaterial ink being 3D (bio) printed and

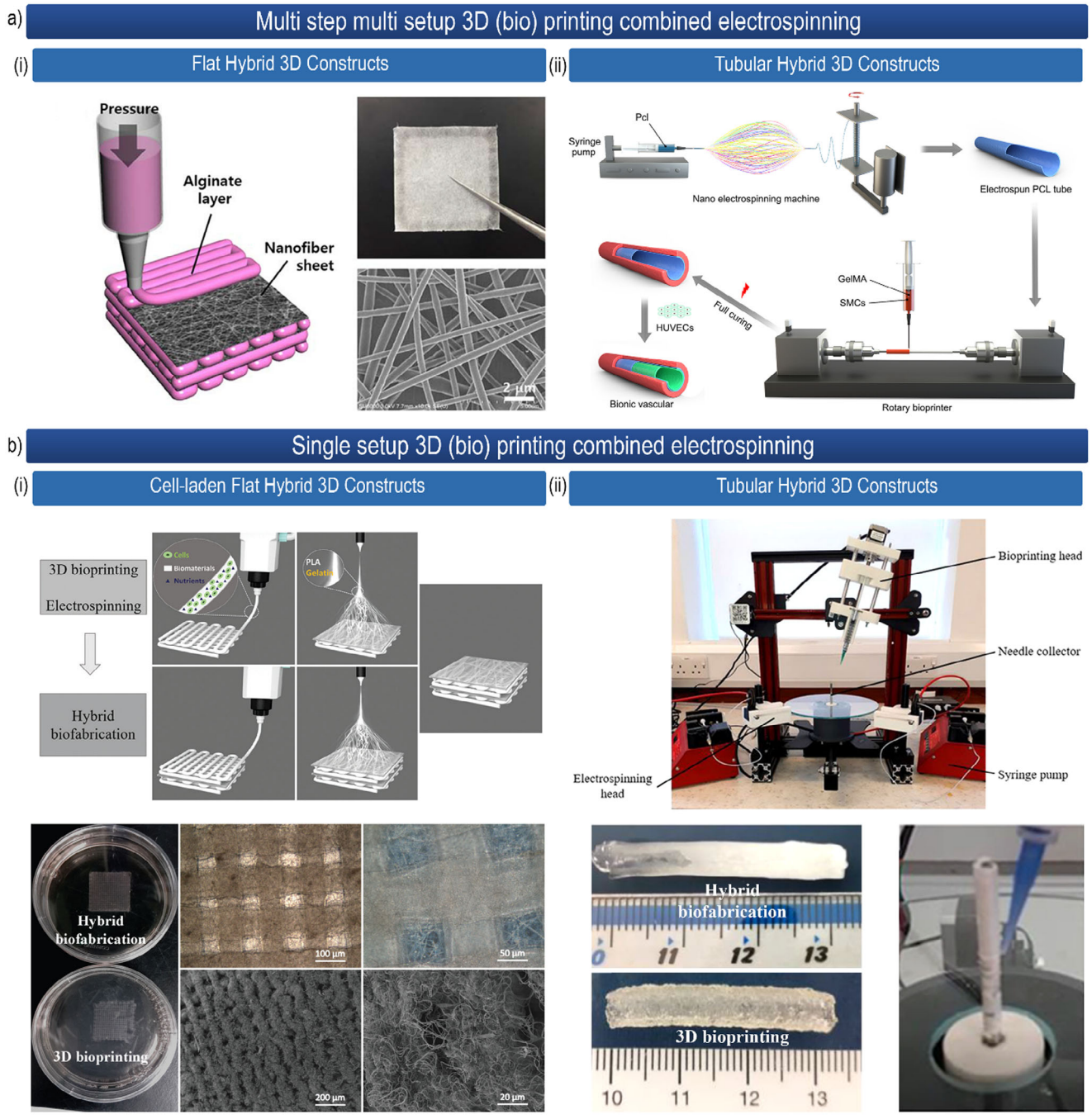

Figure 7. Electrospinning combined 3D (bio) printing for the fabrication of hybrid 3D constructs composed of fibers and 3D printed cell-laden and cell-free hydrogel precursors using a) multi-step multi-setup approach for fabricating, i) flat hybrid 3D constructs for tissue engineering applications. Reproduced with permission.[79b] Copyright 2019, IOP Publishing Ltd. And ii) tubular hybrid 3D constructs for vascular tissue engineering application. Reproduced with permission.[79c] Copyright 2022, The Authors, Published by Elsevier Ltd; and b) single setup approach using i) cell-laden bioink for fabricating flat structures using extrusion-based 3D (bio) printing. Reproduced under terms of the CC-BY license.[79i] Copyright 2024, The Authors, published by AccScience Publishing. ii) And tubular structures using rotary 3D (bio) printing. Reproduced with permission.[79h] Copyright 2021, IPEM. Published by Elsevier Ltd. All rights reserved.

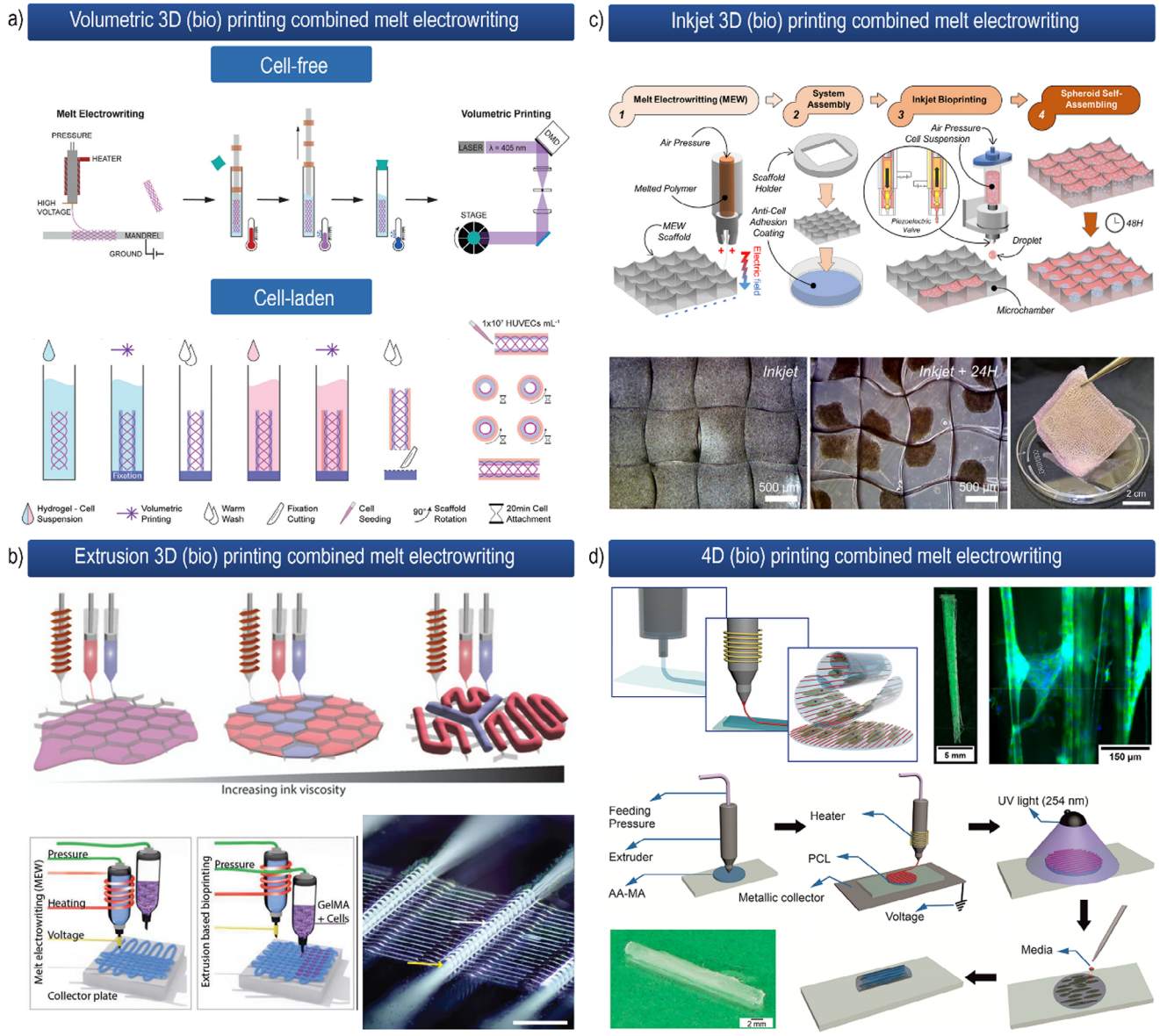

Figure 8. Melt electrowriting combined with different 3D (bio) printing techniques, a) volumetric 3D (bio) printing combined melt electrowriting for vascular tissue engineering applications, in which the process starts with melt electrowriting of fibrous scaffold on a tubular collector, then the tubular fibrous scaffold is transferred into a volumetric 3D (bio) printing vial filled with a bioresin for light-based photocrosslinking of the bioresin to fabricate a hybrid 3D tubular construct, adapted under terms of the CC-BY license.[2a] Copyright 2023, The Authors. Advanced Materials, published by Wiley-VCH GmbH, b) extrusion-based 3D (bio) printing combined melt electrowriting showing the capability of this approach to fabricate tissue interfaces using two different bioinks 3D bioprinted within predefined melt-electrowritten pore geometries for cardiovascular tissue engineering. Reproduced under terms of the CC-BY license.[84] Copyright 2023, The Author(s), Published by IOP Publishing Ltd, as well as the ability of the hybrid approach to produce out-of-plane free-standing fibers. Reproduced under terms of the CC-BY license.[53] Copyright 2018, The Authors. Published by WILEY-VCH. c) Inkjet 3D (bio) printing combined melt electrowriting for articular cartilage tissue engineering showing the localized cell organization within the pore geometry. Reproduced under terms of the CC-BY license.[49a] Copyright 2022, The Authors, Published by Elsevier Ltd. And d) extrusion 3D (bio) printing combined melt electrowriting for skeletal muscle tissue engineering using 4D biofabrication (3D (bio) printing + shape morphing) approach, in which the melt electrowritten fibers guide myoblast cells orientation and folding direction, adapted with permission.[86] Copyright 2021, American Chemical Society.

subsequently incubated in vitro or implanted in vivo.[87a,c–e,g,h,l,p] For instance, it was reported that the compressive stiffness was considerably higher (approx. 150 times) in the hybrid construct (fiber + hydrogel) (few MPa) compared to the alginate-based hydrogel alone (tens of kPa).[32,36c,87l] In addition to that, FDM 3D printed layers provide controlled 3D interconnected porous geometries that ensure proper cell penetration, nutrient diffusion, and oxygen exchange, which consequently allow for creating native tissue-relevant thicknesses compared to hydrogel alone.[36c,87a,b,d–f,h,k] For example, cartilaginous tissue formation similar to native tissue was significantly enhanced in hybrid constructs containing pores in the form of microchannels compared

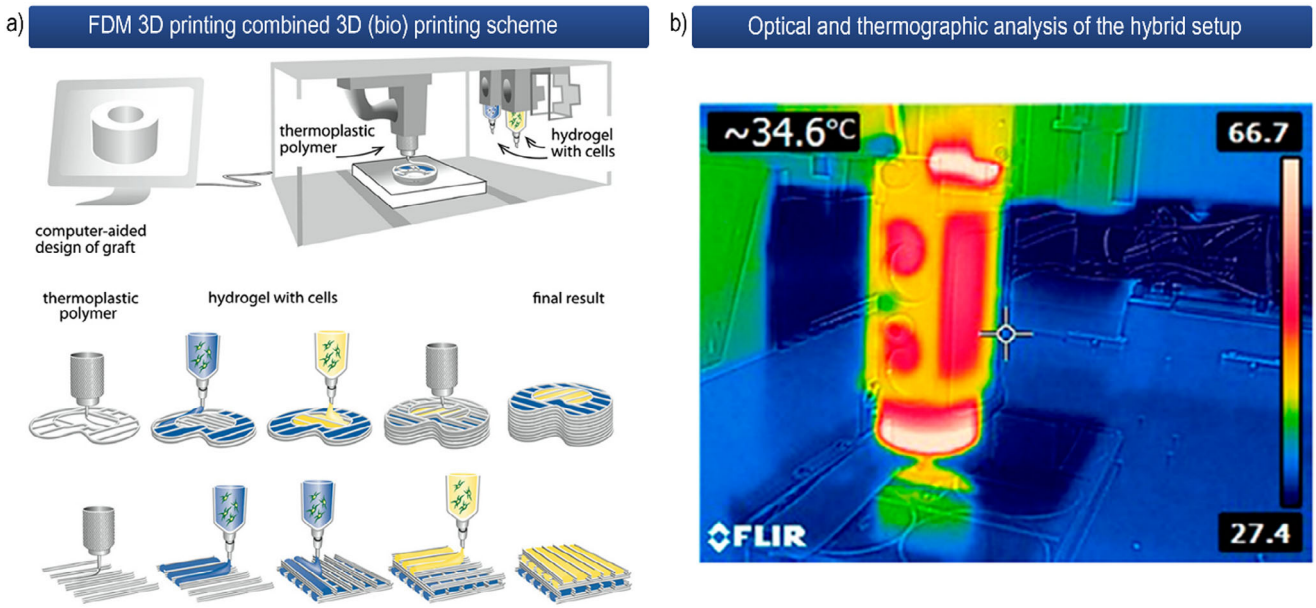

Figure 9. FDM 3D printing combined with 3D (bio) printing, where a) schematic representation of the FDM 3D printing combined 3D (bio) printing of hybrid 3D constructs composed of thermoplastic polymer-based macrofibers with cell-laden bioinks in an alternating manner. Reproduced with permission.[36c] Copyright 2011, The Author(s), Published by IOP Publishing Ltd. b) Optical and thermographic analysis of the FDM 3D printing combined 3D (bio) printing setup using PCL-based thermoplastic polymer printed at 85 °C and 3D bioprinted gelatin-based biomaterial ink at 37 °C. Reproduced under terms of the CC-BY license.[87c] Copyright 2016, The Authors, licensee MDPI, Basel, Switzerland.

to constructs without microchannels, where the tissue formation was limited to the outer edge of the construct with the necrotic center in case of microchannel-free construct.[87f] Moreover, using FDM 3D printing, it is possible to create physical barriers between the deposition of different cell-laden bioinks within the same 3D construct, thus precisely controlling the arrangement of different cell types in empty space.[36c,87a,i,k,n,p] This will allow for the design of more complex 3D constructs composed of different types of cell-laden bioinks and synthetic polymers that can biologically and mechanically mimic different tissue interfaces such as the cartilage-bone interface.[87a,g,i,n,p] Additionally, the mechanical properties of the FDM 3D printed structure can be fine-tuned or modulated by precise control over the fiber deposition to create different infill structures or pore geometries.[32,87f,i,p]

One concern regarding using FDM 3D printing in combination with 3DBP of cell-laden bioinks is that it uses temperatures (usually >80 °C) that are considerably higher than physiological temperatures (37 °C) for extrusion of thermoplastic polymers. This could potentially have an effect on the cell viability while depositing the thermally molten polymer on top of the cell-laden bioink layer. For that, the cell viability within a 3D construct composed of cell-laden bioink with 3D printed PCL fibers at 80 °C was investigated directly after printing and found a decrease in cell viability from 92% to 85% upon further stacking of PCL layers.[87e] In another study, alternating FDM 3D printing of PCL at 60 °C with 3DBP of cell-laden bioink showed a cell viability of ≈66% on day 1. This relatively low cell viability on day 1 of incubation was regarded as the effect of the integrated 3D printing process (FDM + 3DBP), in which heated polymer melt is extruded directly in contact with the cell-laden bioink.[87o] Nevertheless, other studies using PCL have shown that the cells were able to recover upon incubation, reaching a cell viability of greater than 90% at days 7 and 14.[87a,d,o] To further investigate the effect of the used 3D printing temperature of PCL on cell viability, heat distribution maps of the 3D printing setup show an instant cooling of the extruded PCL filament from 85 °C to temperatures below 37 °C within few seconds with no significant decrease in cell viability compared to the control (Figure 9b).[87c,h,j] Similarly, it was found that the biological activity of the cells in vitro, such as cell proliferation, cell differentiation, and ECM protein secretion, were not affected by the fabrication conditions used.[87a,b,d,f,h,i] Although the cell viability tends not to be affected by the used 3D printing temperature when using PCL, which has a relatively low melting/crystallization temperatures and does not need a heated bed for the successful 3D printing, other synthetic polymers need significantly higher printing and deposition temperatures (usually > 140 °C), which may increase the chances for irreversible cell damage and hydrogel dry-out.[87a,h] To study this, the effect of the increased 3D printing temperature of PCL on the cell viability of MSCs cells shows that the cell viability drops down from 65% to 40% upon the increase of temperature from 100 °C to 180 °C, respectively, while the control had a cell viability of ≈70%.[32] In addition to that, the temperature to be chosen affects the mechanical properties and structural stability of the overall construct, in which both the adhesion strength between the extruded filaments and the fracture strength are reduced by using lower 3D printing temperatures closer to the melting point.[32] Moreover, using lower printing temperatures close to the melting point increases the viscosity of the polymer melt, which requires higher printing pressures to maintain a high flow rate as well as more frequent clogging of the 3D printing nozzle may occur.[87h]

5.1.4. Touch Spinning (TS)

In all of the studies mentioned earlier (section 4.2.1) where touch spinning is used, cells were seeded on top of the touch spun fibers (i.e., 2D), which does not provide an aqueous 3D environment that resembles the native ECM environment of many tissues. To resolve this issue, 3DBP was combined for the first time with TS in a single setup for the biofabrication of a 3D scaffold composed of the hydrogel-fiber composite construct.[36b] In this study, an alternating multilayered scaffold composed of touch spun PCL fibers layers and 3DBP bioink layers (biomaterial loaded cells) was fabricated into a composite structure for tissue engineering application. It was found that fibroblast cells tend to adhere to the fibers and align along the fiber main direction with cell body alignment degree of as high as 90% and cell nucleus alignment of higher than 40%. Additionally, the interaction of fibroblasts with the fiber using time-lapse microscopy has shown that cells were able to sense the fibers, adhere to them, and align along them with the ability to snap between fibers and glide along them.[36b] In conclusion, touch spinning allows for the fully automated hands-free integration of fiber spinning with the 3DBP of bioinks (cell-laden hydrogel precursor) in a layer-by-layer approach for the fabrication of fiber-bioink multilayered construct. In addition to that, compared to ES, TS eliminates the need for the manual handling of fibrous mats to yield hybrid constructs composed of alternating fibrous layers and hydrogel precursor layers, thus highly reducing the possibility of contamination as well as reducing the difficulty in handling thin fibrous mats. Moreover, this hybrid technique minimizes the need for physical or chemical crosslinking of hydrogel precursors during or post 3DBP, which is usually needed in the case of 3DBP alone to hold the 3D (bio) printed structure shape and control the degradability both in vitro and in vivo. In the case of the hybrid construct, the hydrogel precursor is supported mechanically by the fibers and acts as a barrier, slowing down the biodegradability of the hydrogel precursor layers. Moreover, no or less crosslinking of the bioink is beneficial for cell motility and migration, thus allowing for dynamic interaction between the cells and the hybrid construct (**Figure 10**).

5.2. Mechanical and Biological Advantages of the Combined Approach

The combination of electrospun fibrous layers with 3D (bio) printed hydrogel layers resulted in enhanced mechanical properties and biological performance compared to hydrogel alone. Therefore, there was a significant increase and improvement in compressive properties (**Figure 11a**),[79a,b,i] tensile properties (Figure 11b),[36a,79e] structural integrity (Figure 11c-i,ii),[36a,79a,b,i] structural stability in cell culture (in vitro) conditions (Figure 11c-iii),[79b] and burst pressure and suture retention strength.[79c] For instance, it was reported that incorporating even a low weight percentage of the electrospun fibrous layer to the hydrogel layers increases the tensile strength and Young's modulus of the composite considerably. Moreover, the toughness of the composite construct can be modulated by adjusting the fibrous layer weight percentage compared to the hydrogel layer (Figure 11b).[88] The hybrid 3D constructs have also shown comparable mechanical properties to native tissues such as native blood vessels[79c,81] and nerve autografts.[79d] In addition to that, the fiber-free constructs have shown noticeably higher geometric mismatch (due to creeping under their own weight and post-crosslinking) to the used 3D CAD model compared to the fiber-containing constructs. Similarly, the shrinkage of the fiber-free scaffold post-crosslinking was significantly higher compared to the fiber-containing counterpart (Figure 11-i).[79a,b] This effect was caused by the fact that the nanofibrous mats have nano topographic features that act as attachment or supporting points for the hydrogel layer during the crosslinking process and thus retain shape uniformity.[79b]

The overall biological properties were also enhanced both in vitro and in vivo, in which higher cell proliferation,[44,79b,c,e,f,i] comparable cell viability,[36a,44,79c,g,i] directed cell orientation,[79e] more homogeneous cell distribution,[79c] enhanced cell adhesion and differentiation,[79d–f] and improved ECM proteins secretion and cell-specific biomarkers expression[79c,i] compared to the fiber-free 3D constructs were reported. For example, in vivo the transplanted hybrid 3D constructs in tissue defect models have shown well-organized tissue-like structure with collagen and glycosaminoglycans formation, angiogenic blood vessels formation, immune infiltration ability, neovascularization ability, and improved integration to the surrounding native tissue comparable to native cartilage tissue,[79i] nerve autografts (**Figure 12d**),[79d] and osteochondral tissue (Figure 12c)[45] compared to 3D printed hydrogel alone. Moreover, transplanted hybrid constructs (3DBP collagen + ES) in mouse defect models have shown improved ankle angle measurements comparable to nerve autografts regaining full ankle functional activity with time compared to the control (bulk collagen + ES).[79d] Thus, this suggests that the implanted hybrid 3D construct has a potential for tissue remodeling. In addition to that, in cases where cell-laden bioinks were 3D (bio) printed in combination with ES in a single setup, it was demonstrated that the cell viability was not affected by the ES process, in which cell viability was high and comparable with that of the positive control while using 20 kV voltage for a total duration of 1.25 h with cell viability of around 82%,[36a] and while using 10 kV for 10–20 s for each ES layer (3 layers in total) with cell viability of around 93%.[79i] Thus, confirming that the fabrication conditions were compatible with cell-laden bioink 3DBP under high voltage ES. Although the beforementioned studies[36a,79i] showed high cell viability while using 3DBP (with cells) in direct combination with ES, there are still concerns regarding the long-term effect on different types of cells and other biological components of the bioink. In addition to that, for long fabrication periods (1.25 h), it was stated that direct ES of PCL into a bath of PBS (phosphate buffered saline) solution was extremely necessary to prevent cell dehydration and subsequent cell death in case of combining ES with inkjet 3DBP.[36a] In summary, in the hybrid constructs, both the mechanical and biological properties were enhanced by better mimicking the native ECM, in which the electrospun layer allows for better cell adhesion, improved mechanical support, and acts as a physical barrier while allowing efficient air exchange and tissue fluid waste discharge. Meanwhile, the 3D bioprinted layer acts as a water-absorbing and cell-supporting layer, allowing for cell encapsulation, aggregation, and migration, as well as ECM protein secretion.[44,45,79c]

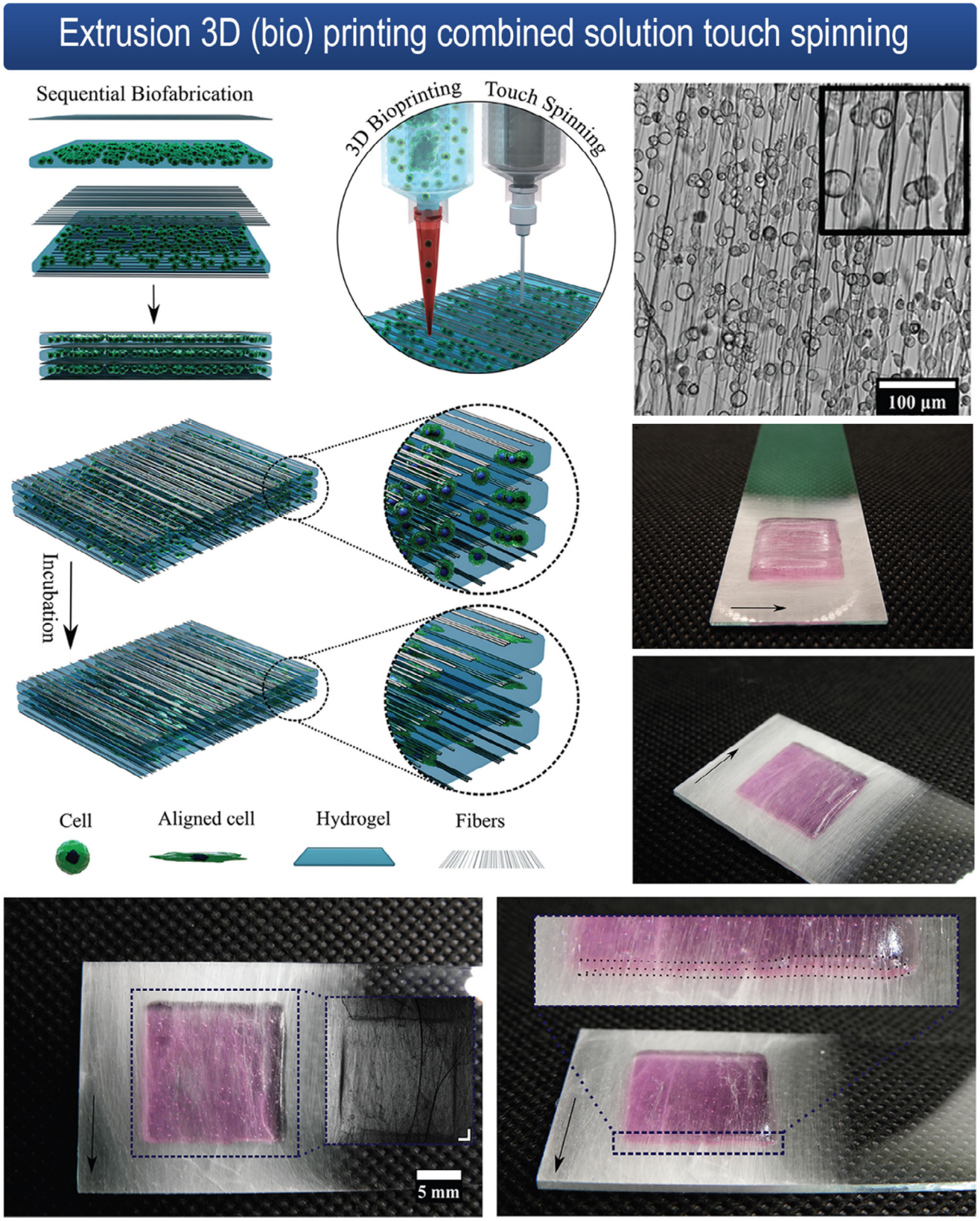

Figure 10. The integration of touch-spinning with 3D (bio) printing of cell-laden bioinks in a sequential multilayered approach to form a hybrid bioink-fiber construct. Reproduced under terms of the CC-BY license.[36b] Copyright 2023, The Authors. Advanced Healthcare Materials, published by Wiley-VCH GmbH.

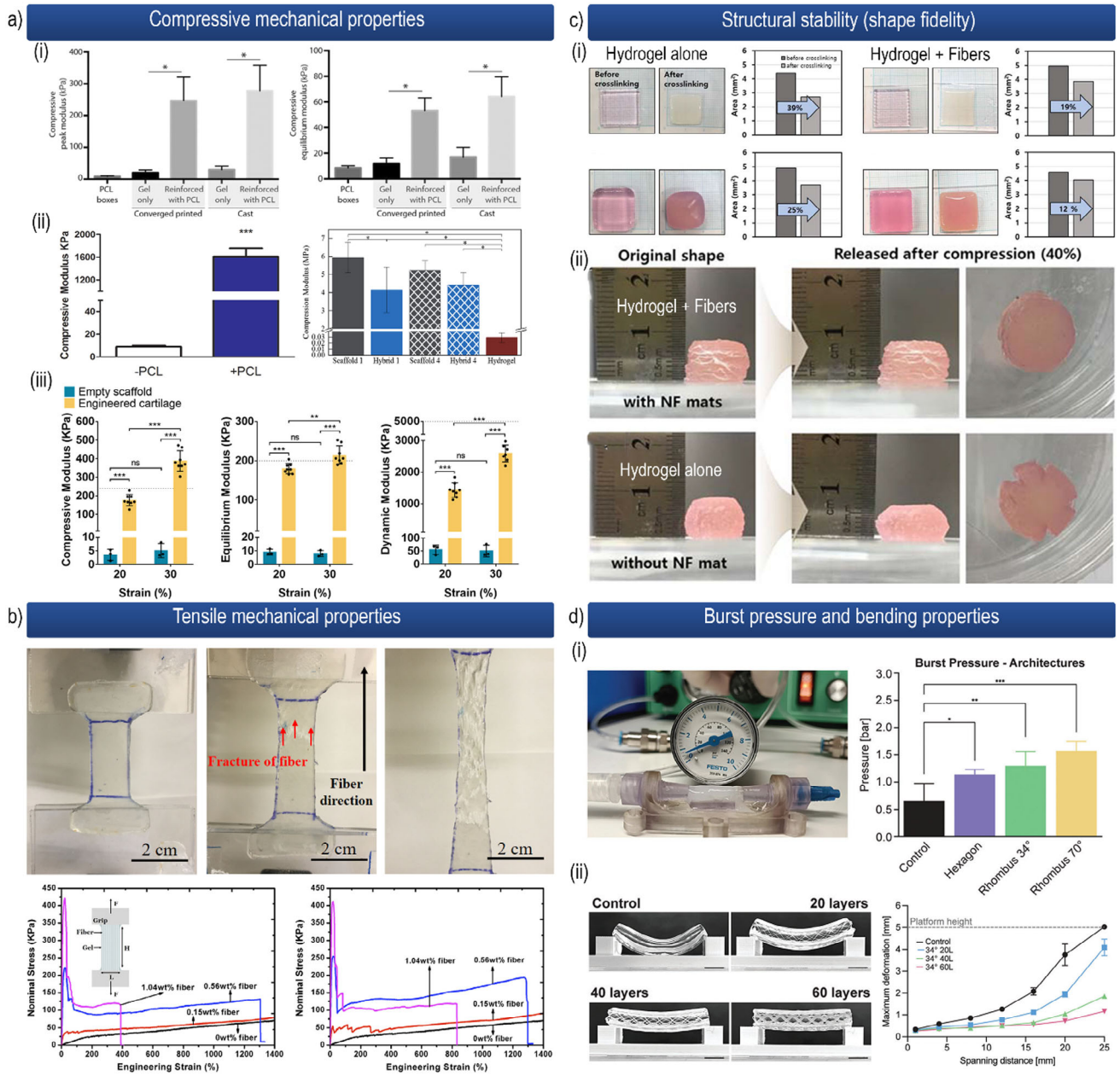

Figure 11. The enhanced mechanical properties of hybrid 3D constructs composed of hydrogel materials combined with fibrous structures. a) The improved compressive mechanical properties of hybrid constructs compared to hydrogel alone and/or fibers alone using 3D (bio) printing combined i) electrospinning. Reproduced under terms of the CC-BY license.[53] Copyright 2018, The Authors. Published by Wiley-VCH. ii) FDM 3D printing. Left) Reproduced with permission.[87l] Copyright 2016, Wiley-VCH. Right) Reproduced under terms of the CC-BY license.[32] Copyright 2022, The Authors. Published by Elsevier Ltd. And iii) melt electrowriting, adapted under terms of the CC-BY license.[49a] Copyright 2022, The Authors. Published by Elsevier Ltd. b) The increased tensile properties of hybrid constructs with the increased fiber content compared to the pristine hydrogel, adapted with permission.[88] Copyright 2016, Elsevier Ltd. c) The structural stability of the hybrid construct upon the addition of fibrous mats in a layer-by-layer approach, in which i) it enhances the shrinkage properties of the construct upon crosslinking and ii) the enhanced structural stability before and after compression. Reproduced with permission.[79b] Copyright 2019, IOP Publishing Ltd. d) The improved mechanical properties of hybrid tubular constructs fabricated using melt electrowriting combined volumetric 3D (bio) printing, in which mechanical properties of the hydrogel tubular construct were enhanced upon changing both the fibrous layer geometry and number of fibrous layers, where i) the burst pressure compared to the control (hydrogel alone) and ii) bending properties of the hybrid construct with increased number of layers compared to the control (hydrogel alone). Reproduced under terms of the CC-BY license.[2a] Copyright 2023, The Authors. Advanced Materials, published by Wiley-VCH GmbH.

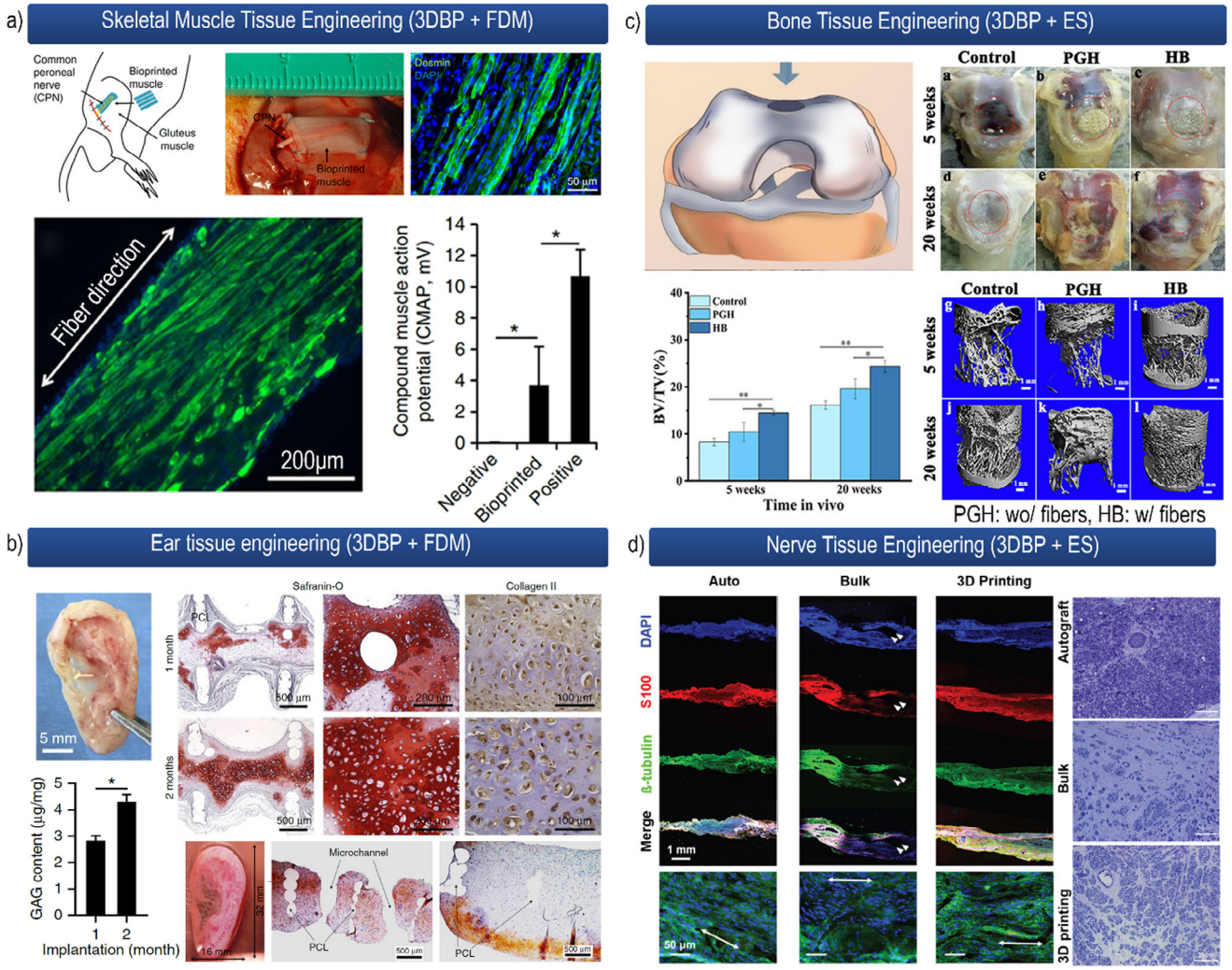

Figure 12. The enhanced biological performance of the hybrid constructs fabricated using combined 3D (bio) printing fiber fabrication methods for different tissue engineering applications. Integrated extrusion-based 3D (bio) printing with FDM 3D printing for a) skeletal muscle tissue engineering, where the mouse-implanted hybrid scaffold was able to induce functional tissue maturation with myotube alignment and sustained structural integrity with nerve tissue integration compared to the control. Reproduced with permission.[87f] Copyright 2016, Springer Nature America, Inc. And b) ear cartilage tissue reconstruction, in which the mouse model implanted (in vivo) hybrid construct was able to maintain its structural and cellular integrity with increased tissue maturation and extracellular matrix (ECM) formation with time. Reproduced with permission.[87f] Copyright 2016, Springer Nature America, Inc. c) The improved biological performance of the hybrid 3D constructs for bone tissue regeneration in vivo, in which the rabbit model implanted hybrid construct was able to remodel the bone tissue and prevented fibrotic tissue infiltration compared to the control. Reproduced with permission.[45] Copyright 2021, The Authors, Published by Elsevier Ltd. d) Nerve tissue regeneration of the rat model implanted hybrid constructs in vivo, in which the hybrid 3D tubular construct supported oriented dense nerve regrowth along the main axis of the tubular construct comparable to the control (nerve autograft). Reproduced with permission.[79d] Copyright 2020, Royal Society of Chemistry.

Similar to the combination of ES with 3DBP, integrating MEW with 3DBP led to improved biological and mechanical performance with the added advantage of the inherent ability of the MEW process to control the spatial arrangement of fibers with predefined pore geometry (e.g., hexagonal and rhombus). This combined approach was found to guide the cellular organization of different cell types, including myoblasts, MSCs, and iPSCs, in which the aligned fibers allowed for an oriented cell alignment along the fiber main direction with higher cell growth and improved cell differentiation as well as tissue-like structure formation with oriented fibrillar collagen organization comparable to native tissue.[49,57,84,85,86] Likewise, the mechanical properties of the hydrogels were significantly improved by their combination with MEW of fibers, in which considerably higher compressive properties,[49a,53] improved tensile properties,[2a] enhanced structural stability,[2a] and improved burst pressure (Figure 11d(i)) and bending properties (Figure 11d(ii))[2a] compared to hydrogel alone. For instance, the peak compressive modulus was increased by 1150% from around 20 kPa for hydrogel alone to 250 kPa for the hybrid construct, thus demonstrating the added advantage of improved mechanical properties.[53] Additionally, the mechanical properties of the hybrid construct can be improved and modulated by controlling the MEW fiber mesh architecture and number of layers to yield mechanical properties

comparable to that of different types of native tissues (Figure 11d(i)).[2a] From the point of view of the freedom in design and controlled geometric properties, integration of MEW with 3DBP allows for the fabrication of different geometrical features such as tissue interfaces,[84] out-of-plane free-standing fibers,[53] and pores and fenestrations[2a] in a complex multiscale hierarchical manner. In conclusion, the melt electrowritten fibers act as both mechanical support to the mechanically soft hydrogels and directional guidance for cells, whereas 3DBP allows for cell encapsulation, proliferation, aggregation, and migration.[2a,84]

FDM combined 3DBP have also shown enhanced biological and mechanical properties. in vitro, these hybrid structures (FDM + 3DBP) were able to guide cell orientation by using the perpendicularly FDM 3D printed PCL fibers as pillars that support the longitudinally aligned 3D (bio) printed cell-laden hydrogel strands extending between the PCL pillars from both sides, thus providing axial mechanical support, which is crucial for supporting cell organization.[87f,89] Thus, myoblasts were able to align and form aligned myotubes upon differentiation along the 3DBP direction with 3D printed PCL fibers as a pillar support, whereas samples without 3D printed PCL showed random orientation of myoblasts (Figure 12a).[87f]

Few studies have investigated the biological properties of the hybrid construct composed of FDM 3D printing combined with 3DBP in vivo.[87e,f,l,o] For instance, hybrid constructs composed of 3D (bio) printed cell-laden alginate and FDM 3D printed PCL fibers were implanted in mouse models and have shown cartilage tissue remodeling with GAGs, proteoglycans, and collagen matrix formation after 4 weeks of implantation, while maintaining the overall structure of the implanted hybrid construct and providing mechanical support for tissue maturation to occur in vivo.[87e,l] Although PCL provided the proper mechanical stability in vivo, it impedes tissue ingrowth due to the slow degradation rate of PCL, which usually takes more than 1 year for complete degradation.[87e,l,90] Similarly, hybrid structures composed of PCL framework and cell-laden fibrinogen hydrogels (1.2 mm thick) were implanted in vivo into a rat bone defect model. The implanted 3D construct was able to integrate with the native tissue by the formation of angiogenic blood vessels and mature bone tissue compared to the formation of fibrotic tissue with minimal vascularization and limited new bone tissue formation for the controls (cell-free construct and untreated defect site) after 5 months of implantation.[87f,l] Biomechanical analysis of the matured tissue after in vivo implantation of the hybrid construct in mouse cartilaginous ear models was also investigated. The results show that the in vivo implanted construct had considerably better mechanical properties compared to the non-implanted construct with higher bending strength and can sustain its mechanical properties over cyclic loading (Figure 12b). The electromechanical properties of in vivo implanted hybrid constructs were also studied for muscle tissue engineering, in which muscle tissue formation with vascular and nerve tissue ingrowth as well as enhanced muscle action potential compared to the negative control and comparable to native muscle tissue after 1 month of implantation have been observed (Figure 12a).[87f]

6. Fiber-Integrated 3D (Bio) Printing Biofabrication Setups

Currently, there are a few setups that integrate 3DBP with the most commonly used fiber fabrication methods: ES, MEW, and FDM. One example is the *R-Gen bioprinter* series (REGENHU, Villaz-St-Pierre, Switzerland); this setup integrates 3DBP (extrusion- and inkjet-based) with MEW, FDM, and ES. REGENHU is one of the very few commercial providers of 3D (bio) printers that integrated multiple biofabrication technologies under a single setup. This setup can accommodate up to five printheads. This includes pneumatic-driven drop-based (inkjet) printhead, pneumatic-driven extrusion-based bioprinting head, pneumatic-driven melt, and syringe pump-based (piston-based) melt extruders. All of these tools and their nozzles can be heat controlled to temperatures up to either 80 or 250 °C, depending on the application (hydrogels or melts). In addition, there are four different options for printing platforms to allow for voltage and heated/cooled options of the printing platforms. This includes a standard, high temperature, physiological temperature, and electro-writing and -spinning printing platforms. A further example, which integrates 3DBP with ES, MEW, and FDM, is a commercial bioprinter called *DomoBIO 4A* 3D Bioprinter from Domotek (Domotek, Donostia-San Sebastian, Spain) and currently distributed by IT3D Group (IT3D Technology, S.L, Valencia, Spain). This setup can accommodate up to four independent printheads of a total of six printheads available. This includes extrusion-based bioprinting head, heated extrusion-based bioprinting printhead (up to 60 °C), solution electrospinning extruder (up to 25 kV), filament-based melt extruder (up to 250 °C), pellet-based melt extruder (up to 250 °C), and melt electrowriting spin head (up to 250 °C and 25 kV). This setup also offers two different printing platforms, a refrigerated/heated and a high-performance heated platform.

A commercial setup that combines 3DBP with both MEW and FDM is the BioScaffolder 3.x and 5.x from GesiM GmbH (GeSiM – Gesellschaft für Silizium-Mikrosysteme mbH, Radeberg, Germany) with a wide range of modular printheads. This bioprinter can accommodate up to four independent printheads with various printhead options, including pneumatic-driven and/or piston-driven printheads with heating/cooling options of the tip and the cartridge and with a gradient mixer. The setup also offers a MEW spin head (± 30 kV), drop-based (inkjet) micro dispenser (piezoelectric, solenoid valve, and others) with droplet mixing, core-shell dispenser, high-temperature piston-driven extruder (up to 250 °C), melt blending extruder, filament extruder (FDM), capillary dispenser, and adhesives dispenser. A further example that integrates 3DBP with both MEW and FDM is *Axo* series from axolotl biosystems (axolotl biosystems Ltd, Istanbul, Turkey). The *Axo 6* bioprinter can accommodate up to six printheads of five different types of printheads available. Available printheads include a pneumatic-driven high-temperature extruder (up to 265 °C), pneumatic-driven low-temperature extruder (as low as 3 °C), pneumatic-driven MEW spin head (up to 265 °C and 15 kV), syringe pump (piston-driven) printhead, and pneumatic-driven cell electrowriting spin head (up to 15 kV). Another example is the *ExploreONE* bioprinter

from biomotion (Biomotion Technologies FlexCo, Vienna, Austria), which has four independent printheads, including, single/dual bioprinting printheads (pneumatic and piston-driven) (4 – 60 °C), pneumatic-based MEW printhead (up to 250 °C), and thermoplastic polymer extrusion (pellet (up to 300 °C), filament (up to 250 °C), and high-temperature pneumatic-driven extrusion (up to 250 °C)) extruders, the electromagnetic droplet-based printhead (up to 60 °C). This bioprinter also provides other printing options such as rotary, non-planar, coaxial, and Freeform Reversible Embedding of Suspended Hydrogels (FRESH) 3D printing.

There are many setups that combine 3DBP with FDM 3D printing; *3D-Bioplotter* (developed by EnvisionTEC GmbH, Gladbeck, Germany and currently distributed by Desktop Metal, Inc, Massachusetts, USA) is one example. 3D-Bioplotter offers up to five independent printhead slots with a high-temperature extruder reaching up to 500 °C. Furthermore, it offers eight different modular printheads (high-temperature (up to 250 °C), ultrahigh-temperature (up to 500 °C), inkjet (up to 70 °C), 2-component (up to 70 °C), co-axial (2 – 70 °C), photocuring (fixed at 25 °C) printheads. A further example is *BioAssemblyBot* (Advanced Solutions Life Sciences, LLC, Kentucky, USA), which is characterized by its robotic arm that is capable of using a wide variety of printheads (13 different printheads) and other tools (four different tools, e.g., eight-channel pipette). Another example is *Dr. INVIVO 4D2* and *Dr. INVIVO 4D6* (Rokit Healthcare, Seoul, South Korea). *Dr. INVIVO 4D2* offers two independent printhead slots and three different types of printheads (pneumatic-driven bioprinting (-4 – 60 °C) and melt (up to 350 °C) printheads as well as standard filament extruder (up to 250 °C)). *Dr. INVIVO 4D6* also offers two independent printhead slots. One of the slots uses a rotary printhead set that can accommodate up to five independent bioprinting printheads (up to 60 °C), and the second printhead is interchangeable and used for melt extrusion (pneumatic-(up to 350 °C) or filament-based (up to 250 °C)). This setup is characterized by having a built-in cell incubator. *REG4LIFE* and *BIO V1* (Regemat, Granada, Spain) offer up to three independent printheads with six types of printheads (syringe pump-based bioprinting head (cooled (-20 – 100 °C) or heated (up to 50 °C) (single or dual)), filament-based (single or dual), and pellet-based melt extruder (up to 250 °C)). An additional example is *Brinter* bioprinter (Brinter, North Carolina, USA), which has an automatically interchangeable printhead slot that offers eight different types of printheads/tools. These tools include a pneumatic-driven bioprinting head (single and triaxial/coaxial (4 – 66 °C)), pneumatic-driven cooled bioprinting head, pneumatic-driven drop-based (inkjet) head, pellet-based melt extruder (up to 250 °C), piston-driven extrusion-based bioprinting head, and microfluidic printhead. Another example is *3DXPrinter* (T&R Biofab, Siheung-si, South Korea), which offers up to six independent pneumatically-driven printheads (melt (up to 200 °C) and 3D bioprinting heads (4 – 60 °C)). A final example is *U-FAB* series (CLECELL, Seoul, South Korea). This setup can use up to three modules, with one having three independent submodules/printheads and two having six independent pneumatic and piston-driven submodules or printheads (melt (up to 180 °C), droplet, and extrusion-based (4 – 50 °C)) and filament-based melt extruder (up to 285 °C). **Table 7** summarizes the commercially available setups integrating 3DBP with the most commonly used fiber fabrication methods in tissue engineering: ES, MEW, and FDM.

Table 7. Available biofabrication setups that integrates 3D (bio) printing with most common fiber fabrication methods for tissue engineering applications.

Bioprinter	3DBP	ES	MEW	FDM
R-Gen bioprinter series	✓	✓	✓	✓
DomoBIO 4A	✓	✓	✓	✓
BioScaffolder	✓	✗	✓	✓
Axo	✓	✗	✓	✓
ExplorerONE	✓	✗	✓	✓
3D-Bioplotter	✓	✗	✗	✓
BioAssemblyBot	✓	✗	✗	✓
Dr. INVIVO 4D2	✓	✗	✗	✓
Dr. INVIVO 4D6	✓	✗	✗	✓
REG4LIFE	✓	✗	✗	✓
BIO V1	✓	✗	✗	✓
Brinter	✓	✗	✗	✓
3DXPrinter	✓	✗	✗	✓
U-FAB series	✓	✗	✗	✓

7. Conclusion and Future Perspectives

In conclusion, although 3DBP alone can provide a favorable environment for cell support by fabricating geometrically relevant cell-encapsulated hydrated 3D structures, which allows for cell maturation and ECM components formation with subsequent tissue maturation for short-term in vitro studies. It lacks the proper structural and mechanical stability for long-term in vitro and in vivo applications due to the inherent poor mechanical properties of the hydrogels used and their noncontrolled degradation rate. This will result in the loss of their initial 3D structure and mechanical properties with time. In addition to that, the isotropic nature of hydrogels and the lack of cell spatial guidance cues would result in non-controlled cell differentiation and function. Despite the fact that the mechanical stability of hydrogels could be increased by increasing the hydrogel precursor concentration or crosslinking degree, it usually results in cell entrapment, which disrupts many crucial cellular functions and imparts tissue in-growth. On the other hand, fiber fabrication methods provide fibrous scaffolds with the needed structural and mechanical properties but lack the ability to encapsulate cells within the hydrated 3D environment.[79i,87a,h,91] Thus, compared to 3DBP alone, hybrid 3D constructs fabricated using the combination of 3DBP and fiber fabrication methods allow for enhanced structural stability and improved mechanical properties as well as better biomimics the structure of native tissues, which is composed of gel-like materials and fibrous structures.[79i] For that, different fiber fabrication methods can be used in combination with 3DBP. The most common techniques are conventional solution ES, FDM 3D printing, and MEW. ES is a relatively slow fiber fabrication method, which yields fibers in the submicrometer range relevant for cells but usually yields 2D structures with non-controlled fiber deposition and limited thickness. Meanwhile, MEW yields relatively thicker fibers in the range of a few

micrometers, which is characterized by the controlled deposition of fibers to yield porous structures with controlled pore geometry. Similar to ES, MEW is a relatively slow fabrication method. The considerably long fabrication time of the most used fiber fabrication methods, including ES and MEW, remains a limiting factor, which adversely affects cell viability due to the drying of the 3D (bio) printed hydrogel precursor with time and the extended exposure of living cells to the harmful fabrication conditions such as the high voltage and high temperatures. On the contrary, from the point of view of scalability and direct integration, FDM 3D printing is a relatively fast fiber fabrication method, but on the other hand, it is characterized by its low-resolution fiber fabrication in the macroscale and the use of high temperatures for fiber extrusion and adhesin. Although many studies have investigated the combination of 3DBP with ES, the majority of them focused on a multi-step multi-setup approach. From the point of view of automation, true integration is only valid when there is minimal human intervention, in which the simultaneous interchange between 3DBP and fiber fabrication is semiautonomous. The advent of machine learning (ML) would allow for further breakthroughs in the field of biofabrication through the development of systemized, fully automated integrated biofabrication technologies.[1c] ML has been recently applied for the optimization of the ES parameters for wearable nanofiber acoustic energy harvesters using a feed-forward neural network.[92] In the biofabrication field, ML was applied for the optimization of MEW fiber fabrication parameters and conditions to yield porous fibrous structures for fibroblast cell confinement. Furthermore, the cell response and adhesion to the MEW fibers as a function of variable substrate geometry and porous structure were studied using ML.[93]

TS is a promising fiber fabrication method that allows automated integration with 3DBP in a cell-friendly environment. Using this technique, fibers are fabricated using pure mechanical drawing, yielding a well-controlled fiber alignment, crystallinity, diameter, and polymer chain alignment compared to ES and MEW. In order to expand the range of polymers that can be used for fiber fabrication and allow for true integration with 3DBP, a variety of promising fiber fabrication methods need to be further investigated for their possible integration with 3DBP. This will open new avenues for more advanced biofabrication processes to better replicate native tissues for several tissue engineering and regenerative medicine applications.

Integrating 3DBP with other fiber fabrication methods can also be applied to different fields of research, such as cellular agriculture. The most common application of cellular agriculture is the production of cultured meat and seafood. The use of this integrated approach would allow for the biofabrication of multimaterial multicellular 3D constructs, which better mimic the texture and structure of different types of natural meats. This is done by incorporating fibrous layers into cell-laden 3D (bio) printed layers in a precise and controlled manner. Additionally, these fibrous structures will support the mechanically soft bioink. Using this approach, multizonal multicellular cultivated meat products can be fabricated.[94] The 3D (bio) printed constructs are usually cultured in a dynamic culture environment using a bioreactor for better control over the culture conditions towards mature constructs.

The biofabricated hybrid constructs could also benefit from using bioreactors to develop fully functional tissues. The design of tissue-specific bioreactors would provide the biofabricated hybrid constructs with a controlled dynamic environment that mimics the native environment of cells. This will further stimulate the embedded or cultured cells with, for instance, mechanical and electrical cues towards fully functional tissue maturation. In addition to that, a dynamic cell culture environment using a bioreactor would enhance the oxygen and nutrient diffusion in thick 3D constructs (>200 μm).[87n,95] Moreover, using integrated biofabrication technologies can facilitate the fabrication of bioreactors and scaffolds for tissue engineering applications in a single setup. This will eliminate the need to use multiple setups to fabricate the bioreactor and 3D (bio) printed construct individually, which reduces the possibility of contamination and the difficulty of handling soft 3D (bio) printed or thin fibrous constructs.

Acknowledgements

The authors would like to acknowledge the German research foundation (Deutsche Forschungsgemeinschaft, DFG) for their financial support—with project funding numbers DFG IO 68/14-1, 68/14-2, and 326998133 – TRR 225 subproject A08.

Open access funding enabled and organized by Projekt DEAL.

Conflict of Interest

The authors declare no conflict of interest.

Keywords

3D (bio) printing, bioink-fiber, fiber spinning, hybrid printing, integrated biofabrication, regenerative medicine, tissue engineering

Received: January 6, 2025
Revised: March 6, 2025
Published online:

[1] a) L. Moroni, T. Boland, J. A. Burdick, C. De Maria, B. Derby, G. Forgacs, J. Groll, Q. Li, J. Malda, V. A. Mironov, C. Mota, M. Nakamura, W. Shu, S. Takeuchi, T. B. F. Woodfield, T. Xu, J. J. Yoo, G. Vozzi, *Trends Biotechnol.* **2018**, *36*, 384; b) J. Malda, J. Visser, F. P. Melchels, T. Jüngst, W. E. Hennink, W. J. A. Dhert, J. Groll, D. W. Hutmacher, *Adv. Mater.* **2013**, *25*, 5011; c) M. Castilho, M. de Ruijter, S. Beirne, C. C. Villette, K. Ito, G. G. Wallace, J. Malda, *Trends Biotechnol.* **2020**, *38*, 1316; d) L. Moroni, J. A. Burdick, C. Highley, S. J. Lee, Y. Morimoto, S. Takeuchi, J. J. Yoo, *Nat. Rev. Mater.* **2018**, *3*, 21; e) R. Levato, T. Jungst, R. G. Scheuring, T. Blunk, J. Groll, J. Malda, *Adv. Mater.* **2020**, *32*, 1906423; f) J. C. Rose, L. De Laporte, *Adv. Healthcare Mater.* **2018**, *7*, 1701067.

[2] a) G. Größbacher, M. Bartolf-Kopp, C. Gergely, P. N. Bernal, S. Florczak, M. de Ruijter, N. G. Rodriguez, J. Groll, J. Malda, T. Jungst, R. Levato, *Adv. Mater.* **2023**, *35*, 2300756; b) M. Tavafoghi, M. A. Darabi, M. Mahmoodi, R. Tutar, C. Xu, A. Mirjafari, F. Billi, W. Swieszkowski, F. Nasrollahi, S. Ahadian, V. Hosseini, A. Khademhosseini, N. Ashammakhi, *Biofabrication* **2021**, *13*, 042002; c) S. C. Neves, L. Moroni, C. C. Barrias, P. L. Granja, *Trends Biotechnol.* **2020**, *38*, 292.

[3] a) C. Frantz, K. M. Stewart, V. M. Weaver, *J. Cell Sci.* **2010**, *123*, 4195; b) N. Khuu, S. Kheiri, E. Kumacheva, *Trends Chem.* **2021**, *3*, 1002; c) J. Z. Gasiorowski, C. J. Murphy, P. F. Nealey, *Annu. Rev. Biomed. Eng.* **2013**, *15*, 155; d) T. J. McKee, G. Perlman, M. Morris, S. V. Komarova, *Sci. Rep.* **2019**, *9*, 10542.

[4] a) P. Datta, V. Vyas, S. Dhara, A. R. Chowdhury, A. Barui, *J. Bionic Eng.* **2019**, *16*, 842; b) G. R. Mitchell, A. Tojeira, *Proc. Eng.* **2013**, *59*, 117.

[5] E. Prince, E. Kumacheva, *Nat. Rev. Mater.* **2019**, *4*, 99.

[6] D. A. D. Parry, G. R. G. Barnes, A. S. Craig, D. C. Phillips, *Proc. R. Soc. Lond. Ser. B. Biol. Sci.* **1997**, *203*, 305.

[7] a) P. Heher, B. Maleiner, J. Prüller, A. H. Teuschl, J. Kollmitzer, X. Monforte, S. Wolbank, H. Redl, D. Rünzler, C. Fuchs, *Acta Biomater.* **2015**, *24*, 251; b) K. Sunadome, A. G. Erickson, D. Kah, B. Fabry, C. Adori, P. Kameneva, L. Faure, S. Kanatani, M. Kaucka, I. Dehnisch Ellström, M. Tesarova, T. Zikmund, J. Kaiser, S. Edwards, K. Maki, T. Adachi, T. Yamamoto, K. Fried, I. Adameyko, *Nat. Commun.* **2023**, *14*, 3060; c) M. Takaza, K. M. Moerman, J. Gindre, G. Lyons, C. K. Simms, *J. Mech. Behav. Biomed. Mater.* **2013**, *17*, 209.

[8] a) C. Papadacci, V. Finel, J. Provost, O. Villemain, P. Bruneval, J.-L. Gennisson, M. Tanter, M. Fink, M. Pernot, *Sci. Rep.* **2017**, *7*, 830; b) N. Tueni, J.-M. Allain, M. Genet, *J. Mech. Behav. Biomed. Mater.* **2023**, *138*, 105600.

[9] a) M. J. Hossain, H. Noori-Dokht, S. Karnik, N. Alyafei, A. Joukar, S. B. Trippel, D. R. Wagner, *J. Mech. Behav. Biomed. Mater.* **2020**, *109*, 103834; b) M. S. Bergholt, J.-P. St-Pierre, G. S. Offeddu, P. A. Parmar, M. B. Albro, J. L. Puetzer, M. L. Oyen, M. M. Stevens, *ACS Cent. Sci.* **2016**, *2*, 885.

[10] a) A. R. Markes, J. D. Hodax, C. B. Ma, *Clin. Sports Med.* **2020**, *39*, https://doi.org/10.1016/j.csm.2019.08.007; b) J. K. Bryceland, A. J. Powell, T. Nunn, *Cartilage* **2016**, *8*, 99.

[11] a) E. M. Feneck, P. N. Lewis, K. M. Meek, *Sci. Rep.* **2019**, *9*, 11277; b) B. Kong, Y. Chen, R. Liu, X. Liu, C. Liu, Z. Shao, L. Xiong, X. Liu, W. Sun, S. Mi, *Nat. Commun.* **2020**, *11*, 1435.

[12] a) L. Wang, Y. Wu, B. Guo, P. X. Ma, *ACS Nano* **2015**, *9*, 9167; b) A. D. Hofemeier, T. Limon, T. M. Muenker, B. Wallmeyer, A. Jurado, M. E. Afshar, M. Ebrahimi, R. Tsukanov, N. Oleksiievets, J. Enderlein, P. M. Gilbert, T. Betz, *eLife* **2021**, *10*, 60145.

[13] a) A. C. B. Allen, E. Barone, N. Momtahan, C. O. Crosby, C. Tu, W. Deng, K. Polansky, J. Zoldan, *Tissue Eng., Part A* **2019**, *25*, 1426; b) B. Liau, N. Christoforou, K. W. Leong, N. Bursac, *Biomaterials* **2011**, *32*, 9180; c) D. G. Hwang, H. Choi, U. Yong, D. Kim, W. Kang, S.-M. Park, J. Jang, *Adv. Mater.* **2024**, *n/a*, 2400364.

[14] a) R. A. Shirwaiker, M. B. Fisher, B. Anderson, K. G. Schuchard, P. B. Warren, B. Maze, P. Grondin, F. S. Ligler, B. Pourdeyhimi, *Tissue Eng., Part C* **2020**, *26*, 364; b) M. Du, K. Liu, H. Lai, J. Qian, L. Ai, J. Zhang, J. Yin, D. Jiang, *Bioactive Mater.* **2024**, *36*, 358; c) W. Niu, W. Guo, S. Han, Y. Zhu, S. Liu, Q. Guo, *Stem Cells Int.* **2016**, *2016*, 4717184.

[15] a) E. M. Espana, D. E. Birk, *Exp. Eye Res.* **2020**, *198*, 108137; b) A. Zhang, W. Zhang, L. J. Backman, J. Chen, *Stem Cells Int.* **2022**, *2022*, 5403995.

[16] a) H. R. C. Screen, D. E. Berk, K. E. Kadler, F. Ramirez, M. F. Young, *J. Orthopaedic Res.* **2015**, *33*, 793; b) P. Kannus, *Scand. J. Med. Sci. Sports* **2000**, *10*, 312; c) S. Zhang, W. Ju, X. Chen, Y. Zhao, L. Feng, Z. Yin, X. Chen, *Bioactive Mater.* **2022**, *8*, 124; d) A. D. Schoenenberger, J. Foolen, P. Moor, U. Silvan, J. G. Snedeker, *Acta Biomater.* **2018**, *71*, 306; e) S. L. Wunderli, U. Blache, J. G. Snedeker, *Connect. Tissue Res.* **2020**, *61*, 262; f) M. L. Bayer, C.-Y. C. Yeung, K. E. Kadler, K. Qvortrup, K. Baar, R. B. Svensson, S. Peter Magnusson, M. Krogsgaard, M. Koch, M. Kjaer, *Biomaterials* **2010**, *31*, 4889; g) C. J. Stender, E. Rust, P. T. Martin, E. E. Neumann, R. J. Brown, T. J. Lujan, *Biomech. Model. Mechanobiol* **2018**, *17*, 543.

[17] a) R. P. Wohlgemuth, S. E. Brashear, L. R. Smith, *Am. J. Physiol.: Cell Physiol.* **2023**, *325*, C1017; b) D. A. Sleboda, K. K. Stover, T. J. Roberts, *J. Morphol.* **2020**, *281*, 160; c) T. K. Borg, J. B. Caulfield, *Tissue Cell* **1980**, *12*, 197; d) T. F. Robinson, M. A. Geraci, E. H. Sonnenblick, S. M. Factor, *Circ. Res.* **1988**, *63*, 577.

[18] a) J. Shao, L. Lin, B. Tang, C. Du, *RSC Adv.* **2014**, *4*, 51165; b) R. Gottardi, U. Hansen, R. Raiteri, M. Loparic, M. Düggelin, D. Mathys, N. F. Friederich, P. Bruckner, M. Stolz, *PLoS One* **2016**, 0163552; c) J. C. Mansfield, V. Mandalia, A. Toms, C. P. Winlove, S. Brasselet, *J. R. Soc., Interface* **2019**, *16*, 20180611.

[19] a) M. Franchi, A. Triré, M. Quaranta, E. Orsini, V. Ottani, *Sci. World J.* **2007**, *7*, 404; b) H. Michna, *Virchows Arch. B* **1986**, *52*, 87.

[20] a) M. Georgiadis, R. Müller, P. Schneider, *J. R. Soc., Interface* **2016**, *13*, 20160088; b) M. Tzaphlidou, *J. Biol. Phys.* **2008**, *34*, 39; c) S. Bakbak, R. Kayacan, O. Akkuş, *J. Biomech.* **2011**, *44*,. d) N. Reznikov, R. Shahar, S. Weiner, *Bone* **2014**, *59*, 93; e) D. J. Buss, R. Kröger, M. D. McKee, N. Reznikov, *J. Struct. Biol.: X* **2022**, *6*, 100057.

[21] a) K. Comley, N. A. Fleck, *Int. J. Solids Struct.* **2010**, *47*, 2982; b) H. Y.-H. Smeland, N. Lu, T. V. Karlsen, G. Salvesen, R. K. Reed, L. Stuhr, *BMC Cancer* **2019**, *19*, 234; c) J. S. Choi, B. S. Kim, J. Y. Kim, J. D. Kim, Y. C. Choi, H.-J. Yang, K. Park, H. Y. Lee, Y. W. Cho, *J. Biomed. Mater. Res., Part A* **2011**, *97A*, 292; d) F. Louis, S. Kitano, J. F. Mano, M. Matsusaki, *Acta Biomater.* **2019**, *84*, 194.

[22] a) W. M. Han, N. L. Nerurkar, L. J. Smith, N. T. Jacobs, R. L. Mauck, D. M. Elliott, *Ann. Biomed. Eng.* **2012**, *40*, 1610; b) J. L. Bron, M. N. Helder, H.-J. Meisel, B. J. Van Royen, T. H. Smit, *Eur. Spine J.* **2009**, *18*, 301; c) D. M. K. Aladin, K. M. C. Cheung, A. H. W. Ngan, D. Chan, V. Y. L. Leung, C. T. Lim, K. D. K. Luk, W. W. Lu, *J. Orthopaedic Res.* **2010**, *28*, 497; d) T. Liang, L.-L. Zhang, W. Xia, H.-L. Yang, Z.-P. Luo, *Spine* **2017**, 42; e) C. M. Disney, K. Madi, A. J. Bodey, P. D. Lee, J. A. Hoyland, M. J. Sherratt, *Sci. Rep.* **2017**, *7*, 16279; f) C. M. Disney, J. Mo, A. Eckersley, A. J. Bodey, J. A. Hoyland, M. J. Sherratt, A. A. Pitsillides, P. D. Lee, B. K. Bay, *Acta Biomater.* **2022**, *138*, 361.

[23] Q. Li, F. Qu, B. Han, C. Wang, H. Li, R. L. Mauck, L. Han, *Acta Biomater.* **2017**, *54*, 356.

[24] a) K. Wolf, S. Alexander, V. Schacht, L. M. Coussens, U. H. von Andrian, J. van Rheenen, E. Deryugina, P. Friedl, *Semin. Cell Dev. Biol.* **2009**, *20*, 931; b) Y. Takeshi, T. Yoshiyuki, A. Tsutomu, *J. Biomed. Opt.* **2004**, *9*, 259; c) W. N. Meigel, S. Gay, L. Weber, *Arch. Dermatol. Res.* **1977**, *259*, BF00562732.

[25] a) J. Wu, Y. Du, S. C. Watkins, J. L. Funderburgh, W. R. Wagner, *Biomaterials* **2012**, *33*, 1343; b) A. J. Quantock, A. E. Meek Km Fau-Ridgway, A. J. Ridgway Ae Fau-Bron, E. J. Bron Aj Fau-Thonar, E. J. Thonar; c) C. Y. Park, J. K. Lee, R. S. Chuck, *Invest. Ophthalmol. Visual Sci.* **2015**, *56*, 5622; d) C. Boote, C. S. Kamma-Lorger, S. Hayes, J. Harris, M. Burghammer, J. Hiller, N. J. Terrill, K. M. Meek, *Biophys. J.* **2011**, *101*. e) K. M. Meek, C. Boote, *Exp. Eye Res.* **2004**, *78*, 503.

[26] a) K. Murata, T. Motayama, C. Kotake, *Atherosclerosis* **1986**, *60*, 251; b) J. A. Niestrawska, A. Pukaluk, A. R. Babu, G. A. Holzapfel, *Microsc. Microanal.* **2022**, *28*, 1649; c) M. J. Merrilees, K. M. Tiang, L. Scott, *Connect. Tissue Res.* **1987**, *16*, 237.

[27] a) D. E. Oken, R. J. Boucek, *Circ. Res.* **1957**, *5*, 357; b) A. J. Pope, G. B. Sands, B. H. Smaill, I. J. LeGrice, *Am. J. Physiol.: Heart Circ. Physiol.* **2008**, *295*, H1243.

[28] J. F. Jameson, M. O. Pacheco, H. H. Nguyen, E. A. Phelps, W. L. Stoppel, *Bioengineering* **2021**, *8*.

[29] a) M. Dey, I. T. Ozbolat, *Sci. Rep.* **2020**, *10*, 14023; b) Y. S. Zhang, G. Haghiashtiani, T. Hübscher, D. J. Kelly, J. M. Lee, M. Lutolf, M. C. McAlpine, W. Y. Yeong, M. Zenobi-Wong, J. Malda, *Nat. Rev. Methods Primers* **2021**, *1*, 75; c) S. V. Murphy, A. Atala, *Nat. Biotechnol.* **2014**, *32*, 773.

[30] J. Groll, J. A. Burdick, D. W. Cho, B. Derby, M. Gelinsky, S. C. Heilshorn, T. Jüngst, J. Malda, V. A. Mironov, K. Nakayama, A. Ovsianikov, W. Sun, S. Takeuchi, J. J. Yoo, T. B. F. Woodfield, *Biofabrication* **2019**, *11*, 013001.

[31] S. Jing, L. Lian, Y. Hou, Z. Li, Z. Zheng, G. Li, G. Tang, G. Xie, M. Xie, *Biofabrication* **2024**, *16*, 012004.

[32] F. Koch, O. Thaden, S. Conrad, K. Tröndle, G. Finkenzeller, R. Zengerle, S. Kartmann, S. Zimmermann, P. Koltay, *J. Mech. Behav. Biomed. Mater.* **2022**, *130*, 105219.
[33] a) X. Li, B. Liu, B. Pei, J. Chen, D. Zhou, J. Peng, X. Zhang, W. Jia, T. Xu, *Chem. Rev.* **2020**, *120*, 10793; b) I. Angelopoulos, M. C. Allenby, M. Lim, M. Zamorano, *Biotechnol. Bioeng.* **2020**, *117*, 272.
[34] a) W. Li, M. Wang, H. Ma, F. A. Chapa-Villarreal, A. O. Lobo, Y. S. Zhang, *iScience* **2023**, 26; b) B. Grigoryan, D. W. Sazer, A. Avila, J. L. Albritton, A. Padhye, A. H. Ta, P. T. Greenfield, D. L. Gibbons, J. S. Miller, *Sci. Rep.* **2021**, *11*, 3171.
[35] C. Dou, V. Perez, J. Qu, A. Tsin, B. Xu, J. Li, *ChemBioEng Rev.* **2021**, *8*, 517.
[36] a) T. Xu, K. W. Binder, M. Z. Albanna, D. Dice, W. Zhao, J. J. Yoo, A. Atala, *Biofabrication* **2013**, *5*, 015001; b) W. Kitana, V. Levario-Diaz, E. A. Cavalcanti-Adam, L. Ionov, *Adv. Healthcare Mater.* **2024**, *13*, 2303343; c) W. Schuurman, V. Khristov, M. W. Pot, P. R. van Weeren, W. J. A. Dhert, J. Malda, *Biofabrication* **2011**, *3*, 021001.
[37] C. C. Cook, E. J. Fong, J. J. Schwartz, D. H. Porcincula, A. C. Kaczmarek, J. S. Oakdale, B. D. Moran, K. M. Champley, C. M. Rackson, A. Muralidharan, R. R. McLeod, M. Shusteff, *Adv. Mater.* **2020**, *32*, 2003376.
[38] H. Onoe, T. Okitsu, A. Itou, M. Kato-Negishi, R. Gojo, D. Kiriya, K. Sato, S. Miura, S. Iwanaga, K. Kuribayashi-Shigetomi, Y. T. Matsunaga, Y. Shimoyama, S. Takeuchi, *Nat. Mater.* **2013**, *12*, 584.
[39] a) O. G. Andriotis, M. Nalbach, P. J. Thurner, *Acta Biomater.* **2023**, *163*, 35; b) R. B. Svensson, A. Herchenhan, T. Starborg, M. Larsen, K. E. Kadler, K. Qvortrup, S. P. Magnusson, *Acta Biomater.* **2017**, *50*, 293.
[40] a) A. Tokarev, D. Asheghali, I. M. Griffiths, O. Trotsenko, A. Gruzd, X. Lin, H. A. Stone, S. Minko, *Adv. Mater.* **2015**, *27*, 6526; b) A. J. Robinson, A. Pérez-Nava, S. C. Ali, J. B. González-Campos, J. L. Holloway, E. M. Cosgriff-Hernandez, *Matter* **2021**, *4*, 821.
[41] D. Asheghali, S.-J. Lee, A. Furchner, A. Gruzd, S. Larson, A. Tokarev, S. Stake, X. Zhou, K. Hinrichs, L. G. Zhang, S. Minko, *Nanomed.:Nanotechnol., Biol. Med.* **2020**, *24*, 102152.
[42] a) R. Rošic, J. Pelipenko, P. Kocbek, S. Baumgartner, M. Bešter-Rogač, J. Kristl, *Eur. Polym. J.* **2012**, *48*, 1374; b) S. Higashi, T. Hirai, M. Matsubara, H. Yoshida, A. Beniya, *Sci. Rep.* **2020**, *10*, 13427.
[43] L. F. Mellor, P. Huebner, S. Cai, M. Mohiti-Asli, M. A. Taylor, J. Spang, R. A. Shirwaiker, E. G. Loboa, *Biomed Res. Int.* **2017**, *2017*, 6956794.
[44] T. Zhang, H. Xu, Y. Zhang, S. Zhang, X. Yang, Y. Wei, D. Huang, X. Lian, *Mater. Des.* **2022**, *218*, 110711.
[45] J. Liu, Q. Zou, C. Wang, M. Lin, Y. Li, R. Zhang, Y. Li, *Mater. Des.* **2021**, *210*, 110047.
[46] T. L. Jenkins, S. Meehan, B. Pourdeyhimi, D. Little, *Tissue Eng., Part A* **2017**, *23*, 958.
[47] H. Lee, K. Watanabe, M. Kim, M. Gopiraman, K.-H. Song, J. S. Lee, I. S. Kim, *Sci. Rep.* **2016**, *6*, 37590.
[48] M. R. Badrossamay, H. A. McIlwee, J. A. Goss, K. K. Parker, *Nano Lett.* **2010**, *10*, 2257.
[49] a) A. Dufour, X. B. Gallostra, C. O'Keeffe, K. Eichholz, S. Von Euw, O. Garcia, D. J. Kelly, *Biomaterials* **2022**, *283*, 121405; b) T. D. Brown, P. D. Dalton, D. W. Hutmacher, *Adv. Mater.* **2011**, *23*, 5651; c) J. C. Kade, P. D. Dalton, *Adv. Healthcare Mater.* **2021**, *10*, 2001232.
[50] A. Nadernezhad, M. Ryma, H. Genç, I. Cicha, T. Jüngst, J. Groll, *Adv. Mater. Technol.* **2021**, *6*, 2100221.
[51] a) A. Reizabal, T. Kangur, P. G. Saiz, S. Menke, C. Moser, J. Brugger, P. D. Dalton, S. Luposchainsky, *Addit. Manuf.* **2023**, *71*, 103604; b) P. B. Warren, Z. G. Davis, M. B. Fisher, *J. Mech. Behav. Biomed. Mater.* **2019**, *99*, 153.
[52] a) J. He, G. Hao, Z. Meng, Y. Cao, D. Li, *Adv. Mater. Technol.* **2022**, *7*, 2101197; b) J. He, B. Zhang, Z. Li, M. Mao, J. Li, K. Han, D. Li, *Biofabrication* **2020**, *12*, 042002.
[53] M. de Ruijter, A. Ribeiro, I. Dokter, M. Castilho, J. Malda, *Adv. Healthcare Mater.* **2019**, *8*, 1800418.
[54] A. Khalf, S. V. Madihally, *Eur. J. Pharm. Biopharm.* **2017**, *112*, https://doi.org/10.1016/j.ejpb.2016.11.010.
[55] S.-J. Lee, D. Asheghali, B. Blevins, R. Timsina, T. Esworthy, X. Zhou, H. Cui, S. Y. Hann, X. Qiu, A. Tokarev, S. Minko, L. G. Zhang, *ACS Appl. Mater. Interfaces* **2020**, *12*, 2067.
[56] J. Uribe-Gomez, A. Posada-Murcia, A. Shukla, H. Alkhamis, S. Salehi, L. Ionov, *ACS Appl. Bio Mater.* **2021**, *4*, 5585.
[57] J. Uribe-Gomez, A. Posada-Murcia, A. Shukla, M. Ergin, G. Constante, I. Apsite, D. Martin, M. Schwarzer, A. Caspari, A. Synytska, S. Salehi, L. Ionov, *ACS Appl. Bio Mater.* **2021**, *4*, 1720.
[58] K. Watanabe, B.-S. Kim, Y. Enomoto, I.-S. Kim, *Macromol. Mater. Eng.* **2011**, *296*, 568.
[59] L. F. Deravi, N. R. Sinatra, C. O. Chantre, A. P. Nesmith, H. Yuan, S. K. Deravi, J. A. Goss, L. A. MacQueen, M. R. Badrossamy, G. M. Gonzalez, M. D. Phillips, K. K. Parker, *Macromol. Mater. Eng.* **2017**, *302*, 1600404.
[60] a) E. D. F. Ker, A. S. Nain, L. E. Weiss, J. Wang, J. Suhan, C. H. Amon, P. G. Campbell, *Biomaterials* **2011**, *32*, 8097; b) A. S. Nain, M. Sitti, A. Jacobson, T. Kowalewski, C. Amon, *Macromol. Rapid Commun.* **2009**, *30*, 1406; c) A. S. Nain, J. A. Phillippi, M. Sitti, J. MacKrell, P. G. Campbell, C. Amon, *Small* **2008**, *4*, 1153.
[61] Z. Ye, A. S. Nain, B. Behkam, *Nanoscale* **2016**, *8*, 12780.
[62] J. Schmidt, S. Shenvi Usgaonkar, S. Kumar, K. Lozano, C. J. Ellison, *Ind. Eng. Chem. Res.* **2022**, *61*, 65.
[63] a) R. Liu, X. Xu, X. Zhuang, B. Cheng, *Carbohydr. Polym.* **2014**, *101*, 1116; b) S. Sinha-Ray, S. Sinha-Ray, A. L. Yarin, B. Pourdeyhimi, *Polymer* **2015**, *56*, 452.
[64] a) N. D. Tien, T. Geng, C. A. Heyward, J. E. Reseland, S. P. Lyngstadaas, J. J. Blaker, H. J. Haugen, *Biomater. Adv.* **2022**, *137*, 212871; b) A. V. Popkov, D. E. Kulbakin, D. A. Popkov, E. N. Gorbach, N. A. Kononovich, N. V. Danilenko, K. S. Stankevich, E. L. Choynzonov, A. A. Zheravin, I. A. Khlusov, L. N. Bondar, V. M. Perelmuter, E. N. Bolbasov, S. I. Tverdokhlebov, *Biomed. Mater.* **2021**, *16*, 055005; c) E. Szymańska, M. Wojasiński, R. Czarnomysy, R. Dębowska, I. Łopianiak, K. Adasiewicz, T. Ciach, K. Winnicka, *Int. J. Mol. Sci.* **2022**, *23*. d) M. Klaas, K. Möll, K. Mäemets-Allas, M. Loog, M. Järvekülg, V. Jaks, *Sci. Rep.* **2021**, *11*, 20165; e) I. Łopianiak, W. Rzempołuch, M. Civelek, I. Cicha, T. Ciach, B. A. Butruk-Raszeja, *J. Biol. Eng.* **2023**, *17*, 20.
[65] D. Jao, V. Z. Beachley, *ACS Macro Lett.* **2019**, *8*, 588.
[66] L. Ren, V. Pandit, J. Elkin, T. Denman, J. A. Cooper, S. P. Kotha, *Nanoscale* **2013**, *5*, 2337.
[67] a) S. Padron, A. Fuentes, D. Caruntu, K. Lozano, *J. Appl. Phys.* **2013**, 113; b) J. J. Rogalski, C. W. M. Bastiaansen, T. Peijs, *Nanocomposites* **2017**, *3*, 97.
[68] a) A. Tokarev, O. Trotsenko, I. M. Griffiths, H. A. Stone, S. Minko, *Adv. Mater.* **2015**, *27*, 3560; b) J.-T. Li, X.-S. Jia, G.-F. Yu, X. Yan, X.-X. He, M. Yu, M.-G. Gong, X. Ning, Y.-Z. Long, *Nanoscale Res. Lett.* **2016**, *11*, 426.
[69] N. S. Yadavalli, D. Asheghali, A. Tokarev, W. Zhang, J. Xie, S. Minko, *Small* **2020**, *16*, 1907422.
[70] W. Wang, Y. Pan, Y. Shui, T. Hasan, I. M. Lei, S. G. S. Ka, T. Savin, S. Velasco-Bosom, Y. Cao, S. B. P. McLaren, Y. Cao, F. Xiong, G. G. Malliaras, Y. Y. S. Huang, *Nat. Electron.* **2024**, *7*, 586.
[71] a) Y. Cheng, F. Zheng, J. Lu, L. Shang, Z. Xie, Y. Zhao, Y. Chen, Z. Gu, *Adv. Mater.* **2014**, *26*, 5184; b) D. Wang, S. Maharjan, X. Kuang, Z. Wang, L. S. Mille, M. Tao, P. Yu, X. Cao, L. Lian, L. Lv, J. J. He, G. Tang, H. Yuk, C. K. Ozaki, X. Zhao, Y. S. Zhang, *Sci. Adv.* **2022**, *8*, abq6900.
[72] E. Kang, S.-J. Shin, K. H. Lee, S.-H. Lee, *Lab Chip* **2010**, *10*, 1856.
[73] E. Kang, G. S. Jeong, Y. Y. Choi, K. H. Lee, A. Khademhosseini, S.-H. Lee, *Nat. Mater.* **2011**, *10*, 877.

[74] F. Serpe, C. M. Casciola, G. Ruocco, G. Cidonio, C. Scognamiglio, *IJB* **2024**, 10.
[75] S.-K. Chae, E. Kang, A. Khademhosseini, S.-H. Lee, *Adv. Mater.* **2013**, *25*, 3071.
[76] a) F. Feng, J. He, J. Li, M. Mao, D. Li, *Int. J. Bioprinting* **2019**, 5; b) G. Addario, S. Djudjaj, S. Farè, P. Boor, L. Moroni, C. Mota, *Bioprinting* **2020**, *20*, 00108; c) C. Colosi, S. R. Shin, V. Manoharan, S. Massa, M. Costantini, A. Barbetta, M. R. Dokmeci, M. Dentini, A. Khademhosseini, *Adv. Mater.* **2016**, *28*, 677.
[77] a) G. Pecorini, S. Braccini, S. Simoni, A. Corti, G. Parrini, D. Puppi, *Macromol. Biosci.* **2024**, *n/a*, 2300538; b) D. Puppi, C. Migone, L. Grassi, A. Pirosa, G. Maisetta, G. Batoni, F. Chiellini, *Polym. Int.* **2016**, *65*, 631; c) S. C. Neves, C. Mota, A. Longoni, C. C. Barrias, P. L. Granja, L. Moroni, *Biofabrication* **2016**, *8*, 025012; d) D. Puppi, A. M. Piras, A. Pirosa, S. Sandreschi, F. Chiellini, *J. Mater. Sci.: Mater. Med.* **2016**, *27*, 44; e) F. Dini, G. Barsotti, D. Puppi, A. Coli, A. Briganti, E. Giannessi, V. Miragliotta, C. Mota, A. Pirosa, M. R. Stornelli, P. Gabellieri, F. Carlucci, F. Chiellini, *J. Bioactive Compatible Polym.* **2015**, *31*, 15.
[78] a) A. F. Quigley, R. Cornock, T. Mysore, J. Foroughi, M. Kita, J. M. Razal, J. Crook, S. E. Moulton, G. G. Wallace, R. M. I. Kapsa, *Front. Chem.* **2020**, 8; b) C. S. Miranda, A. F. G. Silva, C. L. Seabra, S. Reis, M. M. P. Silva, S. M. M. A. Pereira-Lima, S. P. G. Costa, N. C. Homem, H. P. Felgueiras, *Biomater. Adv.* **2023**, *151*, 213488.
[79] a) T. A.-O. Stocco, M. C. Moreira Silva, M. A. F. Corat, G. Gonçalves Lima, A. A.-O. Lobo, *Int. J. Nanomed.* **2022**, *17*, 1111; b) Y. Yoon, C. H. Kim, J. E. Lee, J. Yoon, N. K. Lee, T. H. Kim, S.-H. Park, *Biofabrication* **2019**, *11*, 025015; c) Q. Jin, Y. Fu, G. Zhang, L. Xu, G. Jin, L. Tang, J. Ju, W. Zhao, R. Hou, *Composites, Part B* **2022**, *234*, 109691; d) J. Yoo, J. H. Park, Y. W. Kwon, J. J. Chung, I. C. Choi, J. J. Nam, H. S. Lee, E. Y. Jeon, K. Lee, S. H. Kim, Y. Jung, J. W. Park, *Biomater. Sci.* **2020**, *8*, 6261; e) S.-J. Lee, M. Nowicki, B. Harris, L. G. Zhang, *Tissue Eng., Part A* **2016**, *23*, 491; f) Y.-Z. Yu, L.-L. Zheng, H.-P. Chen, W.-H. Chen, Q.-X. Hu, *Adv. Manuf.* **2014**, *2*, 231; g) T. Carranza, J. Uranga, A. Irastorza, A. Izeta, P. Guerrero, K. d. l. Caba, *IJB* **2023**, 9; h) F. Fazal, F. J. Diaz Sanchez, M. Waqas, V. Koutsos, A. Callanan, N. Radacsi, *Med. Eng. Phys.* **2021**, *94*, 52; i) X. Dai, X. Tian, S. Gu, Y. Yang, H. Li, P. Gao, Q. Lan, H. Cheng, *IJB* **2022**, 9.
[80] a) E. Cojocaru, J. Ghitman, G. G. Pircalabioru, A. Zaharia, H. Iovu, A. Sarbu, *Polymers* **2023**, *15*. b) W. Cao, S. Peng, Y. Yao, J. Xie, S. Li, C. Tu, C. Gao, *Acta Biomater.* **2022**, *152*, 60.
[81] F. Fazal, F. P. W. Melchels, A. McCormack, A. F. Silva, E.-L. Handley, N. A. Mazlan, A. Callanan, V. Koutsos, N. Radacsi, *Adv. Mater. Technol.* **2024**, *9*, 2400224.
[82] L. Liu, Y. A. Dzenis, *Nanotechnology* **2008**, *19*, 355307.
[83] a) B. Elveren, M. Kurečič, T. Maver, U. Maver, *Adv. Biol.* **2023**, *7*, 2300057; b) M. Yeo, G. H. Kim, *Small* **2018**, *14*, 1803491.
[84] M. J. Ainsworth, N. Chirico, M. de Ruijter, A. Hrynevich, I. Dokter, J. P. G. Sluijter, J. Malda, A. van Mil, M. Castilho, *Biofabrication* **2023**, *15*, 035025.
[85] a) X. Barceló, K. F. Eichholz, I. F. Gonçalves, O. Garcia, D. J. Kelly, *Acta Biomater.* **2023**, *158*, 216; b) N. Dubey, M. Rahimnejad, W. B. Swanson, J. Xu, M. de Ruijter, J. Malda, C. H. Squarize, R. M. Castilho, M. C. Bottino, *ACS Macro Lett.* **2024**.
[86] G. Constante, I. Apsite, H. Alkhamis, M. Dulle, M. Schwarzer, A. Caspari, A. Synytska, S. Salehi, L. Ionov, *ACS Appl. Mater. Interfaces* **2021**, *13*, 12767.
[87] a) J.-H. Shim, J.-S. Lee, J. Y. Kim, D.-W. Cho, *J. Micromech. Microeng.* **2012**, *22*, 085014; b) J.-H. Shim, J. Y. Kim, M. Park, J. Park, D.-W. Cho, *Biofabrication* **2011**, *3*, 034102; c) T. Zehnder, T. Freund, M. Demir, R. Detsch, A. R. Boccaccini, *Materials* **2016**, *9*. d) F. Pati, J. Jang, D.-H. Ha, S. W. Kim, J.-W. Rhie, J.-H. Shim, D.-H. Kim, D.-W. Cho, *Nat. Commun.* **2014**, *5*, 3935; e) J. Kundu, J.-H. Shim, J. Jang, S.-W. Kim, D.-W. Cho, *J. Tissue Eng. Regener. Med.* **2015**, *9*, 1286; f) H.-W. Kang, S. J. Lee, I. K. Ko, C. Kengla, J. J. Yoo, A. Atala, *Nat. Biotechnol.* **2016**, *34*, 312; g) J. W. Jung, J.-S. Lee, D.-W. Cho, *Sci. Rep.* **2016**, *6*, 21685; h) Z. Izadifar, T. Chang, W. Kulyk, X. Chen, B. F. Eames, *Tissue Eng. Pt C: Methods* **2015**, *22*, 173; i) J.-S. Lee, J. M. Hong, J. W. Jung, J.-H. Shim, J.-H. Oh, D.-W. Cho, *Biofabrication* **2014**, *6*, 024103; j) F. Koch, O. Thaden, K. Tröndle, R. Zengerle, S. Zimmermann, P. Koltay, *HardwareX* **2021**, *10*, 00230; k) J. H. Shin, H.-W. Kang, *Int. J. Precision Eng. Manuf.* **2018**, *19*, 767; l) A. C. Daly, G. M. Cunniffe, B. N. Sathy, O. Jeon, E. Alsberg, D. J. Kelly, *Adv. Healthcare Mater.* **2016**, *5*, 2353; m) R. Burdis, F. Chariyev-Prinz, D. J. Kelly, *Biofabrication* **2022**, *14*, 015008; n) A. C. Daly, D. J. Kelly, *Biomaterials* **2019**, *197*, 194; o) G. M. Cunniffe, T. Gonzalez-Fernandez, A. Daly, B. N. Sathy, O. Jeon, E. Alsberg, D. J. Kelly, *Tissue Eng., Part A* **2017**, *23*, 891; p) D. Ke, H. Yi, S. Est-Witte, S. George, C. Kengla, S. J. Lee, A. Atala, S. V. Murphy, *Biofabrication* **2020**, *12*, 015022.
[88] Q. He, Z. Wang, Y. Yan, J. Zheng, S. Cai, *Extreme Mech. Lett.* **2016**, *9*, 165.
[89] J. H. Ahrens, S. G. M. Uzel, M. Skylar-Scott, M. M. Mata, A. Lu, K. T. Kroll, J. A. Lewis, *Adv. Mater.* **2022**, *34*, 2200217.
[90] H. Sun, L. Mei, C. Song, X. Cui, P. Wang, *Biomaterials* **2006**, *27*, 1735.
[91] A. D. Augst, H. J. Kong, D. J. Mooney, *Macromol. Biosci.* **2006**, *6*, 623.
[92] N. H. Kouchehbaghi, M. Yousefzadeh, A. Gharehaghaji, S. Khosravi, D. Khorsandi, R. Haghniaz, K. Cao, M. R. Dokmeci, M. Rostami, A. Khademhosseini, Y. Zhu, *Nano Res.* **2024**, *17*, 9181.
[93] F. Tourlomousis, C. Jia, T. Karydis, A. Mershin, H. Wang, D. M. Kalyon, R. C. Chang, *Microsyst. Nanoeng.* **2019**, *5*, 15.
[94] a) F. B. Albrecht, T. Ahlfeld, A. Klatt, S. Heine, M. Gelinsky, P. J. Kluger, *Adv. Healthcare Mater.* **2024**, *13*, 2304058; b) X. Guo, D. Wang, B. He, L. Hu, G. Jiang, *Food Bioprocess Technol.* **2024**, *17*, 1659.
[95] a) M. Thangadurai, S. S. Srinivasan, M. P. Sekar, S. Sethuraman, D. Sundaramurthi, *J. Mater. Chem. B* **2024**, *12*, 350; b) N. Sarkar, S. Bhumiratana, L. Geris, I. Papantoniou, W. L. Grayson, *Nat. Rev. Bioeng.* **2023**, *1*, 361.

Waseem Kitana received his Bachelor's degree in biomedical engineering from the German-Jordanian University Amman, Jordan in 2018. In 2021, he received his Master's degree in biofabrication from the University of Bayreuth. Since 2021, he has been pursuing his Ph.D. degree at the professorship of Biofabrication at the University of Bayreuth. His research focuses on the broad research area of Biofabrication and tissue engineering, including 4D Biofabrication, 3D (bio) printing, and fiber spinning techniques. Currently, focusing on integrated fabrication technologies for the fabrication of anisotropic microtissues using integrated 3D (bio) printing of bioinks and fiber spinning for tissue engineering applications.

Indra Apsite received her Bachelor's and Master's degrees in chemistry from the University of Latvia (Riga) in 2013 and 2015, respectively. She completed her Ph.D. in polymer science at the University of Bayreuth (Germany) in 2020. She is currently a PostDoc at the University of Bayreuth. Her current research focuses on fiber-reinforced tissues utilizing various fiber fabrication techniques and 3D (bio) printing.

Leonid Ionov is a professor of biofabrication at the University of Bayreuth. He graduated in chemistry in 1999 from Lomonosov Moscow State University and completed his Ph.D. in 2005 and habilitation in 2015 at Dresden University of Technology. After that, he worked as a faculty member at the University of Georgia. His main research activities are focused on 3D printing and bioprinting, biomaterials, 4D biofabrication, stimuli-responsive and shape-changing materials, as well as flexible electronics.